

**3-D STRUCTURAL AND SEISMIC STRATIGRAPHIC
INTERPRETATION OF THE GUASARE-MISOA INTERVAL, VLE 196
AREA, BLOCK V, LAMAR FIELD, LAKE MARACAIBO, VENEZUELA**

A Thesis

by

SADUN ARZUMAN

Submitted to the Office of Graduate Studies of
Texas A&M University
in partial fulfillment of the requirements for the degree of

MASTER OF SCIENCE

December 2002

Major Subject: Geology

ABSTRACT

3-D Structural and Seismic Stratigraphic Interpretation of the Guasare-Misoa Interval,
VLE 196 Area, Block V, Lamar Field, Lake Maracaibo, Venezuela. (December 2002)

Sadun Arzuman, B.S., Istanbul Technical University

Co-Chairs of Advisory Committee: Dr. Joel S. Watkins
Dr. Richard Gibson

In this study, the structure, depositional system, and the seismic stratigraphy of the VLE 196 area, Block V in Lamar Field were interpreted using 3-D seismic data and well logs to characterize structural and depositional settings of the Guasare-Misoa interval.

To demonstrate structural settings of the study area 3-D seismic data were interpreted. Three main seismic reflectors, which are the Late Eocene unconformity, Guasare, and La Luna formations, were picked. The most dominant structure in the area is the VLE 400 Fault which was interpreted as a left-lateral strike-slip reverse fault due to its behaviors as a reverse fault in cross sections and as a strike-slip fault in strike sections. The VLE 400 Fault subdivides the VLE 196 area into two main structural blocks, a downthrown block in the western part and the upthrown block in the eastern part of the field where the hydrocarbons were trapped. Several en echelon normal and reverse faults were located along the both sides of the area. The main importance of these faults are that they fractured the La Luna source rock and created migration pathways through the reservoir layers of the Misoa Formation.

To interpret depositional system of the Guasare-Misoa interval, tops of the C4 and C5 intervals and associated C4 layers were picked based on well logs and lithofacies maps were prepared. The results of this part of the study show that the sandstones of the Misoa Formation are delta front and fluvial/distributary channel facies of delta system. The net sand thickness map of the C4 interval also exhibits southeast northwest contour patterns reflecting depositional axes in the area. Shaly units of the C4 interval interpreted as potential seals and are of variable thickness and extend.

Seismic stratigraphic interpretation of the area shows that the four main seismic facies are dominant which mainly represent the recent sediments, “C” sands of the Misoa Formation, underlying Colon and Mito Juan shales, and basement respectively. Some distributary eroded channel fill structures were also observed within the Misoa Formation, but they were not continuous through the area because of the intensive faulting.

DEDICATION

In memory of my mother

ACKNOWLEDGEMENTS

I would like to thank my committee chair, Dr. Joel S. Watkins, for his encouragement, guidance, and friendship. I also thank the rest of my committee members Dr. Richard Gibson and Dr. William Bryant for their support during my research.

I thank Ercin Ozgul, Rasheed Jaradat, and Munji Syarif for their ideas and discussions.

Very special thanks to my sponsors, Turkish Petroleum Company and Turkish Ministry of Education for giving me an opportunity to participate in the TAMU graduate program and for their financial support during my study.

Special thanks go to my sister and brother for their love, patience, and understanding.

Participating a graduate program at the Texas A&M University, Department of Geology and Geophysics has been a very gratifying experience, and I believe it will profoundly impact my professional career.

TABLE OF CONTENTS

	Page
ABSTRACT	iii
DEDICATION	v
ACKNOWLEDGEMENTS	vi
TABLE OF CONTENTS	vii
LIST OF FIGURES	ix
LIST OF TABLES	xiii
CHAPTER	
I INTRODUCTION.....	1
1.1 Objectives	1
1.2 Location	2
1.3 Data Base	4
II BACKGROUND	8
2.1 Tectonic Settings	8
2.1.1 Plate-Scale Settings	8
2.1.2 Tectonic Evolution and Structural Settings of the Lake Maracaibo Basin	11
2.2 Sedimentary Basin Settings	16
2.2.1 Depositional System and Stratigraphy	16
2.2.2 Hydrocarbon Environment	21
III STRUCTURAL INTERPRETATION	26
3.1 Methodology	26
3.2 Main Structure and Faults Network	27
3.2.1 Model: Strike-Slip Faulting, Restraining Bend	27
3.2.2 Structural Interpretation of the Area	30
3.2.3 Hydrocarbon Trapping	42
3.2.4 Results	44

CHAPTER	Page
IV DEPOSITIONAL SYSTEM and SEISMIC STRATIGRAPHY	45
4.1 Depositional System	45
4.1.1 Model: Tide-Dominated Delta	45
4.1.2 Interpretation of the Depositional System	48
4.1.3 Results	64
4.2 Seismic Stratigraphy	66
4.2.1 Principles	66
4.2.2 Seismic Stratigraphic Interpretation	68
4.2.3 Results	86
V DISCUSSION	88
VI CONCLUSIONS	91
REFERENCES CITED	95
APPENDIX A	103
APPENDIX B	104
APPENDIX C	105
APPENDIX D	107
APPENDIX E	108
VITA	109

LIST OF FIGURES

FIGURE	Page
1.1 Location of the study area	3
1.2 Seismic basemap showing the location of the wells	7
2.1 Four-stage depiction of the evolution of the Caribbean region	10
2.2 Tectonic map of the Maracibo-Falcon province showing zones in relation to major fault trends.....	12
2.3 Present structural styles in the Maracaibo Basin	15
2.4 Generalized stratigraphic column for the Lake Maracaibo and surrounding areas	17
2.5 Simplified Early to Middle Eocene paleogeographic map of the Maracaibo Basin showing southwest to northeast transition from fluvial to deltaic to open-marine relations	20
2.6 Generalized stratigraphic column of the central Lake Maracaibo and associated main seismic markers	22
2.7 Location of oil and gas fields in the Maracaibo Basin, within dashed outline	25
3.1 Assemblage of structures associated with divergent wrench faults and simplified strain ellipse for left-slip deformation (inset)	29
3.2 Synoptic diagram illustrating the 3-D geometry of an idealized pop-up structure, which is created by zone of compression in restraining bends or restraining sidesteps	29
3.3 Time structure map of the Late Eocene unconformity	31
3.4 3D perspective visualization of the main structure in the area	32
3.5 (a) Seismic in-line 655 showing main faults and formations in the study area. (b) Shaded relief, time-structure map of the Late Eocene unconformity on the seismic basemap.....	34

FIGURE	Page
3.6 (a) Seismic cross-line 420 showing normal and reverse en echelon faults in the study area. (b) Shaded relief, time-structure map of the Guasare Formation	35
3.7 (a) Seismic cross-line 340. (b) Shaded-relief, time-structure map of the La Luna Formation showing the VLE 400 and complementary fault	36
3.8 Fault polygon map of the Guasare Formation showing the general structure	38
3.9 3D perspective visualization (top view) of the VLE 400 and associated complementary faults and time slice 3.100 s	40
3.10 3D perspective visualization of faults and horizons perpendicular of the strike of the en echelon normal faults which are created migration pathways cutting overlying sediments of the La Luna source rock	41
3.11 3D perspective wireframe visualization of the four-way trapping mechanism in the VLE 196 area	43
4.1 Conceptual model of the tide-dominated delta	47
4.2 Type log (VLE 1063) showing log patterns, reservoir layers, and sedimentary facies	50
4.3 Layer 1 lithofacies maps	52
4.4 Layer 3 lithofacies maps	53
4.5 Layer 5 lithofacies maps	54
4.6 (a) Net sand thickness map of the C4 interval. (b) Isopach map of the C4 interval	56
4.7 (a) Average porosity map of the C-4 interval. (b) Log facies map of the C-4 interval	57
4.8 Stratigraphic cross-section A-A' along the depositional dip (northeast-southwest)	60

FIGURE	Page
4.9 Stratigraphic cross-section B-B' along the depositional strike (northwest-southeast)	61
4.10 Stratigraphic cross-section C-C' along the depositional strike (northwest-southeast)	62
4.11 (a) Seismic stratigraphic reflection terminations within idealized seismic sequence. (b) Various seismic reflection configurations and modifications. (c) Seismic reflection patterns interpreted as prograding clinoforms	67
4.12 Isochron map of the C4 interval	70
4.13 Isopach (true vertical thickness) map of the C4 interval	72
4.14 Enlarged image of the dotted line area in Figure 4.13	73
4.15 Correlation plot of the C4 interval thickness from well and seismic data	74
4.16 Seismic facies recognized in this study and their characteristics and geological interpretation	76
4.17 Locations of the seismic lines in Figure 4.18 to Figure 4.22 on the seismic basemap	80
4.18 (a) Seismic line A-A' (amplitude display) showing the general reflection character of the Guasare-Misoa interval. (b) Interpreted phase display of the line A-A'	81
4.19 (a) Seismic line B-B' (amplitude display) along the depositional dip (southwest-northeast) showing the stacking pattern of the Guasare-Misoa interval. (b) Interpreted phase display of the line B-B'	82
4.20 Seismic line C-C' (amplitude display) showing the aggradational deposition of "C" sands in the Misoa Formation. (b) Interpreted phase display of the line C-C'	83
4.21 Seismic line D-D' (amplitude display) along the depositional strike (southeast-northwest) showing progradational reflection patterns within the Misoa Formation. (b) Interpreted phase display of the line D-D'	84

FIGURE Page

- 4.22 Seismic line E-E' (amplitude display) showing the reflection pattern of the Misoa and Guasare formations in the west side of the area (downthrown block). (b) Interpreted phase display of the line E-E' 85

LIST OF TABLES

TABLE	Page
1.1 3-D seismic data acquisition parameters for the VLE 196 area	5
1.2 Well log data used in this study	6

CHAPTER I

INTRODUCTION

1.1 Objectives

The Lake Maracaibo Basin is one of the most prolific oil producing fields in the world. Because of its complex structure, it is very important to understand detailed relationships between fault networks and stratigraphy of the area for future field development.

The Lamar Field is one of the most producing fields in the Lake Maracaibo Basin, which is discovered in 1958. The use of 3D seismic data to interpret old producing fields is very important in assessing in field development and the VLE 196 area exhibits one of the best examples of old producing fields. When integrated with well log data, 3D seismic provides the best tool to determine the seismic stratigraphic and structural framework for an area.

The main purpose of this study to define the structural and depositional settings of the VLE 196 area and to demonstrate a seismic stratigraphic model for the Guassare-Misoa interval within its depositional environment in the VLA 196 area, Block V, Lamar Field. To do this, structure, depositional system, and seismic stratigraphy of the area were interpreted using 3-D seismic data and existing well logs. Time horizons, faults,

The style and format of this thesis follow that of the Bulletin of the American Association of Petroleum Geologists.

seismic stratigraphic relations, and lithofacies were mapped. Results gathered from well log interpretation correlated with seismic data and they were tried to determine possible secondary recovery areas.

1.2 Location

The Maracaibo Basin is located in northwestern Venezuela, South America as shown in Figure 1.1. The basin occupies an area approximately of 24,200 sq. ml. (62,000 sq. km.), of which about 5,000 sq. ml. (12,900 sq. km.) are covered by Lake Maracaibo. Within the lake proper elevation is more than 328 ft. (100 m.) (Sutton, 1946). The basin is limited to the north by the Oca fault, to the west by the Sierra de Perija, to the southeast by Merida Andes Mountains, and to the east by Serrania de Trujillo.

The Maracaibo Basin is one of the most prolific oil-producing basins in the world. Approximately 35 billion barrels (bbl) of oil have been produced from this basin since 1946 and containing an estimated 200 billion stock-tank barrels of original oil in place (Tyler et al., 1994) (Ambrose and Ferrer, 1997).

The Lamar field is owned and operated by Maraven S.A., one of the national oil companies of the Venezuela which is responsible for operations in the Lake Maracaibo and it is located in south central lake, in the eastern part of the Lama-Icotea fault. It covers an area of 8,700 acres. The study area VLA 196, Block V is located in the northwestern part of the Lamar field (Figure 1.1).

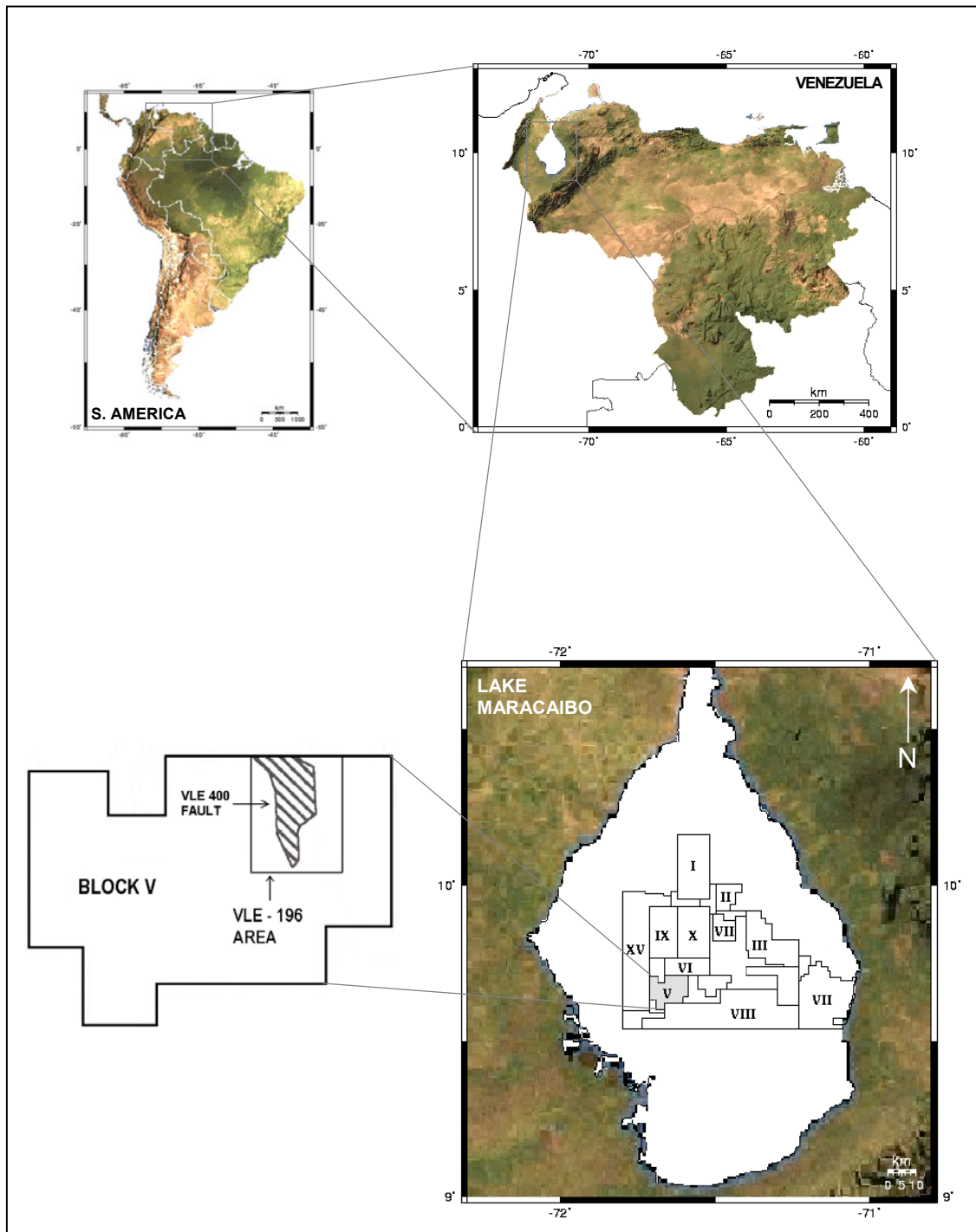


Figure 1.1 Location of the study area.

1.3 Data Base

Data set used in this study includes seismic and well logs. The 3-D seismic amplitude data covers an area of 37 km² subset of the 609 km² survey shot in the Lake Maracaibo. Seismic survey was shot and processed by Western Geophysical in 1992. The bin spacing of the data is 30 by 30 m and record length is 6.1 s. Detailed acquisition parameters of time migrated seismic data are listed in Table 1.1. The reflection quality of the data is very good and faults and stratigraphic picks for horizons are easily recognizable (Holditch and Associates Inc., 1997).

24 well logs were used in this study to integrate seismic and well-log data. Well data include time depth curves and digital well curves. These wells were drilled in the western side of the study area, leaving the eastern side with no well control. Therefore, well log analysis was done mainly for the area covered by well logs. Locations of the wells are shown on the basemap in Figure 1.2 and well types are shown in Table 1.2.

Table 1.1 3-D seismic data acquisition parameters for the VLE 196 area (Holditch and Associates Inc., 1997).

Sampling rate	2 milliseconds
Record length	6.1 seconds
Energy source	Air guns
Receiver and source array	East-West receivers and North-South shots
Number of instrument channels	256
Line of configuration of 128 hydrophones	
Distance between receivers	60 meters
Hydrophone frequency	10 Hz
Distance between receiver lines	600 meters
Patch	2 lines of 128 hydrophones each
Shot line	80 shots
Distance between shot points	60 meters
Distance between shot lines	240 meters
Bin size	30 m * 30 m
Coverage	$8 * 4 = 3200\%$

Table 1.2 Well log data used in this study. (ACAL: caliper, ASN: short normal resistivity, LLD: laterolog deep resistivity, LN: log normal resistivity, LLS: laterolog shallow resistivity, CNLLC: neutron porosity, RHOCN: bulk density, DT: sonic, GR: gamma ray, (*): type log)

Well ID	ACAL	ASN	LLD	LN	LLS	CNLLC	RHOCN	DT	GR
VLE 0096	x	x	x			x	x		x
VLE 0196	x	x		x					x
VLE 0400	x	x					x		x
VLE 0449	x	x					x		x
VLE 0504	x	x					x		x
VLE 0506	x	x					x		x
VLE 0510	x	x					x		x
VLE 0516	x	x					x		x
VLE 0571	x	x					x		x
VLE 0619	x	x					x		x
VLE 0631*	x	x					x		x
VLE 0651	x	x					x		x
VLE 0674	x	x					x		x
VLE 0675	x	x				x	x		x
VLE 0677	x		x		x	x	x		x
VLE 0973	x		x		x	x	x		x
VLE 1004	x		x		x				x
VLE 1063*	x		x		x		x	x	x
VLE 1101	x		x		x		x		x
VLE 1130	x		x		x		x		x
VLE 1139	x		x		x		x		x
VLE 1140	x		x		x		x		x
VLE 1148	x		x		x		x		x
VLE 1155	x		x		x		x		x

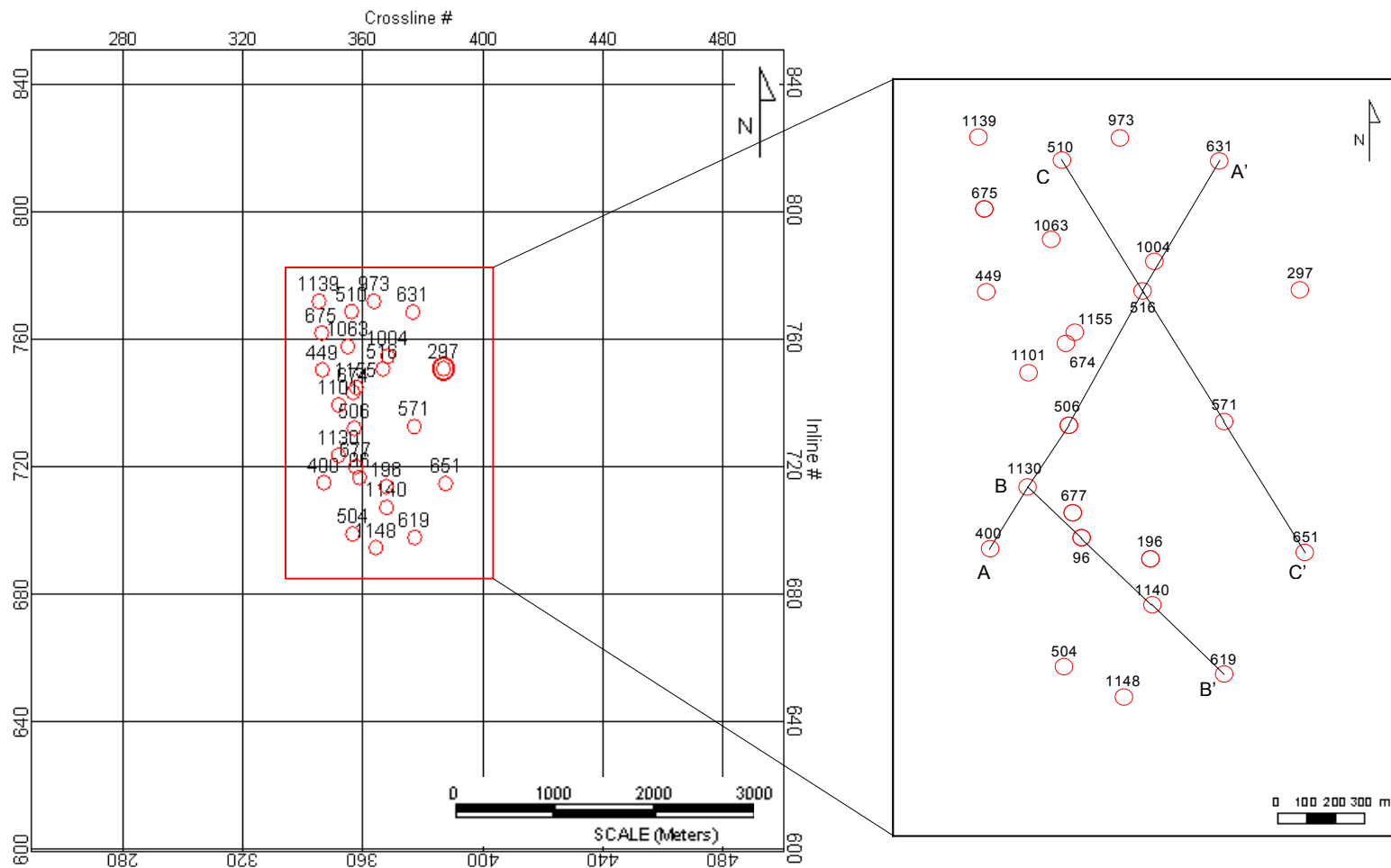


Figure 1.2 Seismic basemap showing the location of the wells. Enlarged figure shows the well data extend and locations of cross-sections.

CHAPTER II

BACKGROUND

2.1 Tectonic Settings

2.1.1 Plate-Scale Settings

It is accepted by most workers (e.g., Burke, 1988; Pindell and Barrett, 1990; Montgomery et al., 1992) that the Caribbean region originated in the eastern Pacific and was transported into its present position between the North and South American plates along large-scale strike-slip faults and oblique subduction zones of Cenezoic age (Lugo and Mann, 1995).

It appears from reconstructions (see Burke, 1988) that west facing coast of northwestern South America rifted from the eastern margin of Mexico, and that the north-facing coast rifted from Yucatan. Since that time, the west coast has develop as an Andean margin that has experienced two arc collisions, while the north coast has experienced intense deformation (Burke, 1988).

Figure 2.1 summaries Caribbean relative-motion history as follows: Jurassic rifting accompanied rifting between the North and South American continents. Early-Late Cretaceous passive margin subsidence followed rifting and the creation of oceanic crust between North and South America and Paleocene-Eocene foreland basin

subsidence followed the oblique collision of an Pacific-derived Caribbean plate with the South American passive margin (Lugo and Mann, 1995).

The Proto-Caribbean ocean basin has been progressively consumed by subduction beneath the Caribbean plate during Caribbean-American relative motion. This subsidence diachronously produced numerous notable basins at the Caribbean Plate boundaries during Caribbean migration and the following aspects of Caribbean evolution may be particularly important for hydrocarbon potential:

The first is the Paleocene-Eocene opening of the Yucatan (Rosencrantz, 1990), Grenada (Speed and Westbrook, 1984), and the early Cayman Trough basins (Rosencrantz et al., 1988). Early deposition of these three basins may have occurred in restricted conditions above stretched-arc or juvenile oceanic basement with high initial heat-flow, and portions of these basins may therefore be prospective.

A second important aspect of Figure 2.1 is the probable onset of underthrusting of Proto-Caribbean crust beneath northern South America in the Eocene, which Pindell et al., (1991) interpreted as having caused moderate regional uplift and local erosional shoaling, and widespread deposition of shallow-water sandstones along the Eocene shelf section of eastern Venezuela and Trinidad (Pindell, 1991).

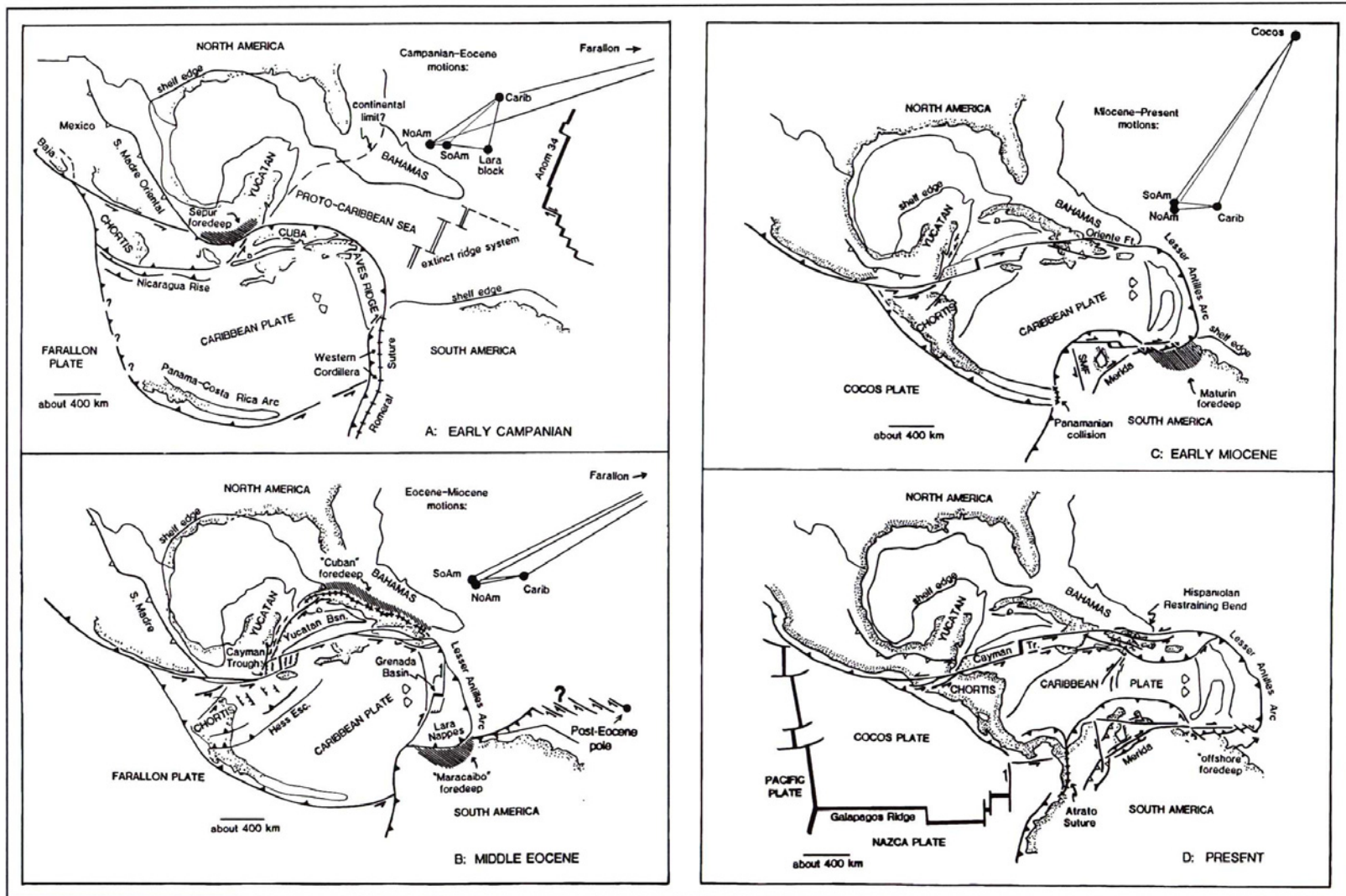


Figure 2.1 Four-stage depiction of the evolution of the Caribbean region (Pindell, 1991).

2.1.2 Tectonic Evolution and Structural Settings of the Lake Maracaibo Basin

The Maracaibo basin is located within broad band of active deformation in the center of the Maracaibo Block, a triangular lithospheric wedge of the northwestern South America continent that actively “escaping” northward over a thinner crust of the Caribbean Sea along the right-lateral Bocono and left-lateral Santa Marta-Bucaramanga strike-slip fault zones (Mann and Burke, 1984) (Lugo and Mann, 1995).

Three principal deformation periods responsible for the present structural configuration of the Maracaibo Basin (Figure 2.2).

The first period of deformation was a minor epirogenic uplift, which took place during the Late Cretaceous and Paleocene. This period of deformation was responsible for the formation of small anticlines and north-northeast-trending strike-slip and normal faults (Icoeta, Sibucara, Sol, Pueblo Viejo) (Gonzales et al., 1980) (Azpiritxaga, 1991). During this deformation, parts of the Venezuelan Andes and Perija Range began to emerge as topographic highs. During the Cretaceous, the Maracaibo Basin began to subside and eventually formed part of an extensive basin occupying the continental shelf of proto-South America, to the east of the primitive Central Cordillera, the middle Magdalena Basin and the Cesar Basin (Talukdar and Marcano, 1994).

The second deformation during the Late Eocene-Early Oligocene was related to a northeastward compression against northwestern South America due to movement of the Cocos plate and the northern part of the Nazca plate (James, 1990). During this time, transverse faulting occurred, producing a major high in the center of the Lake Maracaibo that is bounded on the west by Icotea fault. Transverse faults, mostly with left lateral

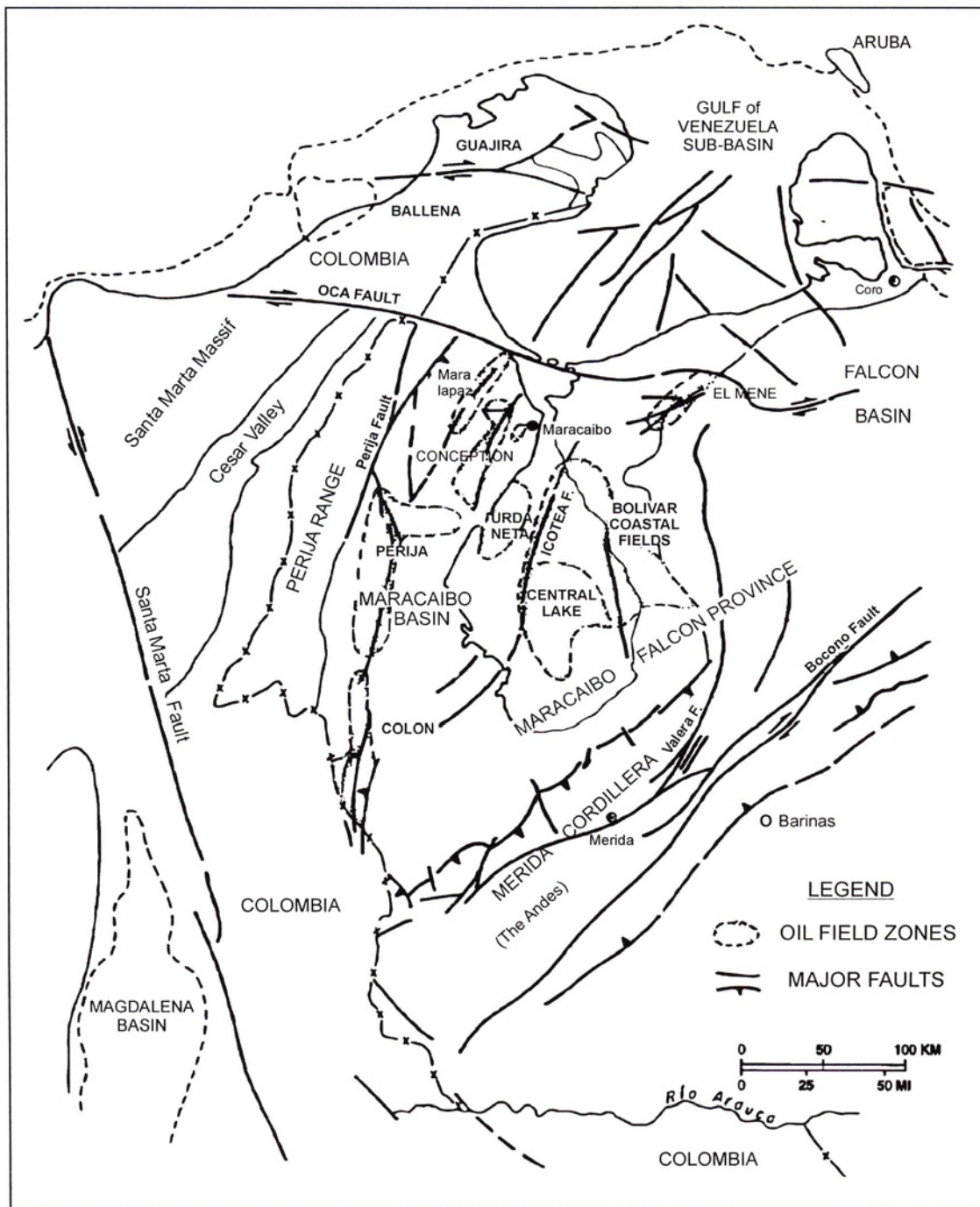


Figure 2.2 Tectonic map of the Maracaibo-Falcon province showing zones in relation to major fault trends (Modified from Molina, 1993).

displacement, seal of the major oil accumulations in the basin such as, Tarra, Lama, and Lamar oil fields (Delgado, 1993). During this deformation, structures developed earlier were also reactivated. This deformation marked the structural inversion of the platform, with the thickest Eocene section being deposited in the northeast, to an intermontane foreland basin with the depocenter to the southwest (Zambrano et al., 1971) (Talukdar and Marcano, 1994).

At the end of Upper Eocene, folding, faulting, and internal erosion took place. The major geological feature was a north-northeast-trending anticlinal dome. A series of en echelon faulted anticlinal folds located on the flanks of the structure (Delgado, 1993). The post-Eocene structural phase was dominated by the uplift of the Sierra de Perija in the west and the Merida Andes in the south. The formation of these two mountain ranges also was responsible for numerous compressional faults parallel to the two ranges (Stauffer and Croft, 1995).

The last period of deformation in the Miocene-Pliocene-recent is characterized by intense structural development in the area and this deformation in general related to the oblique compression of the Caribbean plate with respect to the South American plate. Open folds, minor faults, and some uplifts were formed in the post-Eocene sedimentary rocks as well as the reactivation of the earlier structures in Eocene and older rock units. Compressional structures (such as thrust faults) developed at the north end of the Venezuelan Andes and in the east end of the Perija Range and locally older extensional structures became inverted. Therefore, the basin contains a variety of structural trap types (Kulke, 1994). In the Maracaibo foreland basin, the general

structure that related to this period is a southward-opening fan whose ribs are north-northeast and north trending sinistral faults. Of these, the Icotea, left-lateral strike-slip fault, which extends over 200 km, is the best known example (James, 1990) (Talukdar and Marcano, 1994). This regime also produced a down-to-basin system of normal faults that cut most of the Eocene section (Kulke, 1994).

During the last deformation period, the Maracaibo foreland basin became part of an independent block or microplate that appears to have a northward translation toward the Caribbean plate. This northward shift is due to dextral movement along the northeast-southwest trending Bocono Fault, which extends through the entire Venezuelan Andes. Transpression along this fault is the cause of uplift and northwestward thrusting of the Venezuelan Andes against the adjacent Andean foredeep in the south Maracaibo foreland basin (Talukdar and Marcano, 1994). The final uplift of the Venezuelan Andes took place during this time, resulting in the current configuration of the Maracaibo (Figure 2.3) (Delgado, 1993).

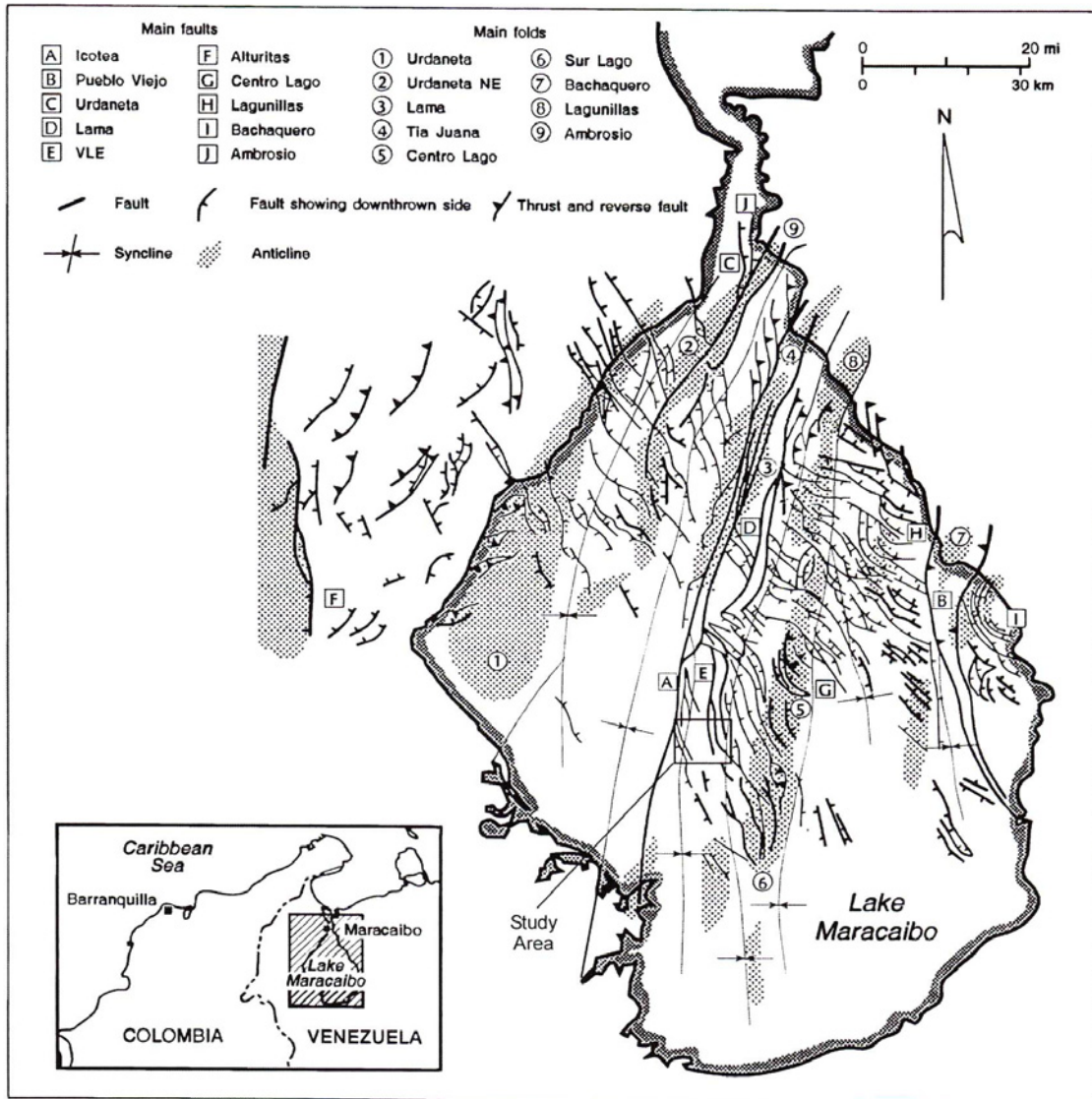


Figure 2.3 Present structural styles in the Maracaibo Basin (Modified from Lugo, 1991).

2.2 Sedimentary Basin Settings

2.2.1 Depositional System and Stratigraphy

The area of the Maracaibo Basin is approximately 23,572 sq. ml. (61,45 sq. km.), with the total drainage area of approximately 50,000 sq. km., of which about 5,000 sq. ml. (12,900 sq. km.) are covered by Lake Maracaibo which is connected to the Gulf of Venezuela through the El Tablazo Bay (Sutton, 1946). The greatest known depth of the lake is about 100 m. and receives water drained from the Perija range, Venezuelan Andes, and Trujillo ranges (Talukdar and Marcano, 1994).

Deposition in the pre-Cambrian is represented by the igneous and metamorphic rocks of the Perija and Iglesias series, which form the cores of the bordering mountain ranges. These are followed by the largely metamorphosed Mucuchachi series of Upper Cambrian to Upper Ordovician age (Sutton, 1946).

The sedimentation of the Cretaceous sequence in the Maracaibo Basin started up with the deposition of coarse continental clastic sediments of the Rio Negro Formation which consists of conglomerates and sandstones with minor shale intercalations. In the Lake Maracaibo Basin the Rio Negro Formation is unconformably overlie the Jurassic to early Cretaceous age of the La Quinta Formation (Figure 2.4). In the Aptian-Albian, the Cretaceous marine transgression led to the deposition of thick shallow water platform carbonates and associated sediments which include, the Apon, Lisure and Maraca Formations (or their equivalents) of the Cogollo Group. The formation consists of deposits of hard, fossiliferous limestones, interbedded with shales (Bartok and Reijers,

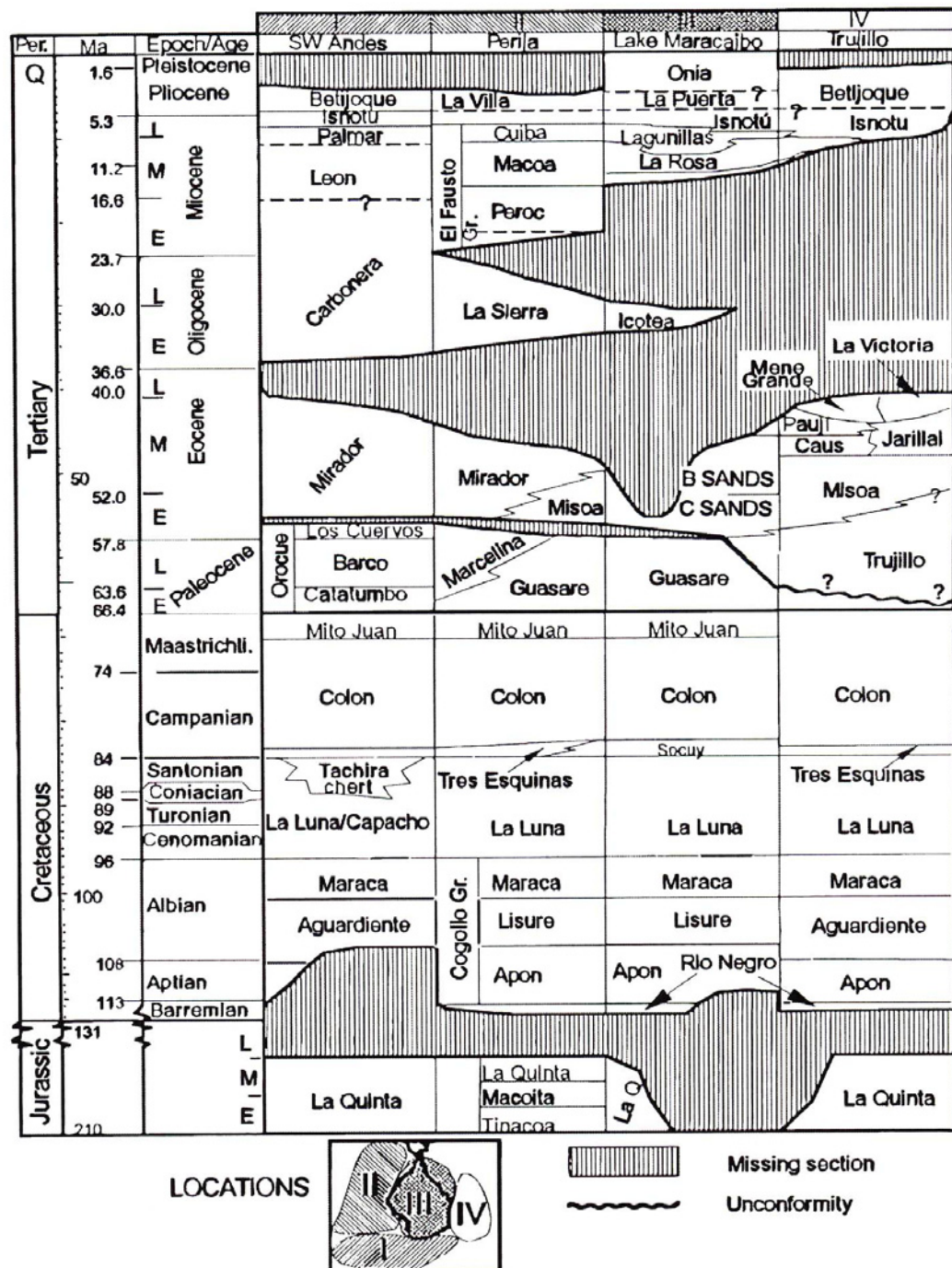


Figure 2.4 Generalized stratigraphic column for the Lake Maracaibo and surrounding areas (Modified from Lugo and Mann, 1995).

1977) (Delgado, 1993). During maximum marine transgression between the Cenomanian and the Coniacian (Upper Cretaceous), the sedimentation was typically of pelagic and euxinic facies, represented predominantly by organic-rich limestones (La Luna Formation) main source rock in the basin (Bertagne et al., n.d.). During the Santonian to Maestrichtian time, the sedimentation took place in an open marine (oxic) condition represented by the thick shales of the Colon Formation which consists of almost entirely of massive, hard shale (Sutton, 1946) and in addition, by the overlying more sandy Mito Juan Formation in the western part of the basin (Talukdar et al., 1985). The Mito Juan is composed principally of massive, black, gray, or greenish gray shales that are locally sandy (Sutton, 1946).

The Late Cretaceous and Lower Paleocene orogeny caused uplifting and subsequent erosion of the Paleocene formations, resulting in an unconformity identified within the basin sediments (Delgado, 1993). Sedimentation changed from marine to nonmarine in some areas during the Paleocene. In the southwest of the basin, non-marine shale, sandstone, and coal of the Orocue Formation were deposited. In the western part of the basin deposition took place in shallow-marine to near-shore deltaic conditions. In the rest of the basin, sedimentation occurred on a shallow-water marine platform, represented mostly by limestone and marl of the Guasare Formation. The formation consists of thick sequence of fossiliferous, glauconitic limestones intercalated with thin layers of shales and sandstones (Van Andel, 1958) (Sutton, 1946).

Because of the coastline of the Caribbean Sea during Eocene time was in the vicinity of what is now the Lake Maracaibo (Bockmeulen et al., 1983), during early-

middle Eocene time the great river built a stream flowed from southwest to northeast (Figure 2.5). It built a series of deltas, but subsidence of the sea bottom was very rapid and the successive deltas did not prograde seaward, but piled on top of each other (Zamora, 1977). The combination of fluvial, fluvio-deltaic, and deltaic sedimentation resulted in the thick, sandy/shaly Eocene sequence that covers the entire basin. The most important oil reservoirs of the Maracaibo Basin accumulated during this period (Delgado, 1993). Eocene sedimentation was mostly fluvial (Mirador Formation) in the southwest, fluviodeltaic to deltaic (Mirador and Misoa Formations), which are contain mostly sandstones, on the platform up to the hinge line (shelf break), deep water marine shale (Pauji Formation) overlying the Misoa Formation in the northeast (Figure 2.6), and turbidite and flysch deposits in the Barquisimeto trough beyond the northeastern limit of the basin (Talukdar and Marcano, 1994).

In the Lake Maracaibo, at the end of the Upper Eocene, uplifting, folding, faulting, and intense erosion took place, giving rise to an unconformity between the Eocene and the overlying continental valley-fill sandstones of the Oligocene Icotea Formation. This was followed by a transgressive period of sedimentation, beginning with a regional basal conglomerate, the Santa Barbara Member of the La Rosa Formation, in which were later accumulated huge quantities of hydrocarbons. Overlying this unit is the lower-middle Miocene Lagunillas Formation, which consists of sandstone, shale, and coal deposited in fluvial to deltaic environments. The Lagunillas formation is subdivided into the lower Lagunillas, Laguna, and Bachaquero members, which contain the three principal Miocene producing sands (Bockmeulen et al., 1983)

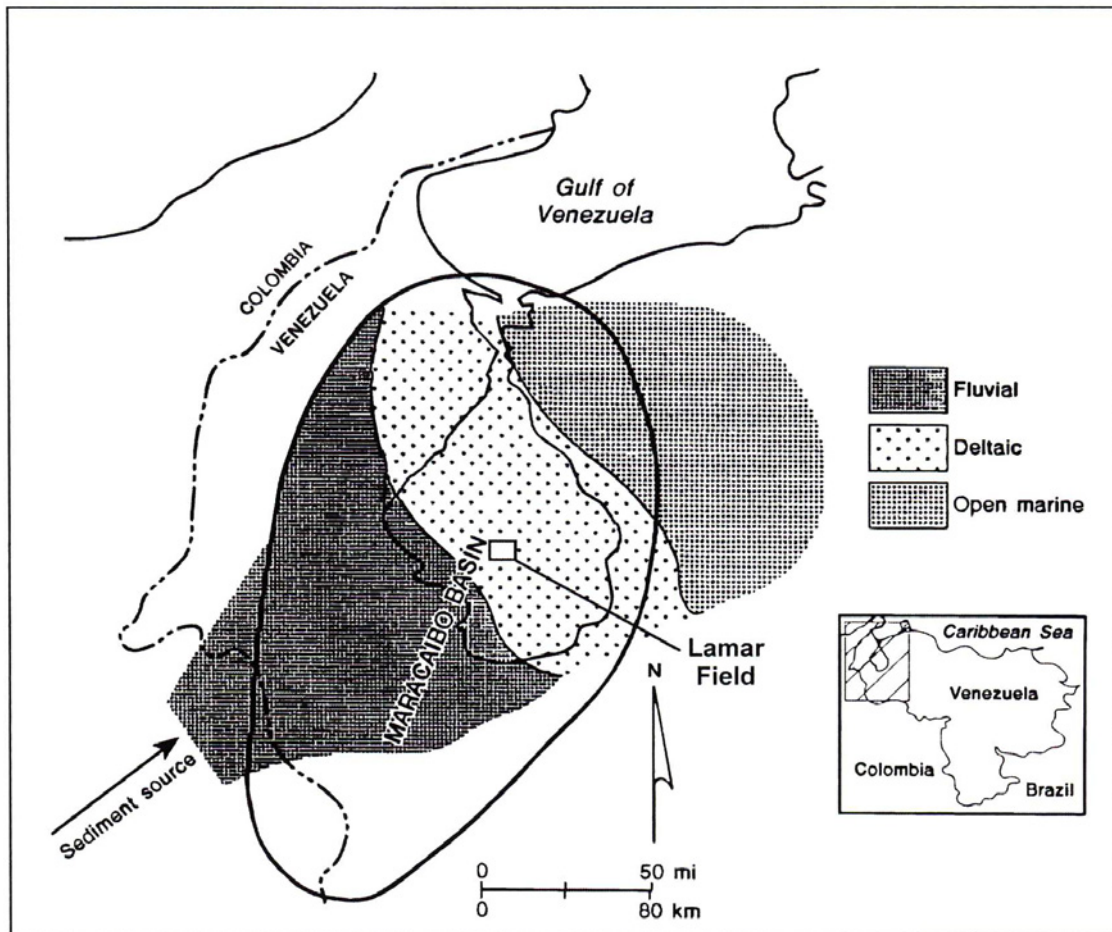


Figure 2.5 Simplified Early to Middle Eocene paleogeographic map of the Maracaibo Basin showing southwest to northeast transition from fluvial to deltaic to open-marine relations (Modified from Maguregui and Tyler, 1991).

(Talukdar and Marcano, 1994).

The subsidence of this foreland basin continued throughout Late Miocene-Pliocene time during which the direction of maximum subsidence shifted from north to south along the Venezuelan Andes foredeep. Thick siliciclastic continental sedimentary rocks of the Late Miocene Betijoque Formation were deposited in this foredeep. In general, since Late Miocene time, continental sedimentation has filled more and more of the foredeep. Presently, the filling of Lake Maracaibo is the continuation of this sedimentation process (Talukdar and Marcano, 1994).

2.2.2 Hydrocarbon Environment

Most of the oil in the Maracaibo Basin originated mainly from the marine organic matter of the La Luna Formation and in minor amount from the marine organic matter of the Capacho and Apon Formations (Talkudar et al., 1987).

Coarse continental clastics of the Rio Negro Formation is in places an excellent reservoir rock, but mostly it is a poorly sorted mixture of clastics with moderate reservoir capabilities (Stauffer and Croft, 1995). Conformably overlying the Rio Negro clastics are the thick limestones of the Cogollo group. The Cogollo is an also good reservoir where it has sufficient primary porosity and has also been fractured, as in Mara and La Paz fields (Stauffer and Croft, 1995).

On top of the Cogollo group lies what is perhaps the world's most prolific oil source rock; the La Luna formation. It consists of black, organic-rich limestones that are characteristically thin bedded and fracture readily because of a high content of chert.

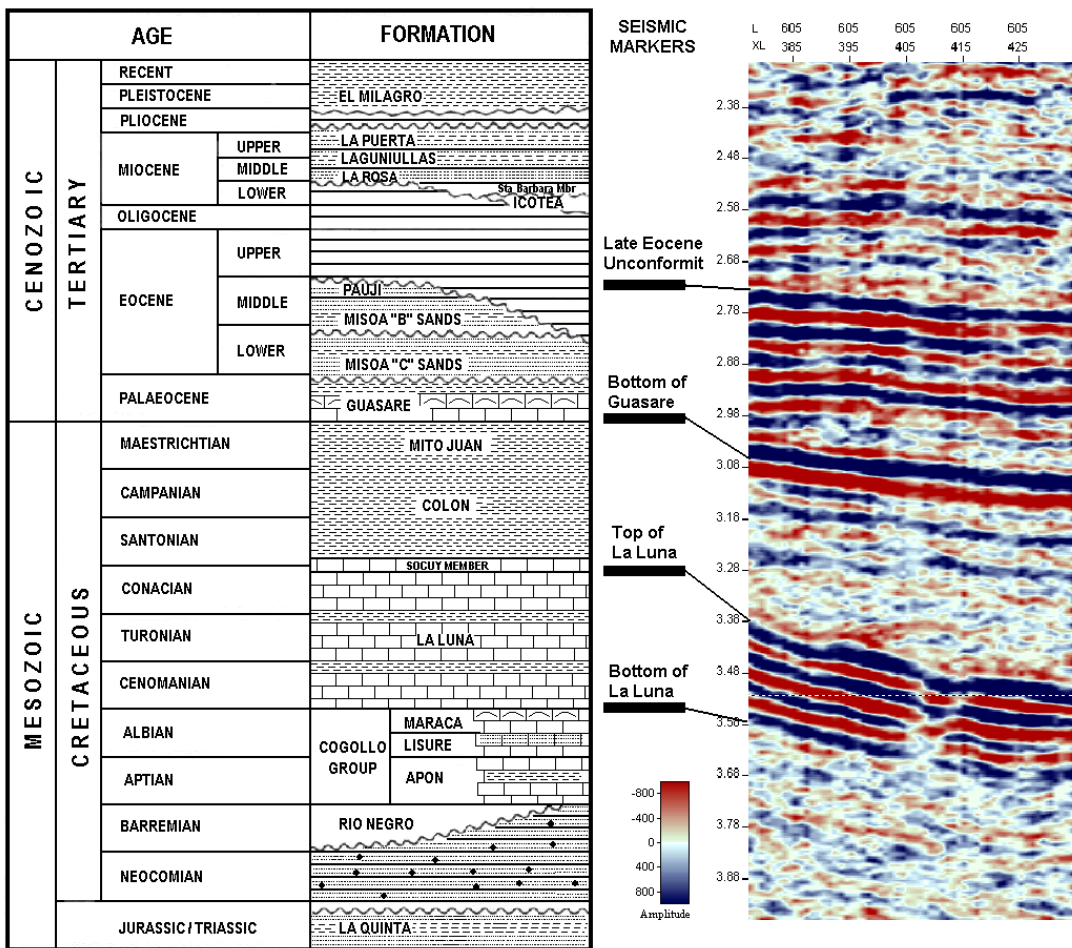


Figure 2.6 Generalized stratigraphic column of central Lake Maracaibo and associated main seismic markers. The Santa Barbara Member is the basal unit of the La Rosa Formation. Lamar field, which is located in the central lake, shows same stratigraphic characteristics with the stratigraphic column presented in this figure. Beside, the Lagunillas Formation is subdivided into the lower Lagunillas, Ojeda, Laguna, and Bachaquero members and the Misoa “C” sands are subdivided into several lower and upper “C” members by some authors (e.g., Garcia, 1988; Holditch and Associates Inc., 1997) which are not shown in this stratigraphic column (Modified from Delgado, 1993).

The Colon Formation comprises a thick shaly sequence, which was deposited in an open marine oxic condition during Santonian-Maestrichtian (Talukdar et al., 1985). The Colon shale conformably overlies the La Luna formation and forms a regional seal over the whole Maracaibo basin. It is this shale that seals most of the Cretaceous traps. In the southwest part of the basin sand lobes in the upper part of the Colon are called the Mito Juan Formation, which consists fine-grained sandstone, and are often good oil reservoirs (Stauffer and Croft, 1995).

During the Paleocene, in the southwest of the basin, non-marine shale, sandstone, and coal of the Orocue Formation were deposited. Among its three members, the Catatumbo, Barco, and Los Cuervos Members, the lower Catatumbo and the upper Barco contain coal that is a secondary source rock for oil. In the rest of the basin, sedimentation represented mostly by limestone and marl of the Guasare Formation. Siliciclastic sandstone of Paleocene age acts as secondary reservoir rock (Talukdar and Marcano, 1994).

Eocene sedimentation was mostly fluvial (Mirador Formation) in the southwest, fluviodeltaic to deltaic (Mirador and Misoa Formations) on the platform and deep water marine shale (Pauji Formation) overlying the Misoa Formation in the northeast. Sandstones in the Misoa and Mirador formations are primary and secondary reservoir rocks, respectively (Talukdar and Marcano, 1994).

During Late Oligocene-Early Miocene time, the La Rosa Formation was deposited first. Overlying this unit is the lower-middle Miocene Lagunillas Formation, which contains Miocene producing sands (Bockmeulen et al., 1983). Sandstones of the

Lagunillas and La Rosa are the primary and secondary reservoir rocks, respectively (Talukdar and Marcano, 1994).

Several important north-south faults developed during the Miocene. The most important in the Bolivar Coastal area are the Icotea-Lama horst and the Pueblo Viejo fault and these faults created very important seal mechanisms through the Lake Maracaibo Basin (Bockmeulen et al., 1983).

In particular, producing units in the Lamar field (Figure 2.7) discovered in 1958 consists of sandstones of the La Rosa, Icotea, and Misoa formations. Most of the oil in the field trapped in faulted anticline and producing depth approximately ranged between 3000-5000 m. Cumulative oil production and estimated oil reserves from these formations are $119,301,7 \cdot 10^3$ bbl and $464,445 \cdot 10^3$ bbl respectively (Talukdar and Marcano, 1994).

In general, accumulations of oil and gas in the Maracaibo basin are related to two petroleum systems. The main petroleum system, which contributes more than 98% of the total oil reserves (produced plus proven) of 52.20 bbo, involves the genetic relationship between the Upper Cretaceous La Luna source rock and the resulting petroleum accumulations (Talukdar and Marcano, 1994).

The other petroleum system encompasses the upper Maastrichtian-Paleocene Orocue Group source rocks and the resulting oil accumulations. This system is restricted to the southwestern part of the Maracaibo basin and has contributed less than 2% (0.7 bbl) of the oil discovered (Talukdar and Marcano, 1994).

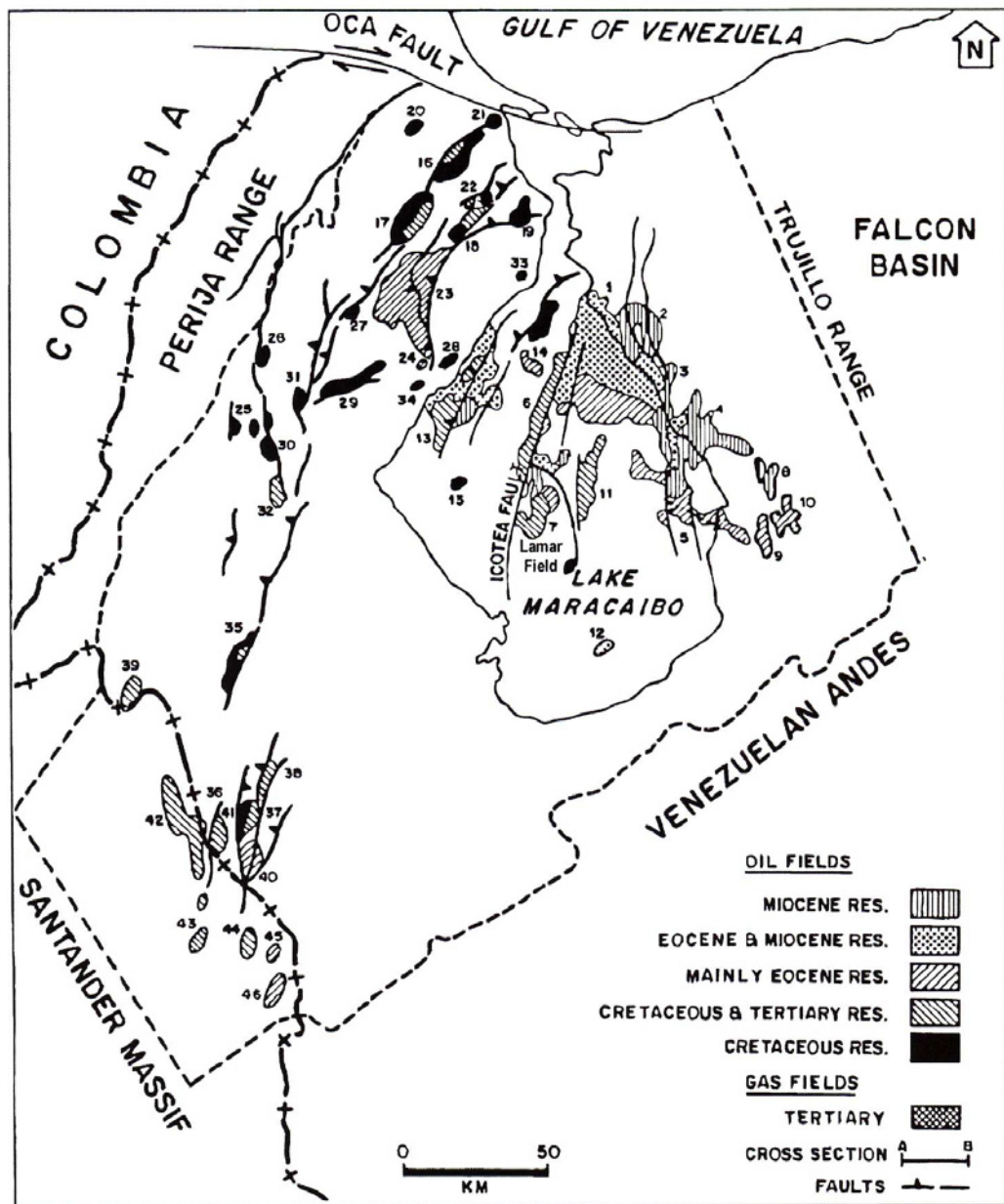


Figure 2.7 Location of oil and gas fields in the Maracaibo Basin, within dashed outline. Shown are ages of reservoir rocks, important faults. Numbers refer to name of the oil fields (for details see Talukdar and Marcano, 1994) (Modified from Talukdar and Marcano, 1994).

CHAPTER III

STRUCTURAL INTERPRETATION

3.1 Methodology

The structure and seismic stratigraphy of VLE 196 area in Block V were re-interpreted using 3-D seismic data integrating with well logs. Both Kingdom Suite and GeoGraphix softwares with NT workstations were used to interpret seismic data and to construct maps, cross sections, and various 3-D graphic presentations. Because of the study area has only one well log which has both sonic and density log, seismic interpretation was done mainly on the seismic reflectors.

Interpretation procedure of the main structure can be summarized as follows: 1) identification of main seismic reflectors, which are the Late Eocene unconformity (seal), bottom of the Guasare Formation (secondary reservoir), and top of the La Luna formation (main source rock), 2) identification of faults networks (VLE 400 and related secondary faults).

To interpret depositional system of the area, GeoGraphix Prizm and GeoAtlas applications were used. 3D seismic data were integrated with well logs and confirmed tops of the C4 interval and the Guasare Formation picked on well logs smoothly followed the seismic reflectors, which are time lines representing these picks. Gross-thickness, net sand-thickness, log facies, and average porosity maps of the C4 interval

and associated layers were prepared by correlating the tops through the seismic volume, which allowed interpretation of structure between wells and in areas of no well control.

Seismic stratigraphic interpretation of the area was based on isochron, isopach, and seismic amplitude maps due to target interval (Guasare-Misoa) has lack of well data. Results gathered from seismic stratigraphic interpretation were also correlated with the results obtained from well log interpretation for C4 interval because existing well logs only penetrated to this interval.

3.2 Main Structure and Faults Network

3.2.1 Model: Strike-Slip Faulting, Restraining Bend

Strike-slip faults are characterized by a linear or curvilinear principal displacement zone (PDZ) in map view (Figure 3.1). Typically, they consist of a relatively narrow, sub-vertical PDZ at depth, and within the sedimentary cover, of braided splay that diverge and rejoin both upwards and laterally. Arrays of upward-diverging fault splay are known as “flower structures”, or less commonly “palm tree structures”. Some strike-slip faults terminate at depth (or upward) against low-angle detachments that may be located entirely within the sedimentary section or involve basement rocks as well (Christe-Blick and Biddle, 1985).

A most distinctive features of many strike-slip faults are the occurrence of “en echelon” faults and folds within and adjacent to the PDZ. The term en echelon refers to a stepped arrangement of relatively short, consistently overlapping or underlapping

structural elements that are approximately parallel to each other, but oblique to the linear zone in which they occur. In strike-slip regimes, it can also be distinguished between en echelon arrangements of structures along a given principal displacement zone. Releasing oversteps and restraining bends are also other prominent features of strike-slip regimes. The presence of both normal and reverse separation ceases to distinguish the two styles (Christe-Blick and Biddle, 1985).

Releasing overstep (bend) is a zone in which the PDZ shifts laterally in an en echelon pattern. A releasing overstep is caused by a change in overall direction of the PDZ. The direction of the bend is such that fault blocks on opposite sides of the bend tend to pull apart. A restraining bend is the opposite of a releasing bend. Opposite sides of the fault tend to become a high-angle reverse fault separating a subsiding footwall from a rising hangingwall. Flower structures are relatively small structures that develop in zones where the upper part of PDZ fault splits due to local tension or compression.

Pop-ups and transpressional uplift are also an integral part of intraplate and interplate strike-slip fault zones. Figure 3.2 shows the typical idealized pop-up structure which is created by the zone of compression in restraining bends. They typically form anticlinal uplifts, commonly with doubly plunging arrangements of folds, and are of limited strike extent. In plan view they are broadly lozenge-shaped to rhomboidal in form, whereas in cross section they commonly bounded convex-up faults that flatten upward toward the surface forming positive flower or palm tree structure.

Bends and stepovers (jogs or offsets) in the PDZs of a strike-slip fault system generally produce either zones of extension (pull-apart or stepover basins) at releasing

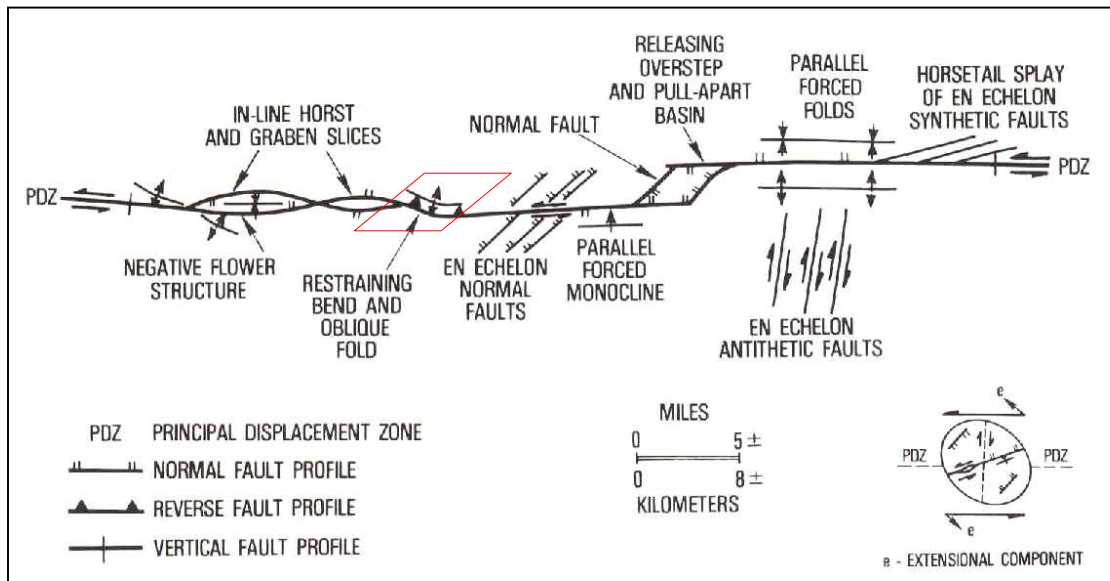


Figure 3.1 Assemblage of structures associated with divergent wrench faults and simplified strain ellipse for left-slip deformation (inset) (Modified from Harding et al., 1985).

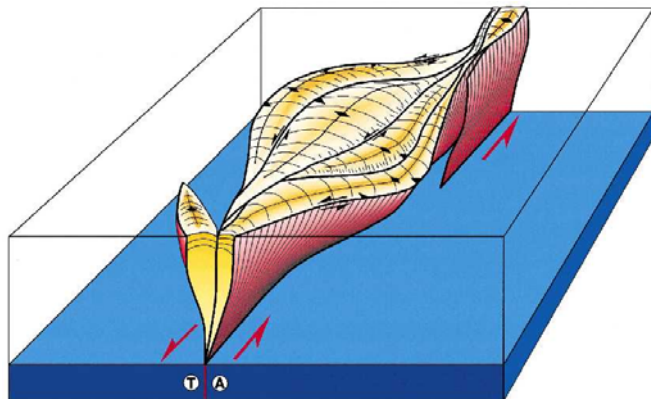


Figure 3.2 Synoptic diagram illustrating the 3-D geometry of an idealized pop-up structure, which is created by zone of compression in restraining bends or restraining sidesteps. T= baseplate movement toward viewer; A= baseplate movement away from viewer (Modified from McClay and Bonora, 2001).

bends or stepovers or regions of compression, uplifts, or pop-up structures (including positive flower – palm tree structures) at restraining bends or restraining stepovers. The latter characteristically produce anticlinal uplifts in the overlying sedimentary section with older strata or basement exposed in the core (McClay and Bonora, 2001).

3.2.2 Structural Interpretation of the Area

The seismic interpretation in the area is based primarily on the seismic reflectors. Main structures of the area consist of three main horizons, which are the Late Eocene Unconformity, the Guasare and Misoa Formations, and the La Luna Formation respectively and complex faulting which is mainly created by the VLE 400 Fault (Figure 3.3 and Figure 3.4).

The unconformity is spread all over the field and easily recognizable. Average depth of unconformity is about 2.75 s and it is characterized by a strong, very clear zero crossing and continuous reflection. The structural map of the Late Eocene unconformity is shown in Figure 3.3. It is clear in this picture that the deformation increases in the northeast direction, particularly along the VLE 400 Fault. This erosional structure in the area is possibly related to the renewed transpression of the Maracaibo Basin during Middle Miocene or tectonic uplift during the Late Eocene to the Early Oligocene (Lugo Lobo, 1991). The unconformity acted as a seal in the area and inhibited the migration of the hydrocarbons. It is relatively flat structure and all structures below toplap the overlying unconformity.

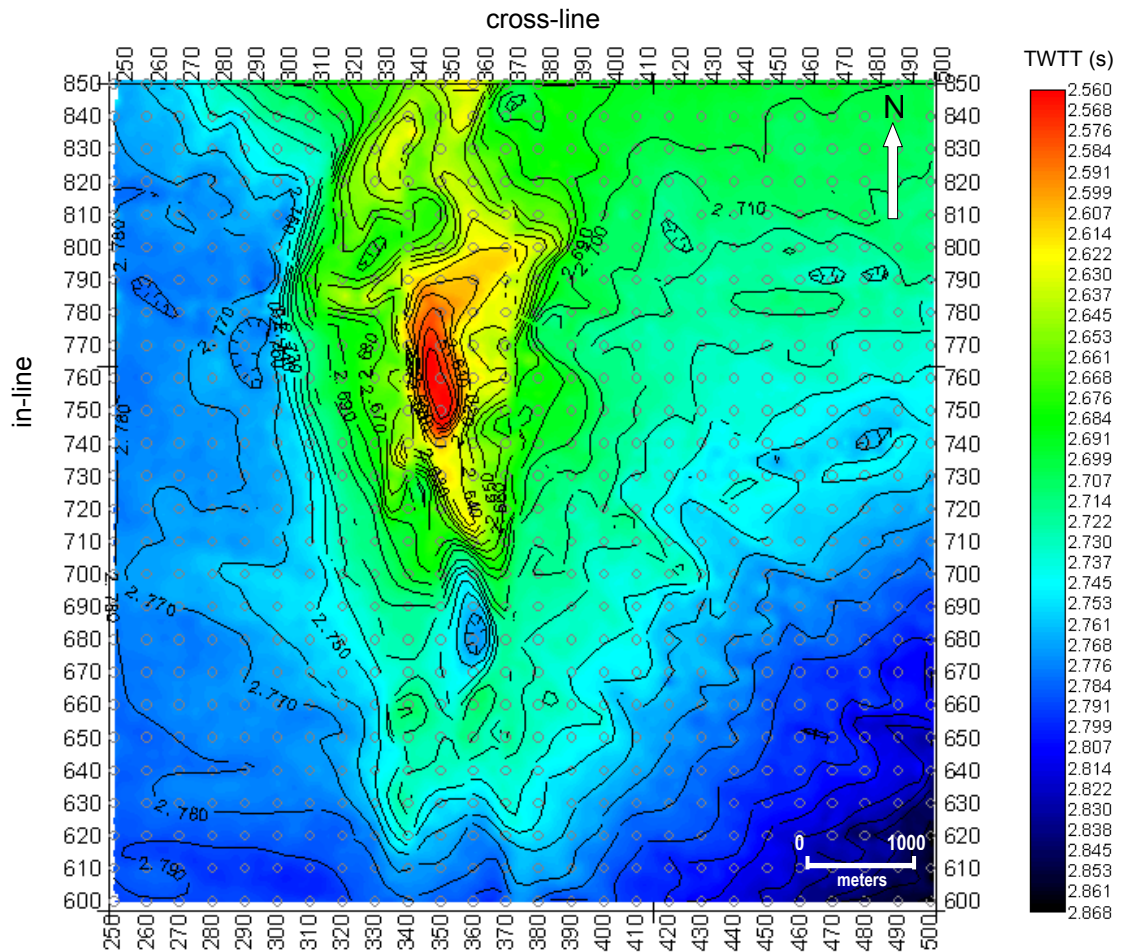


Figure 3.3 Time structure map of the Late Eocene unconformity. As it can be seen in the figure, deformation related with unconformity increases to the northeast especially along the VLE 400 Fault. Contour interval is 10 ms (two way travel time).

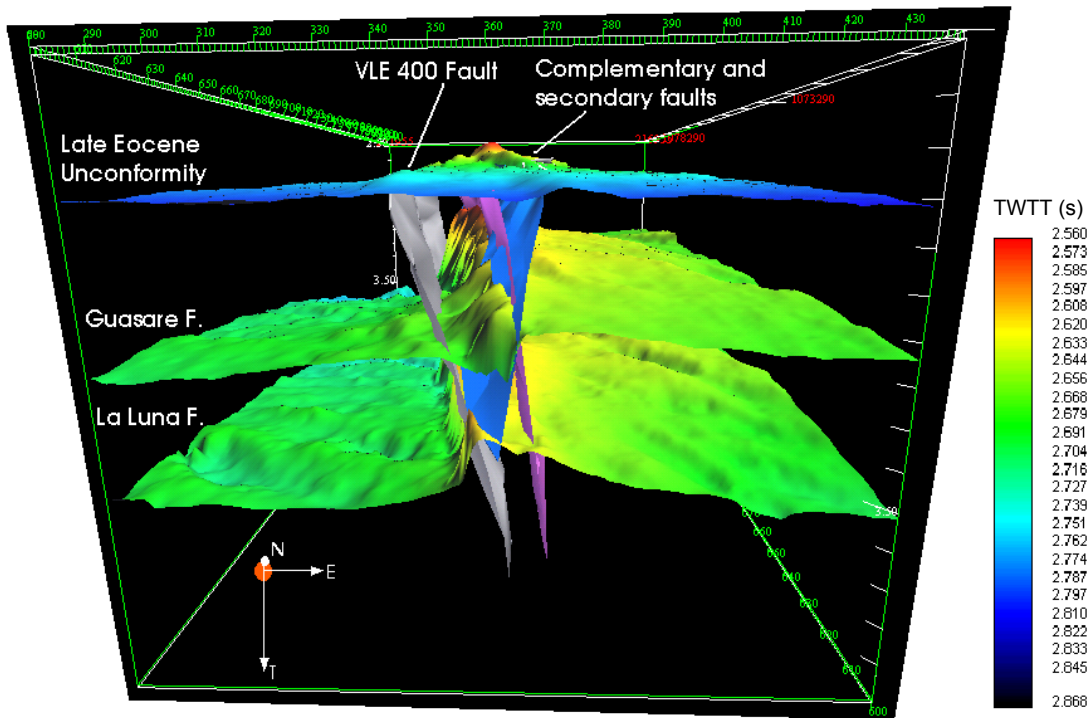


Figure 3.4 3D perspective visualization of the main structure in the area. The VLE 400 fault separates the area in two main parts and creates upwelling in the overlying unconformity and shifted the Guasare and La Luna Formations. (Note that the figure horizontally exaggerated and normal and reverse faults on the east and west side of the area were not shown.)

Figure 3.5 (a) shows positive flower structure, which is created by strike-slip faulting, in the middle of the area and Figure 3.5 (b) shows shaded relief – time-structure map of the unconformity. As it can be seen in these figures, intensive faulting did not affect the overlying unconformity but strike-slip faulting created uplifting in the west side of the area.

Second main seismic reflector in the area is the Guasare Formation, which is secondary reservoir, located middle of the study area and overlain by the Misoa Formation. The Guasare Formation affected by faulting especially in the vicinity of the VLE 400 Fault. Figure 3.6 (a) shows normal and reverse faulting in the area and Figure 3.6 (b) shows the shaded relief – time structure map of the Guasare Formation. In these figures, orientation of the normal and reverse faults is approximately 50° to the VLE 400 Fault and the dipping direction of the faults can easily be seen.

Third main seismic reflector is the La Luna Formation, which is the main source rock in the Lake Maracaibo basin, was interpreted based on its strong seismic reflectors. The average depth of source rock is around 0.2 s. Source rock was characterized by four seismic reflector packages. These reflectors are recognizable in the eastern part of the area but in the western part, they are quite difficult to pick because of the complex structure especially in the vicinity of the VLE 400 Fault. As seen in the Figure 3.6, both the Guasare and La Luna Formations were affected by the VLE 400 Fault.

The main deformation process in the area is strike-slip movement created by the VLE 400 Fault. It creates a significant vertical displacement of the Guasare and La Luna Formations (Figure 3.7). Vertical separation is approximately 75 m (150 ms two-way

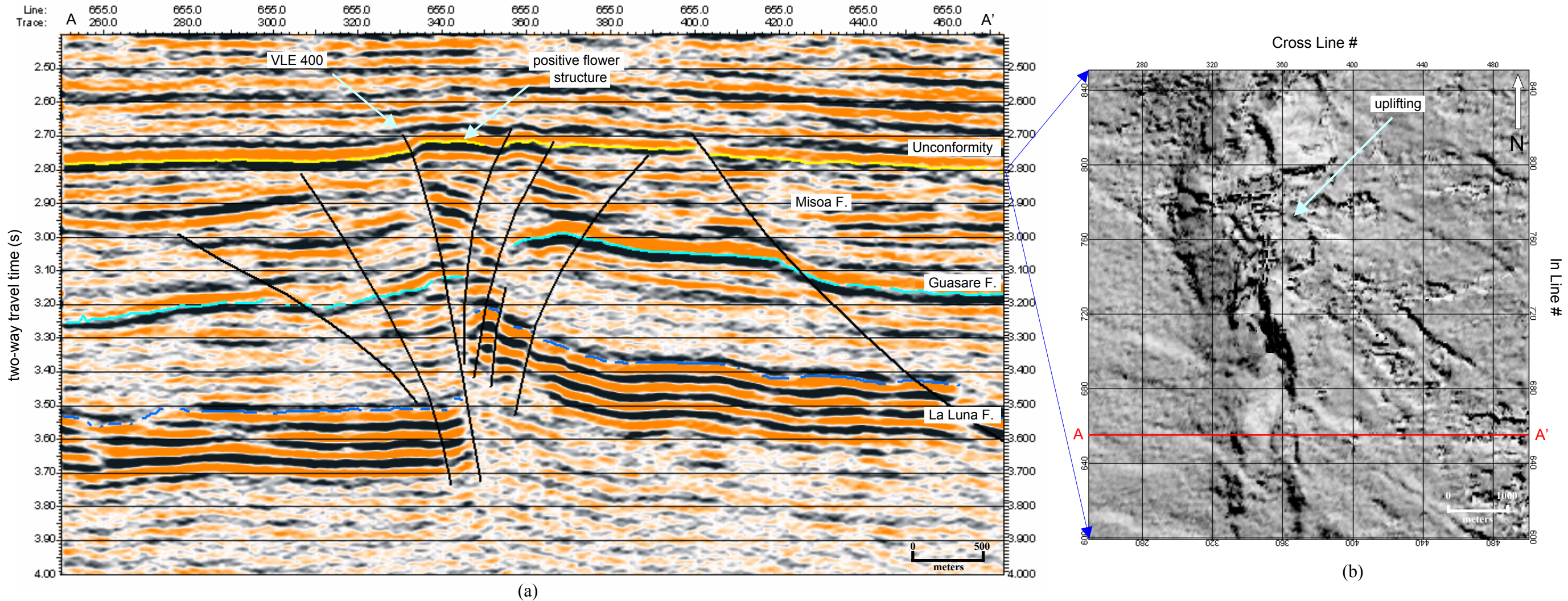


Figure 3.5 (a) Seismic in-line 655 showing main faults and formations in the study area. Three main reflectors are the unconformity, Guasare and La Luna formations respectively. The unconformity has strong reflector, mainly sub-horizontal; bottom of Guasare Formation (secondary reservoir) has strong reflector, clear zero-crossing. The La Luna source rock is composed of four seismic reflectors, which are easily identified. Note that the strike-slip faulting created positive flower structure in the west side of the area. (b) Shaded relief, time-structure map of the Late Eocene unconformity on the seismic basemap. Note that the uplifting created by the VLE 400 strike-slip reverse fault very clear in the west side of the base map. Horizontal red line on the basemap shows the location of in-line 655.

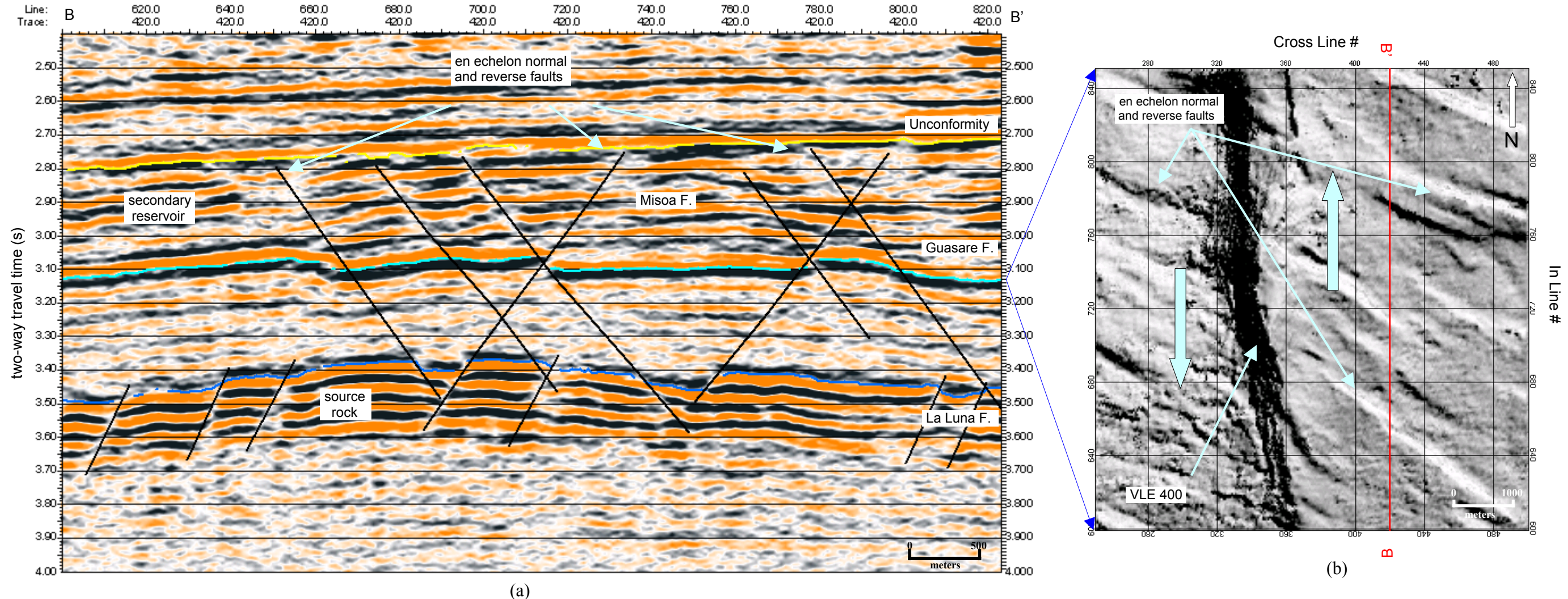


Figure 3.6 (a) Seismic cross-line 420 showing normal and reverse en echelon faults in the study area. Almost all faults parallel to each other and most of them effect the La Luna source rock and created migration pathways through reservoir layers of the Misoa and secondary reservoir Guasare Formation. Note that the La Luna source rock highly fractured and most of these faults did not penetrate thorough reservoir layers and the VLE 400 Fault can not be seen in this cross-line (see location of the cross-line). (b) Shaded relief, time-structure map of the Guasare Formation. Orientation of the VLE 400 Fault and associated secondary faults indicated that main deformation process created by left-lateral movement. Horizontal red line on the basemap shows the location of cross-line 420.

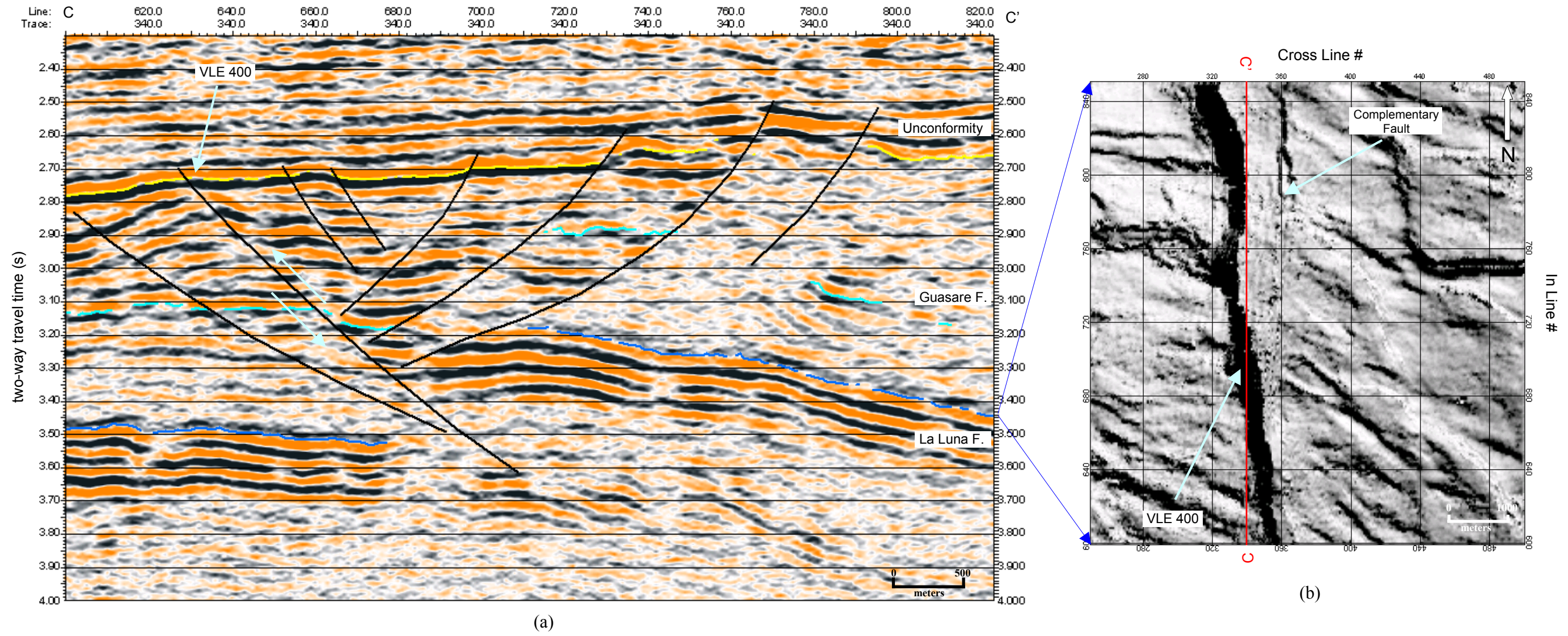


Figure 3.7 (a) Seismic cross-line 340. Figure shows complex faulting in the area and the cross-line over the VLE 400 Fault shows the reverse component of the VLE 400 strike-slip fault. Faulting caused shifting of the La Luna and Guasare formations. Note that the changes of thickness of both formations from south to north. (b) Shaded-relief, time-structure map of the La Luna Formation showing the VLE 400 and complementary fault. Horizontal red line on the basemap shows the location of the cross-line.

travel time) and 150 m (250 ms two-way travel time) for the Guasare and La Luna formations respectively.

The VLE 400 Fault is interpreted as a left lateral strike-slip reverse fault (term adapted from Hill, 1958). Because the VLE 400 Fault behaves as a strike-slip in strike sections and acts as a reverse faults in dip sections and I believe that dual classification, which is consider both strike and dip separation, is the most appropriate definition for this fault. Comparison of Figure 3.5 (a) and Figure 3.6 (a) show this behavior clearly. Vertical displacement along the VLE 400 Fault is about 100 m is down to the west. As it can be seen in Figure 3.8, the trend of the principal displacement zone is north south and dips westward and it is situated right in the middle of the field and as it stated above it appears in cross sections as a reverse fault with the upthrown block on the east side of the principal displacement zone. The VLE 400 Fault was also interpreted as a splay of the Icotea Fault (Figure 2.3) which is the major north fault that traverses trending that the center of the Maracaibo Basin. Associated secondary faults have same trend with the VLE 400 Fault and they created a positive flower structure in the central area and created uplift on the overlying unconformity. General interpretation and the 3D perspective visualization of the structure (Figure 3.9) and comparison of the model (Figure 3.2) show that the area was subjected northeast southwest compression and the VLE 196 area situated in the restraining bend area.

The VLE 400 Fault separates the VLE 196 area into two main parts. The eastern part of the area has been producing oil for years whereas the western part has not. The eastern part is gently dipping on the east direction. It is affected by some normal faults

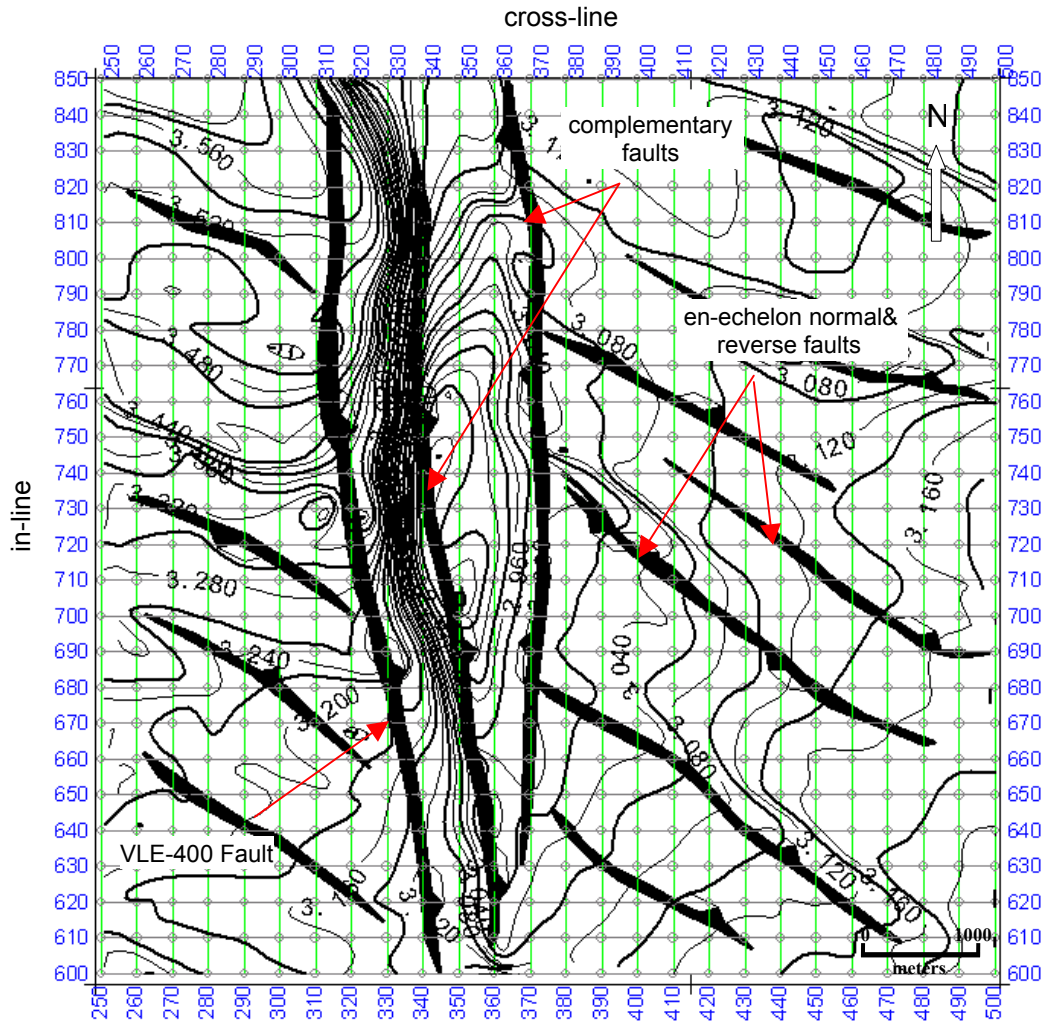


Figure 3.8 Fault polygon map of the Guasare Formation showing the general structure. The main fault, VLE 400, can easily be identified by its north-south trend as well as its associated faults. Eastern part of the area appears to be affected by faults more than western part. Trend of normal and reverse faults is northwest southeast. The contour interval is 40 ms (two-way travel time).

that have important lateral extension. The western part is affected by reverse faults in the southern area and normal faults in the northern area. This structure is dipping very steeply on the north direction.

Strike-slip faulting and tectonic activity created numerous faults on the both parts. These northwest southeast trending secondary faults are oriented approximately 50° to the VLE 400 Fault. Secondary faults also interpreted as a second order wrench faults (Holditch and Associates Inc., 1997) because (1) there are kinks or local offsets of the VLE 400 Fault near the ends of secondary faults, (2) the displacement diminish across the secondary faults with proximity to the VLE 400 Fault, (3) most of the secondary faults terminate at the Eocene unconformity. Most of these faults located in the eastern part of the area. These are mainly northwest southeast oriented en echelon normal and reverse faults (Figure 3.10) and they compartment the reservoir. Both reverse and normal faults have same orientation and they mostly created vertical displacements in the Guasare-Misoa interval but some of them also penetrated through the La Luna Formation.

One of the most important problems arises in the structural interpretation part, which is if the area situated in the restraining bend or releasing bend within the strike slip movement. As it can be seen in Figure 3.1, restraining bends characterized by reverse faults and en echelon normal faults form parallel to the direction of the principal stress. Comparison of Figure 3.6 (b) and Figure 3.1 suggest that the area situated in the restraining bend area because orientation of normal faults show left lateral movement and southwest northeast compression other than extension. On the other hand, fault trace

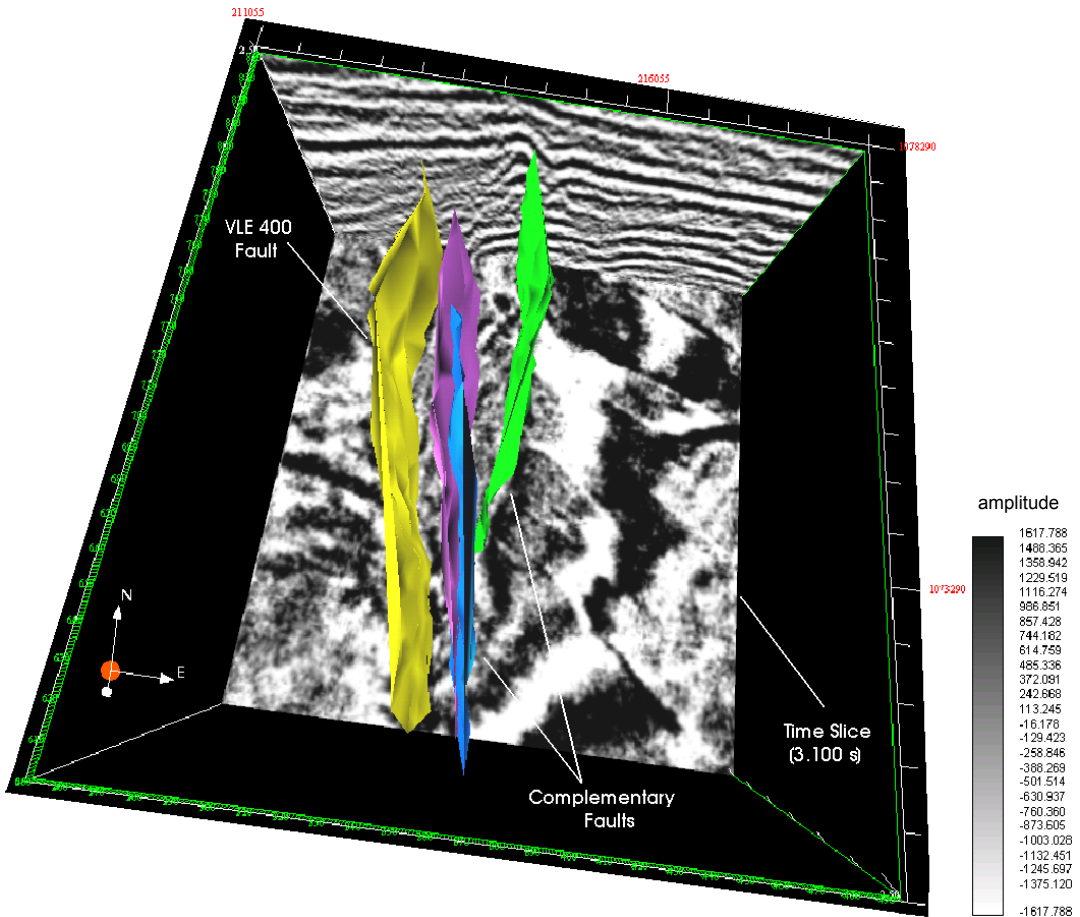


Figure 3.9 3D perspective visualization (top view) of the VLE 400 and associated complementary faults and time slice 3.100 s. Note that the orientation of en echelon normal and reverse faults in time slice, which are not shown in this figure, are southeast northwest.

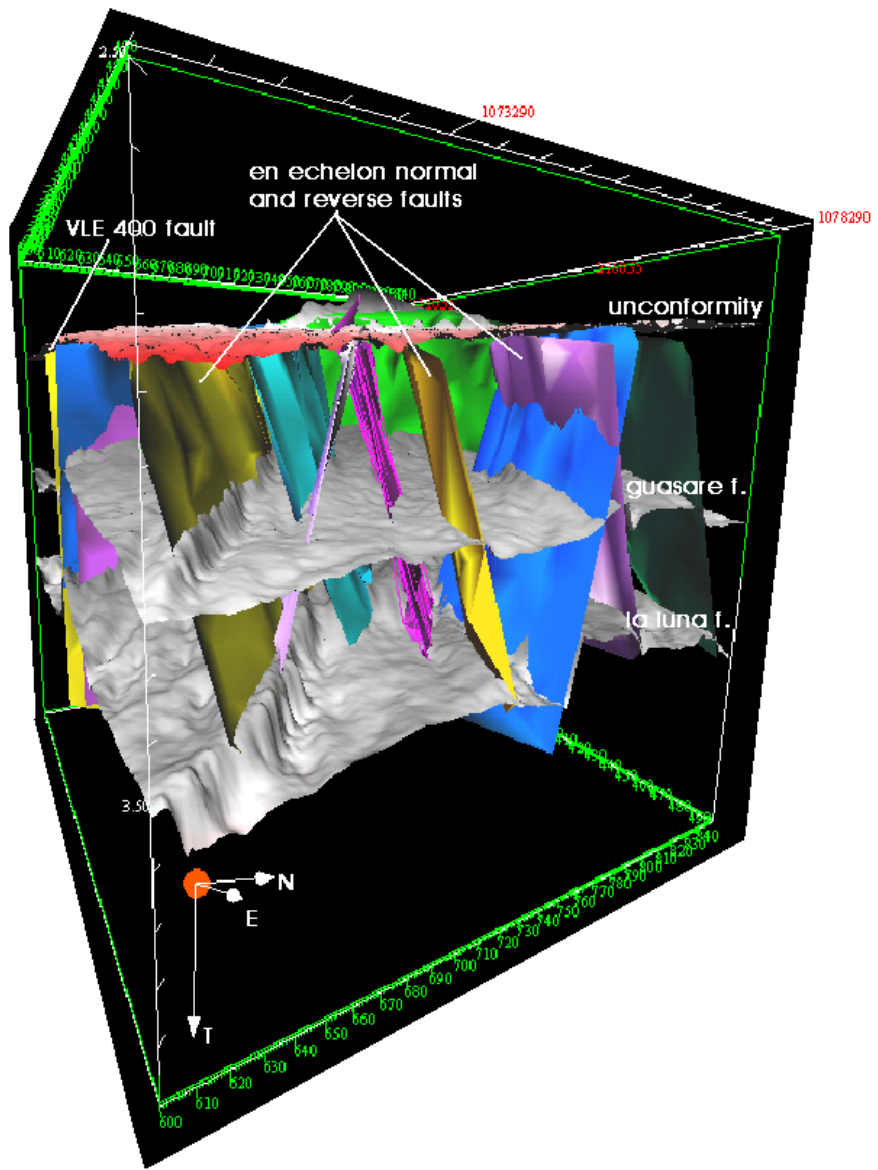


Figure 3.10 3D perspective visualization of faults and horizons perpendicular of the strike of the en echelon normal faults which are created migration pathways cutting overlying sediments of the La Luna source rock.

of the PDZ (VLE 400 Fault) in Figure 3.6 (b) and Figure 3.7 (b) indicate extension which shows that the area situated in the releasing bend (see Appendix E, figure part B). The most possible explanation for this contradiction can be that the area was situated in the releasing bend but afterward, it was subjected to inversion tectonics (see discussion for details) and the VLE 400 Fault gained its reverse component and the VLE 196 area showed restraining bend characteristics.

3.2.3 Hydrocarbon Trapping

The major trapping mechanisms in the VLE 196 Field are the four-way closure of the anticline and offset of strata by the VLE 400 Fault (Figure 3.11). The anticline trends northward across most of the field, but the axis turns northeastward on the north, as the fold enters Block VI. Strata on the east flank of the anticline dip approximately 20° eastward (Holditch and Associates Inc., 1997). The VLE 400 Fault is a sealing fault that prevents migration of hydrocarbons from the eastern to western block. Because overlying Late Eocene unconformity was not affected by the faults, it acts as a seal and inhibits further migration of hydrocarbons.

The most distinctive feature in the study area is the existence of the source and reservoir rocks together. Because en echelon normal and reverse faults penetrated through source rock, they created excellent migration pathways to reservoir sandstones of the Misoa Formation through overlying shaly layers of Colon and Mito Juan formations. The main producing area is situated in the positive flower structure, which is located in the middle of the VLE 196 area.

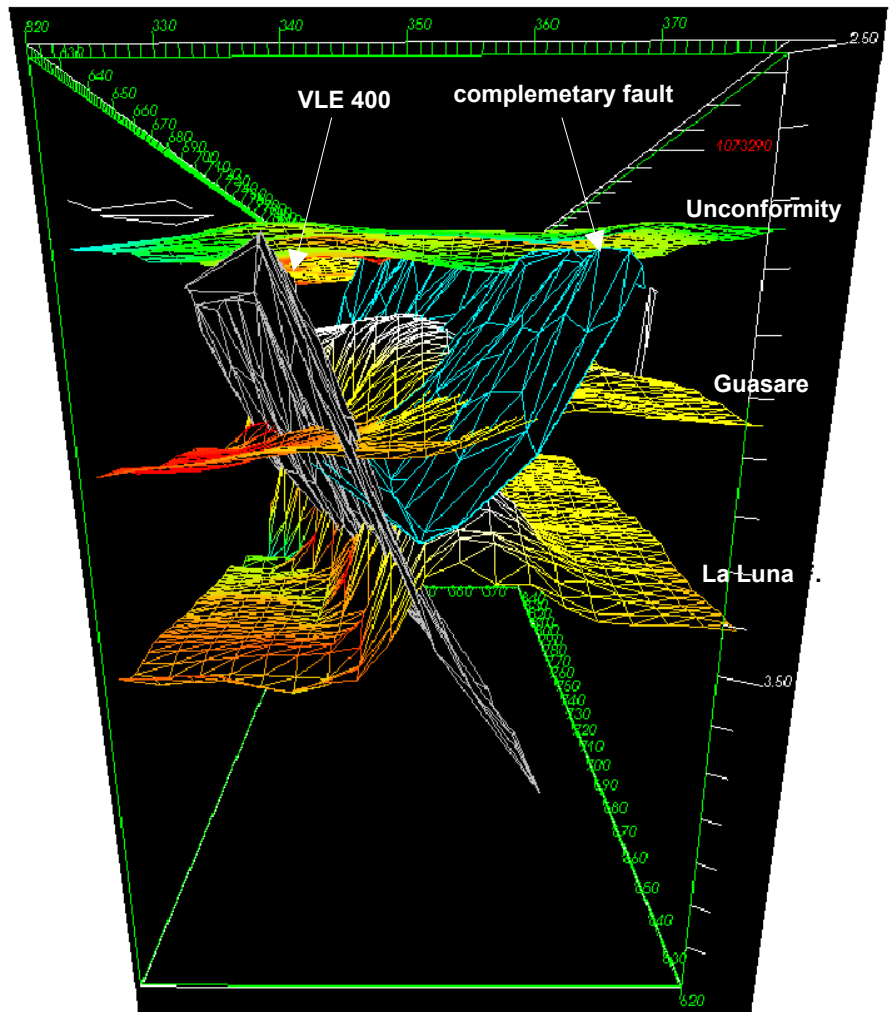


Figure 3.11 3D perspective wireframe visualization of the four-way trapping mechanism in the VLE 196 area. The unconformity on the top, the VLE 400 Fault and complementary faults on the sides and the anticline on the bottom.

3.2.4 Results

- 1) The VLE 196 area, Block V, Lamar Field, represents a complex structure because of its previous long tectonic activity.
- 2) The main deformation process in the area is the strike-slip movement created by the VLE 400 Fault, a left-lateral strike-slip reverse fault, separated the area in two main parts.
- 3) The trend of PDZ (principal displacement zone) is north south and dips westward.
- 4) Associated complementary faults have same trend with the VLE 400 Fault whereas en echelon normal and reverse faults are oriented approximately 50 degrees to the VLE 400 Fault and they compartment the reservoir.
- 5) General structural interpretation shows that the area was subjected northeast southwest compression and the VLE 196 area situated in the restraining bend.
- 6) Three main reflectors in the study area are the Late Eocene unconformity, Guasare Formation, and La Luna Formation. The unconformity is spread all over the field and because of it was not affected by faulting, it acted as a seal and inhibited the migration of the hydrocarbons. The Guasare and La Luna formations were affected by faulting especially in the vicinity of the VLE 400 Fault. The VLE 400 Fault created a significant vertical displacement of the Guasare and La Luna formations. Vertical separation is approximately 75 m (150 ms two-way travel time) and 150 m (250 ms two-way travel time) for Guasare and La Luna formations respectively.
- 7) The major trapping mechanism in the VLE 196 area is the four-way closure of the anticline and offset of strata created by the VLE 400 Fault.

CHAPTER IV

DEPOSITIONAL SYSTEM and SEISMIC STRATIGRAPHY

4.1 Depositional System

4.1.1 Model: Tide-Dominated Delta

Deltaic depositional facies result from interacting dynamics processes (wave energy, tidal regime, currents, climate, etc.), which modify and disperse fluvial clastic deposits. Depositional features include distributary channels, river-mouth bars, interdistributary bays, tidal flats, tidal ridges, beaches, eolian dunes, swamps, marshes, and evaporite flats. A significant deltaic accumulation necessarily requires the existence of a river system carrying substantial quantities of clastic sediment from an inland drainage basin to the coast, where the deposits form the delta plain (Coleman and Prior, 1982).

Delta environments and facies can be conveniently grouped into delta plain, delta front, and bounding delta destructional and flank assemblages. Delta geometry and distribution of framework sand facies are determined by three basic processes: (1) sediment input, (2) wave energy, and (3) tidal energy flux. This process of framework provides the basis for recognition of a tripartite classification of end member delta types, which are fluvial-, wave-, and tide-dominated deltas.

Framework sand bodies of tide-dominated deltas (Figure 4.1) are the products of deposition in tidally modified estuarine distributary channels, delta-fringing tidal sand

flats, and tidal current ridges and shoals. The distributary fill and tidal sand ridge facies merge as distributary mouths flare and open onto the broad subtidal platform that fronts most tide-dominated deltas. Tide-dominated deltas display few to many estuarine distributary channels, which are characterized by broad, funnel-shaped mouths, and narrow, sinuous upper reaches (Galloway and Hobday, 1996). Distributary mouth bars and channel deposits also comprise the best reservoir quality bodies within a delta system. The general upward-coarsening character of distributary mouth bars tends to produce sandstone bodies are usually upward-fining and have their greatest permeability at the base (Scheibling and Atkinson, 1992).

The channel fill deposit is composed of multiple, superimposed, and variably preserved upward-fining depositional units. Estuarine distributary channels are flanked by diverse facies of the lower and upper delta plain. Landward, channel fill boundaries are abrupt and erosional, but in distal portions of the distributary, where surrounding flats and splays are flooded during high tide, channel-fill deposits grade in part into surrounding finer-grained sediments.

Recognition of delta types can be differentiated primarily by the geometry and orientation of the progradational sand facies, their spatial relationships to the distributary channel system and, to a lesser extent, the geometry of the distributary channel fills (Galloway and Hobday, 1996).

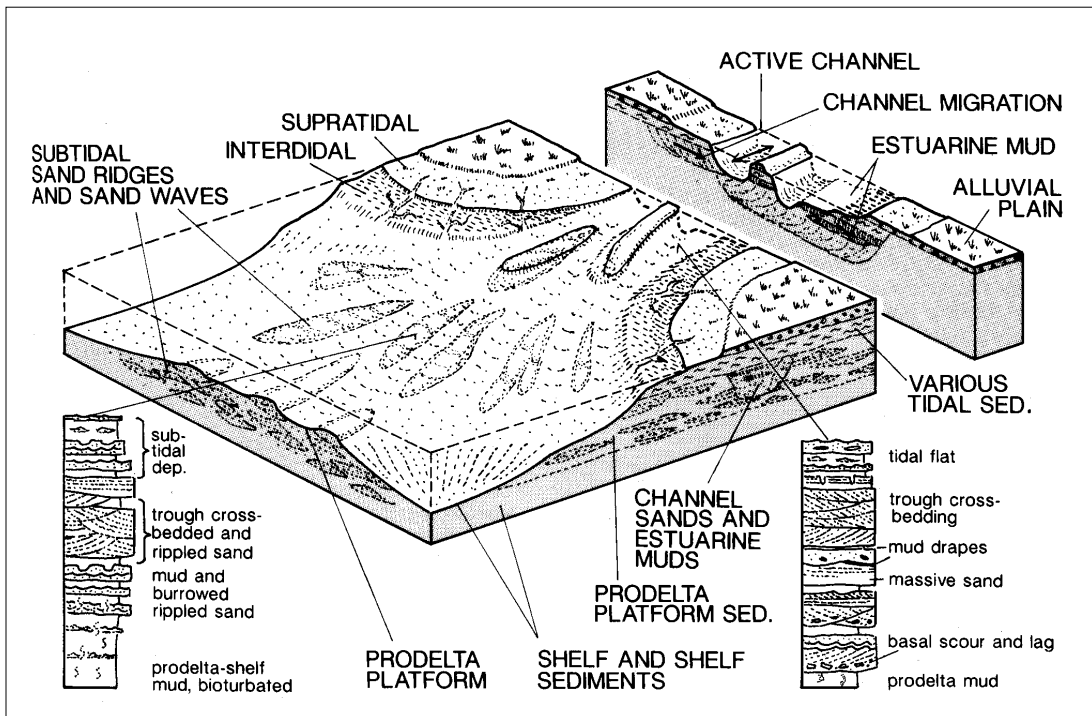


Figure 4.1 Conceptual model of the tide-dominated delta. Vertical sections show estuarine channel fill and tidal sand ridge on prodelta platform of tide-dominated delta (Modified from Einsele, 1992).

4.1.2 Interpretation of the Depositional System

In this part of the study to interpret depositional system of the VLE 196 area, Block V, 3D seismic data integrated with well logs and confirmed that tops of the C-4 interval and the Guasare Formation picked on well logs smoothly followed the seismic reflectors, which are time lines representing these picks. Gross-thickness, net sand-thickness, log facies, isopach, net to gross ratio, and average porosity maps of the C-4 interval and associated layers were prepared by correlating the tops through the seismic volume, which allowed interpretation of structure between wells and in areas of no well control. In the study area, most wells were drilled in the western portion leaving the eastern portion with no well control. Most of the wells fully penetrated the C-4 interval but partially penetrated the other “C” intervals. Log information for the C-4 interval was much more complete and representative than those of the other intervals. Therefore, interpretation of depositional system of the area was done based on C-4 interval with the area in well log control.

Three cross sections were used to divide the C-4 interval into three sandstone and three shaly layers. For each sandy layer, gross interval thickness, net average porosity, and log facies maps were prepared for the area which includes well logs (see Figure 1.2 for the well log data extend). Net-to-gross ratio maps were prepared dividing net thickness to gross thickness. Average porosity maps were done based on density logs using following equation:

$$\phi_D = \frac{\rho_{ma} - \rho_b}{\rho_{ma} - \rho_{fl}}$$

ρ_{ma} = matrix density, ρ_b = bulk density, and ρ_{fl} = density of the fluid

The average porosity and net sand thickness map were done using cut-off 5% effective porosity and 45% shale volume.

Figure 4.2 shows one of the type logs (VLE 1063) in the study area. In this type log C-4 interval was separated into three sandy and three shaly layers. Sandy layers of C-4 interval show upward-coarsening, blocky and, upward fining log patterns on the gamma ray trace. Log patterns and their order of occurrence suggest that the sandstone are delta front and stacked fluvial/distributary channel facies of delta system. This conclusion supported by the stratigraphic cross sections and associated lithofacies maps.

Layer 1 is predominantly sand, the top of the interval exhibits a shaly zone with thin sandy interbeds (especially on gamma ray logs). Well log response of this layer is fining-upward, blocky which is interpreted as a delta front. Gross thickness map (Figure 4.3 a) of this interval shows that sediments deposited along the southeast northwest and thickest sediment body (approximately 250 ft) located in the middle of the area. Average porosity and log facies maps of Layer 1 also indicated SW-NE trend of sedimentation. Most porous part is situated in the north and has 27% average porosity (Figure 4.3 b) and blocky log pattern. Comparison of gross thickness, average porosity and log facies map (Figure 4.3 c) show thickest sediment part with 27% porosity has blocky log pattern and fining-upward sequences surrounded by blocky part. Based on these informations, Layer 1 was interpreted as delta front.

Layer 3 consists of massive sand within thin, shaly interbeds (Figure 4.2). Gross thickness and average porosity maps (Figure 4.4 a and b) of this layer suggested that the sediment source was SW to NE. Maximum gross thickness of this interval is 100 ft and

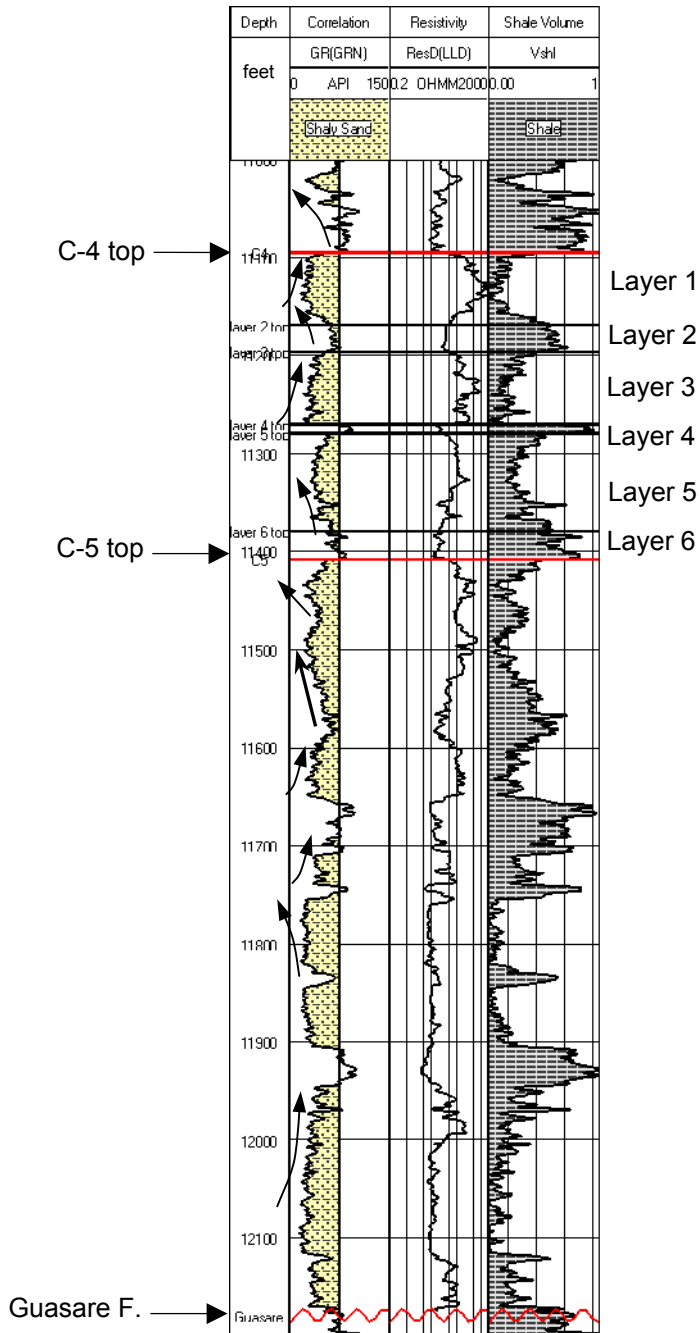


Figure 4.2 Type log (VLE 1063) showing log patterns, reservoir layers, and sedimentary facies. Note that left curve is gamma ray and right curves are laterolog deep resistivity and shale volume respectively. See Figure 1.2 for location.

average porosity is 30%. Log facies map (Figure 4.3 c) shows that the most porous parts have blocky, serrate, and coarsening-upward log signatures.

Layer 5 is mostly sandy with shaly interbeds. Gross thickness (Figure 4.5 a) of this layer is approximately 150 ft and elongated to SE NW direction and become thinner through to southeast. Average porosity and log facies maps (Figure 4.5 b and c) of this layer show that maximum porosity (30%) located in the middle of the area and has upward-fining facies pattern which is indicator of distributary channel.

Shaly layers of C-4 interval interpreted as potential seals and they were deposited in low-energy interdistributary, and shallow marine environments. The percentage of shale increases upward from C5 to C-4. Shales are of variable thickness and extend and they make up almost 40% of the C-4 interval. These layers are believed to be potential seals. Shales are of variable thickness and some shaly layers pinch out between C-4 layers. In addition, sandy facies commonly occur within the shales. Layer 6 at the base of the C-4 interval is the most extensive shaly layer in the section, and most likely it represent a marine flooding surface which is identified in electric logs as low resistivity and high gamma peak. In contrast, many other shaly layers have more sand content. Thus, the extend of shale layers as reservoir or no-flow units vary from layer to layer.

To interpret all layers together, similar maps were also prepared for C-4 strata. Figure 4.6 (a) and (b) show isopach and net sand thickness of C-4 interval. The net sand thickness map exhibits southeast northwest contour patterns, reflecting depositional control on the interval. The maximum sand is 250 ft thick and become thinner in the southeast direction.

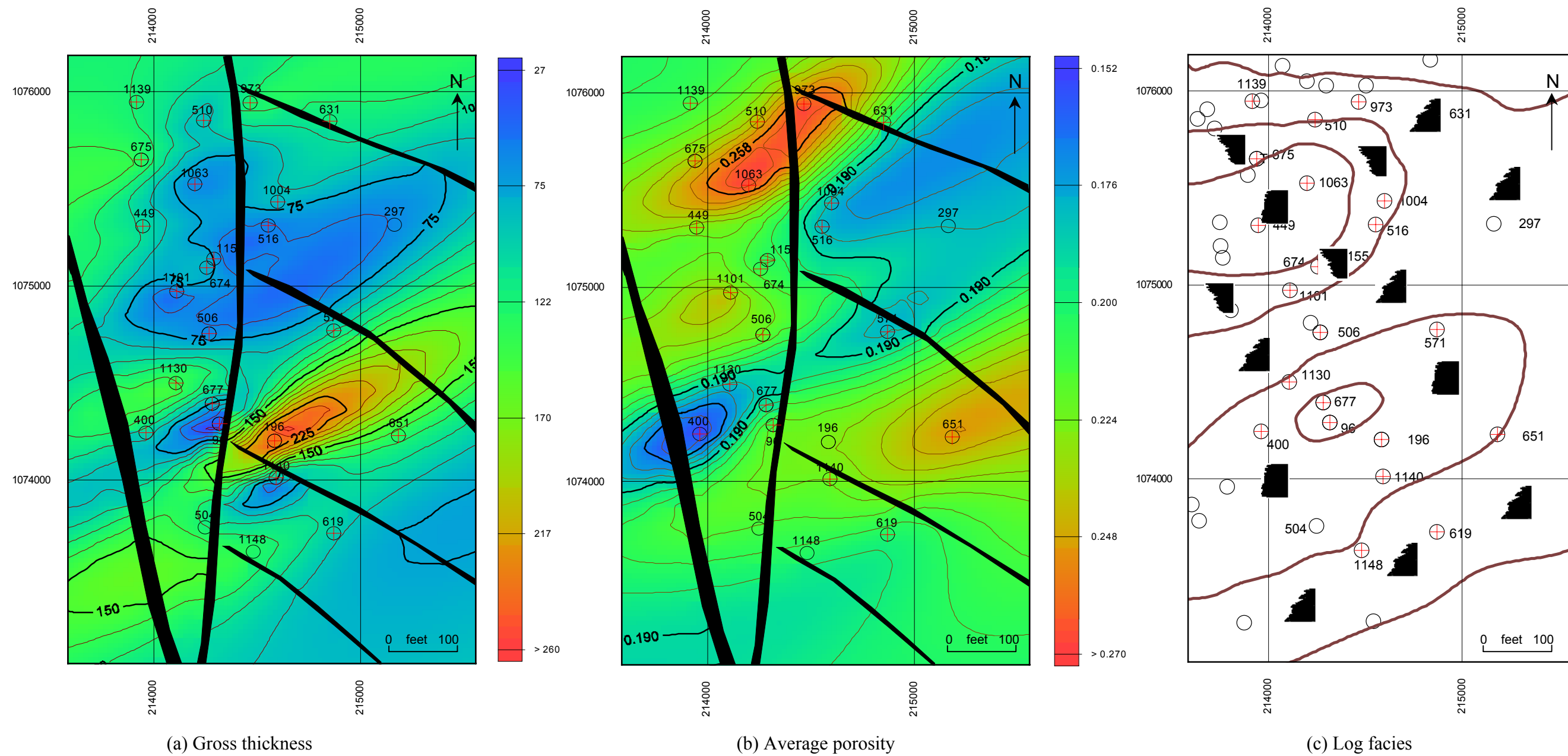


Figure 4.3 Layer 1 lithofacies maps (see Figure 1.2 for log data extend). (a) Gross thickness map of Layer 1 shows that sediments deposited along the southeast northwest and thickest sediment body (approximately 250 ft) located in the middle of the area. Contour interval is 15 ft. (b) Average porosity map of Layer 1 also indicates that depositional axis is trending southeast northwest. Most porous sand body located in the north of the area with 27% average porosity. Note that the thickest sand bodies have higher porosities than those of the thinner. Contour interval is 0.75%. (c) Log facies map of Layer 1 shows that dominant log responses are fining-upward and blocky. SE NW trending two lobes with their blocky and coarsening-upward log responses interpreted as a delta front. (⊕ : well data control, log patterns: : fining-upward, : coarsening-upward, : blocky)

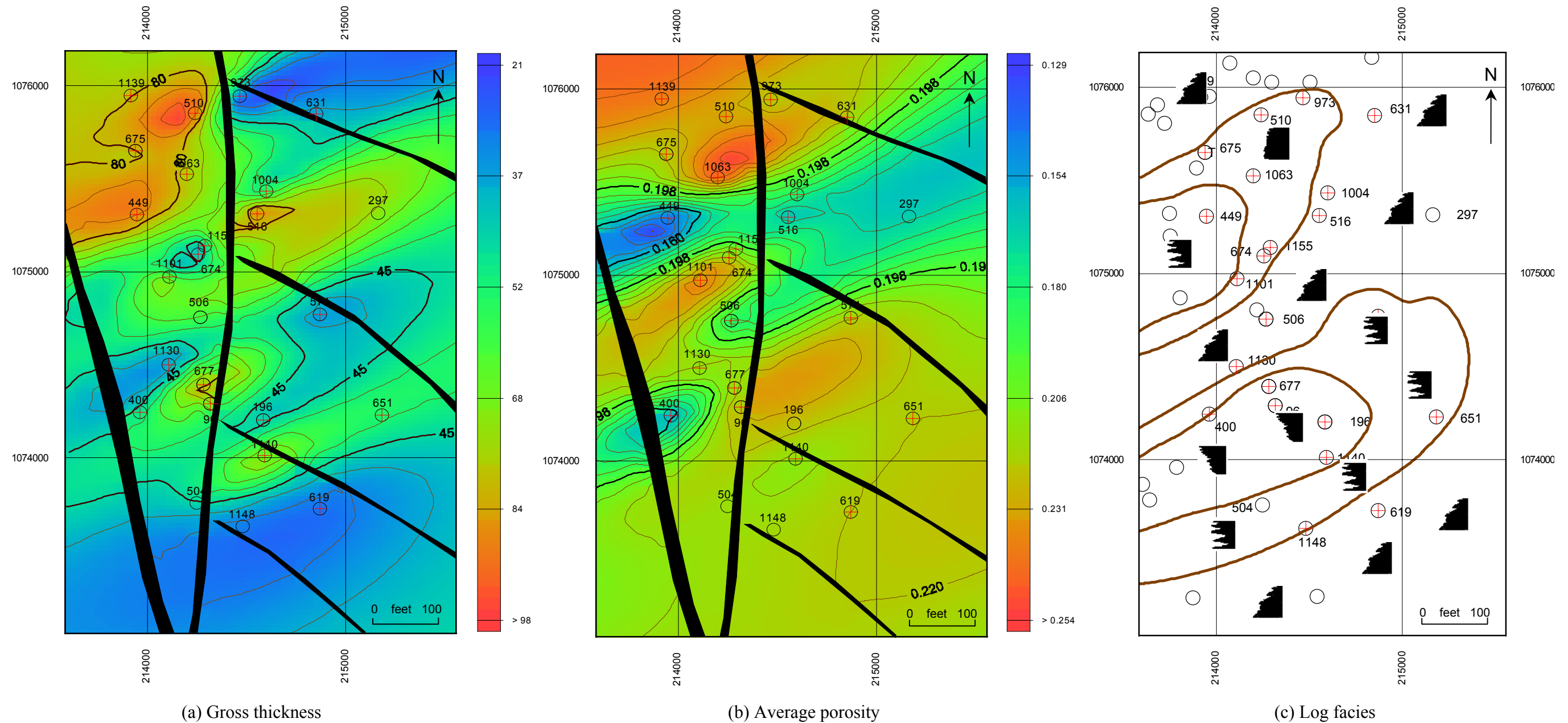


Figure 4.4 Layer 3 lithofacies maps (see Figure 1.2 for log data extend). (a) Gross thickness map of Layer 3 shows that sediments deposited along the southeast northwest and thickest sediment body (approximately 90 ft) located in the northern part of the area. Contour interval is 8 ft. Massive sands were interbedded with shaly units. (b) Average porosity map of the Layer 3 also shows southwest northeast trending of sediments. Most porous sand bodies concentrated in three areas, which have 25%, 20% and 23% average porosity values respectively. Contour interval is 0.75%. (c) Log facies map of the Layer 3 shows that the SW NE trending sand bodies have serrate and coarsening upward log responses. These sand bodies interpreted as interdistributary channels. Interdistributary channels flanked by fining-upward log sequences. (⊕: well data control, log patterns: ▲: fining-upward, ■: coarsening-upward, ▨: serrate, ▨: blocky)

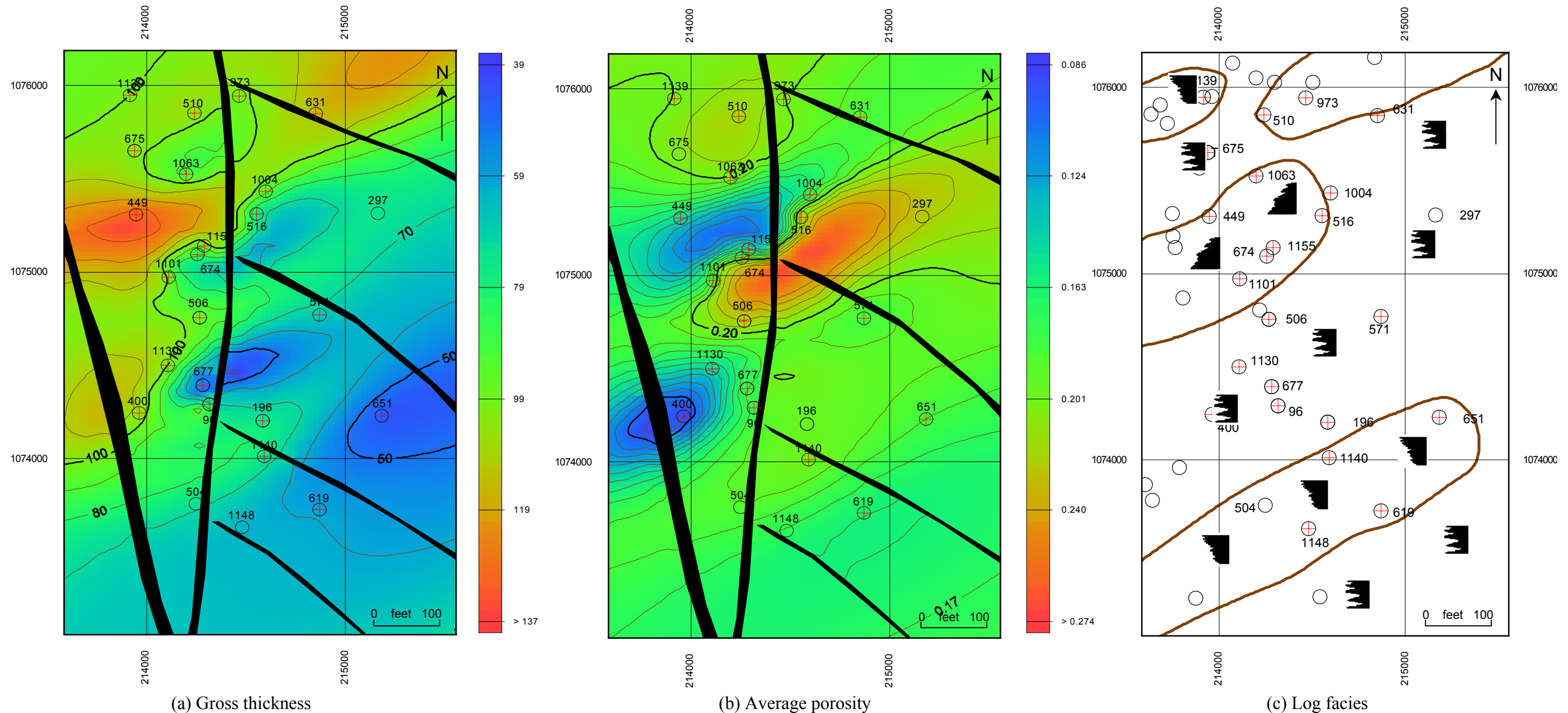


Figure 4.5 Layer 5 lithofacies maps maps (see Figure 1.2 for log data extend). (a) Gross thickness map of the Layer 5 shows the same trend (southwest northeast) of sediment source. Layer 5 is mostly sandy on the north but with shaly interbeds in the southeast. Maximum gross thickness is about 130 ft. Contour interval is 10 ft. (b) Average porosity map of the Layer 5. Maximum average porosity is 24% located in the middle of the area. Contour interval is 1%. (c) Log facies map of the Layer 5 shows that the most porous part coincides with fining-upward log responses, which are indicator of typical channel system. Between fining-upward log sequences, serrate log patterns cover whole area. (⊕: well data control, log patterns: ▲: fining-upward, ▨: coarsening-upward, ▨: serrate)

Figure 4.6 (a) shows the net sand thickness map of the C-4 interval. In this map, thickest sands located in the north part of the area and they also show SE NW trend. As it can be seen in Figure 4.6 (b), sandstone geometry parallel to each other and separated by two shaly units. Thickness of sand packages is 200 ft, 100 ft, and 120 ft and average porosities are 25%, 22%, and 23% respectively (Figure 4.7 a). Comparison of average porosity and log facies maps (Figure 4.7 b) show that the sandy parts in the C-4 interval have fining-upward log pattern. When porosity, net sand thickness, and log facies maps interpreted together, it shows that depositional axes of these southwest northeast trending sandy packages coincide with fining-upward log responses and they can be interpreted as distributary channels. Serrate log patterns flanked fining-upward log responses and they can be interpreted as interdistributary channels with their high shale content. They usually deposited during over flooding times.

In general, depositional axes in the C-4 interval defined by trends of more than 200-250 ft of gross sandstone, occur in narrow, northeast-trending dip-parallel belts, separated by relatively sandstone-poor area containing less than 75 ft of gross sandstone. C-4 depositional axes coincide with blocky and upward-fining log responses, flanked by sandstone-poor deposits exhibiting upward-coarsening and serrate log response. These blocky and upward-fining sandstones are interpreted to have been deposited several sandstone-rich tidal channels or upward-coarsening tidal-bar and tidal-shelf deposits.

In the VLE 196 file, C-4 stratum is sand rich and is composed of around 70% sandstone. These sediments were deposited by a delta system that prograded eastward to northeast through the area. Reservoir quality is mostly controlled by sandstone facies.

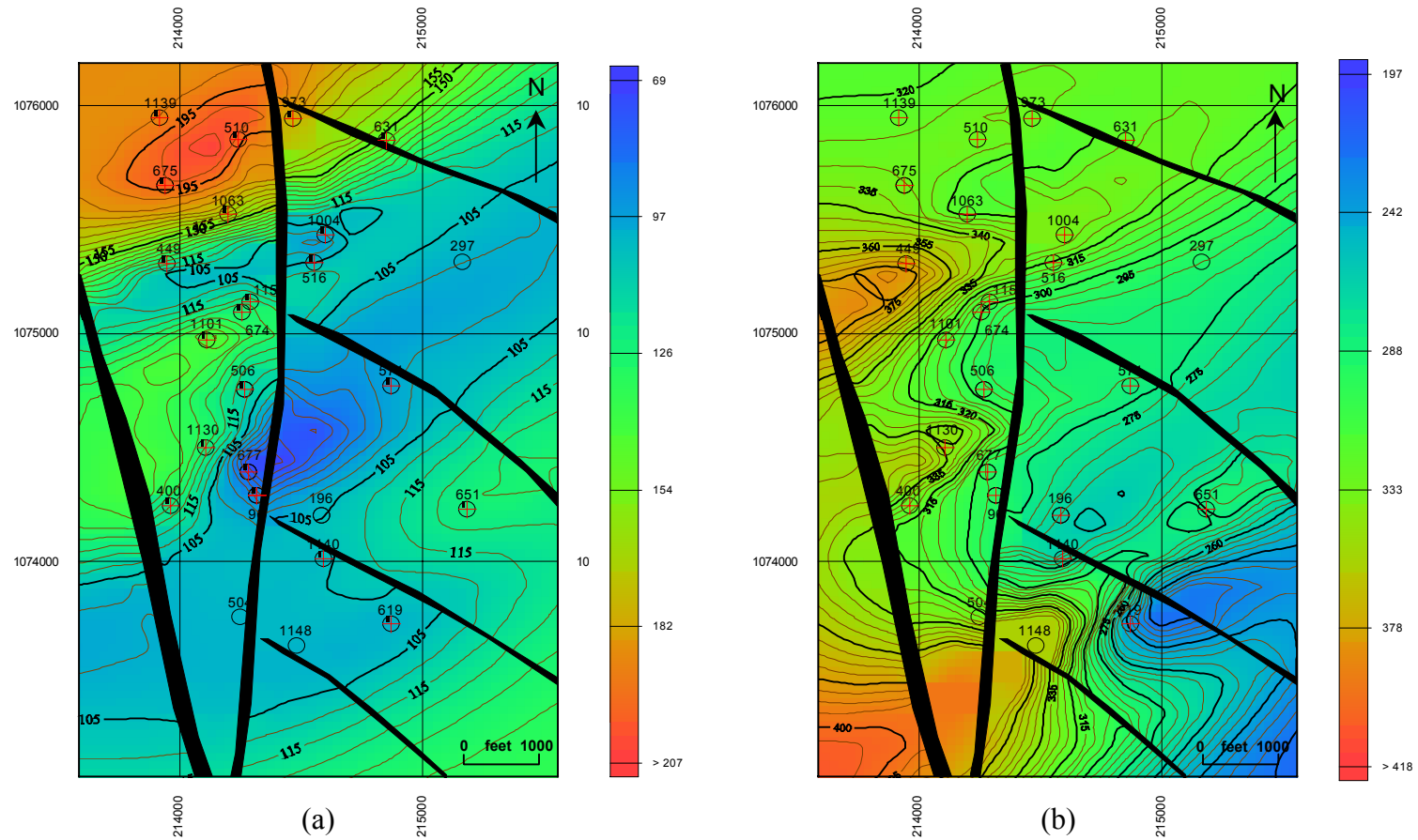


Figure 4.6 (a) Net sand thickness map of the C-4 interval. Figure exhibits southeast northwest contour patterns, reflecting depositional control in the interval. Thickest sands located in the northern part and 200 ft value. Contour interval is 5 ft. (b) Isopach map of the C-4 interval. This figure also shows same trend with net sand thickness map. Note than the shaly units interbedded the depositional dip trending sandy units. Contour interval is 5ft. (\oplus : well data control)

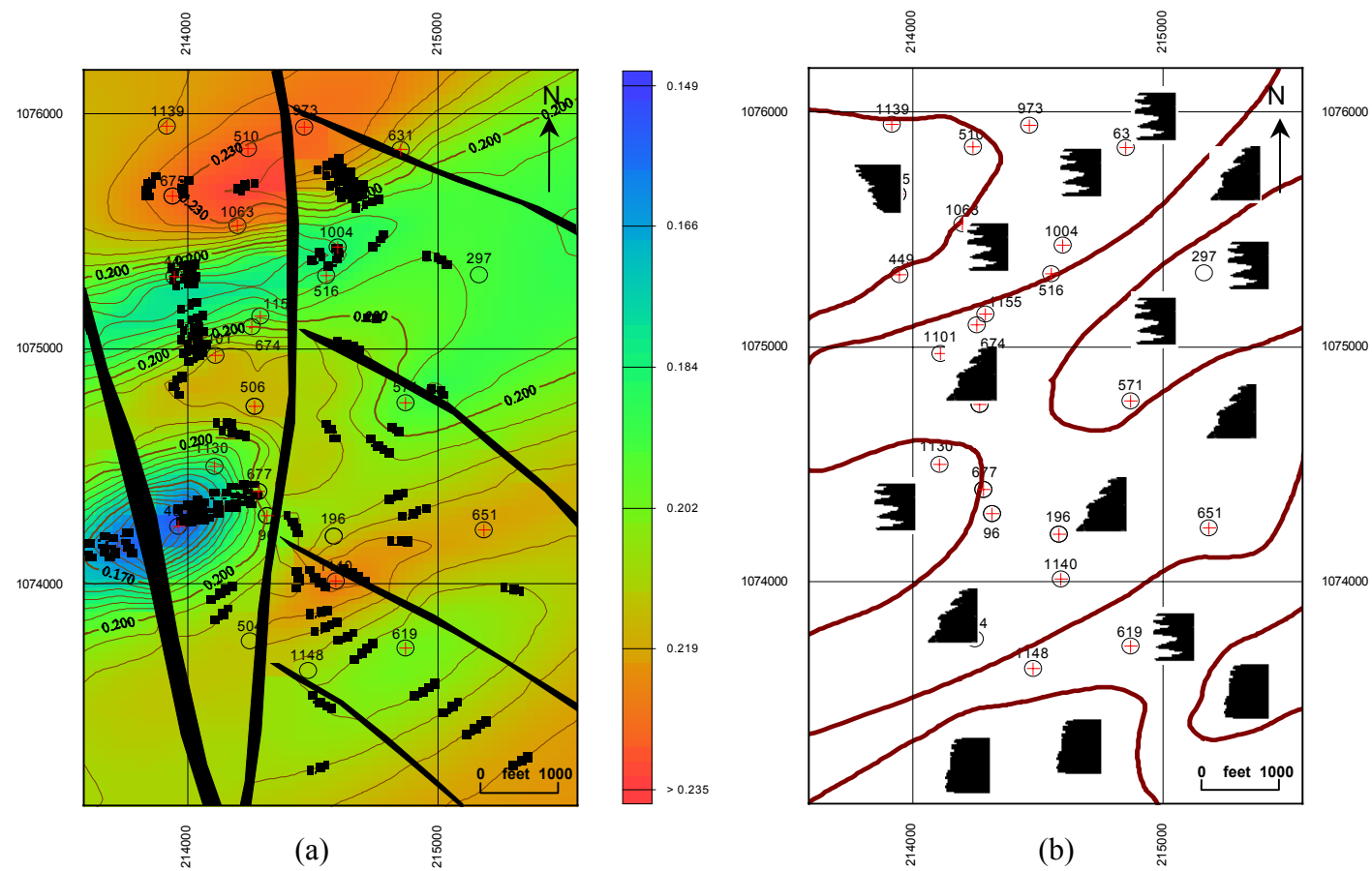


Figure 4.7 (a) Average porosity map of the C-4 interval. Figure shows three most porous bodies are trending through depositional dip. (b) Log facies map of the C-4 interval. In this figure southwest northeast trending sand packages coincide with fining-upward log responses which are interpreted as distributary channels. (\oplus : well data control, log patterns: : fining-upward, : coarsening-upward, : serrate, : blocky)

The oil-bearing facies in the VLE 196 area are mainly channel-fill sandstones that have upward-fining and block patterns and delta-front sandstones that have upward-coarsening and blocky patterns. These sandstones are more continuous in the east-west than the north-south directions.

The log patterns and their order of occurrence in C-4 strata suggest that the sandstone are delta front and stacked fluvial/distributary channel facies of a delta system. This conclusion supported by the sand-body geometry shown on net sandstone maps. On these maps, sand bodies trend eastward and northeastward, and they have distributary patterns. The most persistent input of sediments was in the northwest of the area, between wells VLE 1063 and VLE 1139.

I used processed well logs to construct two stratigraphic cross sections along the depositional strike (northwest-southeast) and one stratigraphic cross section along the depositional dip (northeast-southwest). Figure 4.8, 4.9, and 4.10 show representative cross sections (see Figure 1.2 for locations). Stratigraphic cross-sections are drawn using electric log correlation techniques to recognize identical sand/shale bodies between wells. The gamma and resistivity curves are used to identify the major sandstone and shale sections.

Using the cross sections made with normalized well logs, Misoa C-4 interval was divided into six layers. Odd-numbered layers are potential reservoir sandstones, whereas even-numbered layers are shaly and are potential seals. Cross-section A-A' (Figure 4.8) is along the depositional dip. In this figure, reservoir facies of C-4 interval consist of stacky, massive sand bodies from gamma ray log. Sandy layers have generally blocky,

serrate, and fining-upward log responses. The gamma ray log especially serrated in well #400 and #1130 as compared to other wells in the cross section showing increasing shaliness in the southeast direction. The shaliness is most probably caused by pinching out of sandy layers 3 and 5. Stratigraphic cross-section B-B' (Figure 4.9) is along the depositional strike (northwest-southeast) and all wells in this section are producer. In this cross-section, sand body thickness of Layer 1 increases through well #1140 and then decreases. Its fining-upward – serrate log response shows possible distributary channel. Sand body thickness is same for Layer 3 and 5 but shaly content of Layer 2, 4, and 6 varies through the cross-section and it is believed that they do not sufficient enough to create seals in the area. Cross-section C-C' is also along the depositional strike and parallel to cross-section B-B' (see Figure 1.2 for locations). This cross-section shows similar characteristics with cross-section B-B'. Sandy layers of C-4 have dominantly fining-upward, blocky, and serrate log responses. Layer 1 in well #571 also shows increase in sand body with its fining upward log pattern shows the existence of distributary channel. Interpretation of cross sections B-B' and C-C' together shows that the channel system in well #571 is same as the channel observed in well #1140 in cross-section B-B' (note that the well #1140 and well #571 are approximately in the same direction, see for Figure 1.2). Shaly layers of cross- section C-C' are also varies in thickness and distribution through the area and thickness decreases from C-5 to C-4. Interpretation of cross sections reveals that the study area consists several distributary

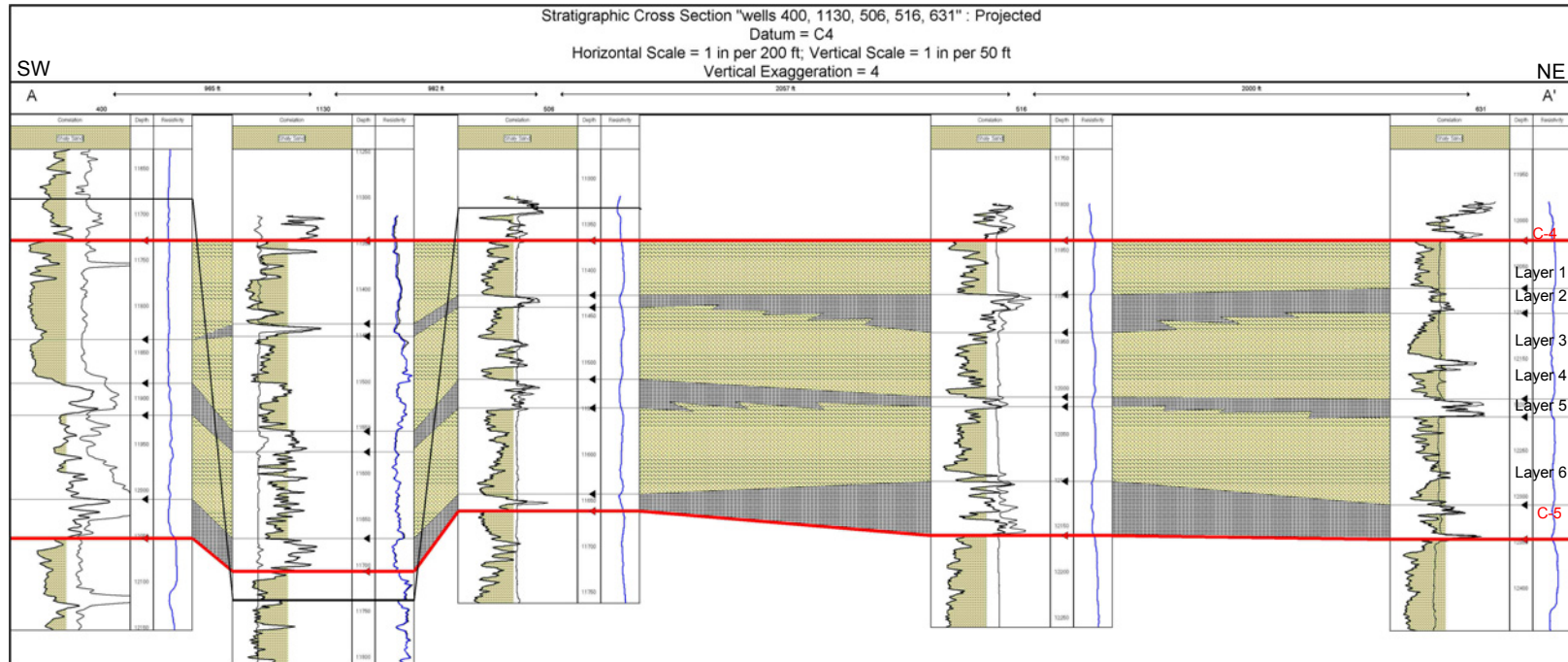


Figure 4.8 Stratigraphic cross-section A-A' along the depositional dip (northeast-southwest) (see Figure 1.2 for location). The gamma ray and resistivity curves were used to identify the major sandstone and shale sections. Misoa C-4 interval divided into three sandy and three shaly layers. In this cross-section, reservoir facies of C-4 strata consist of stacky, massive sand bodies. Sandy layers have generally blocky, serrate, and fining-upward log responses. Shaliness of layers increase in the southeast direction, especially in wells #400, and #1130. The shaliness is most probably caused by pinching out of sandy layers 3 and 5.

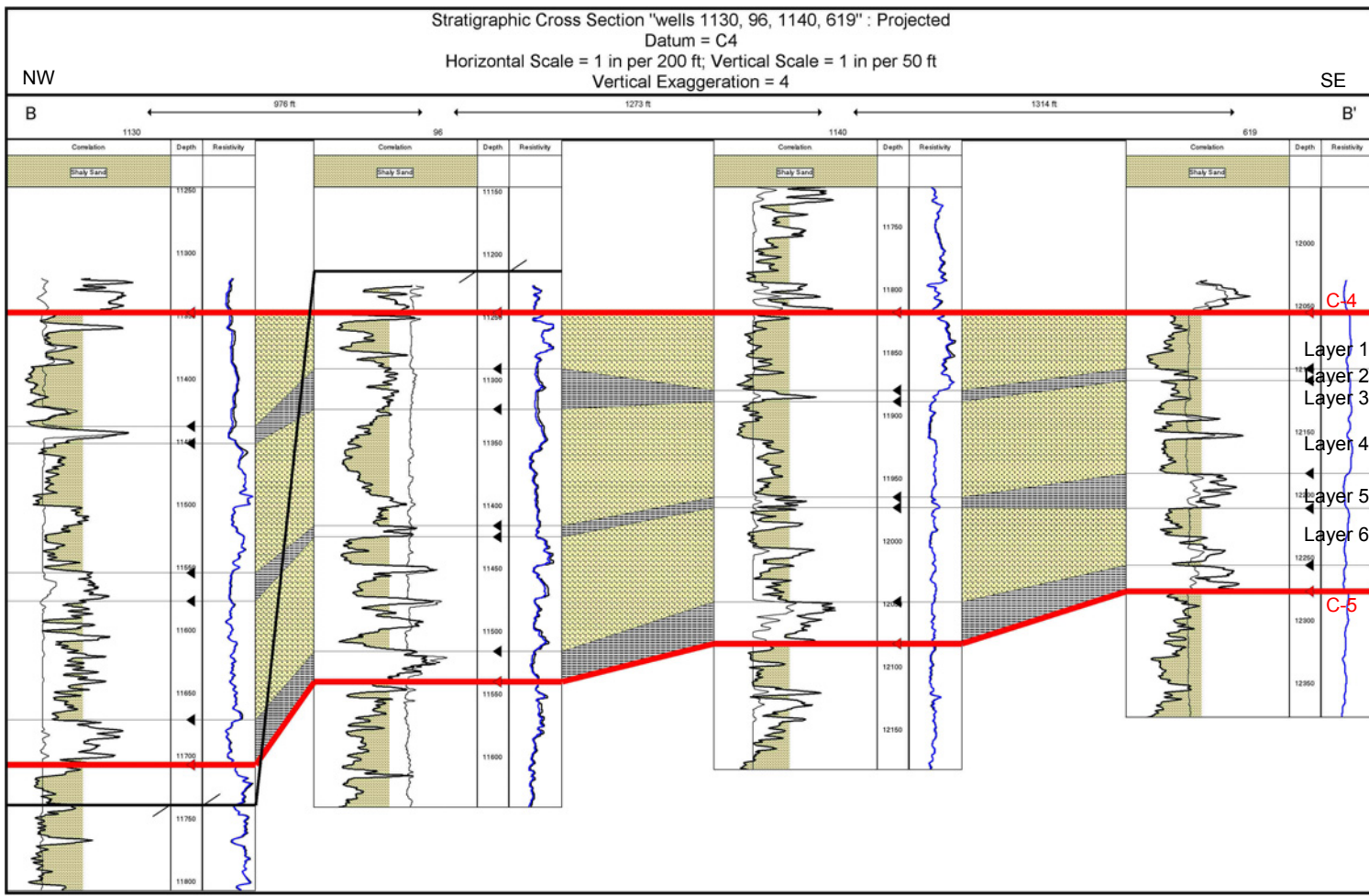


Figure 4.9 Stratigraphic cross-section B-B' along the depositional strike (northwest-southeast) (see Figure 1.2 for location). Layer 1 in the well #1140 shows increases in sand content with fining-upward – serrate log response interpreted as a distributary channel.

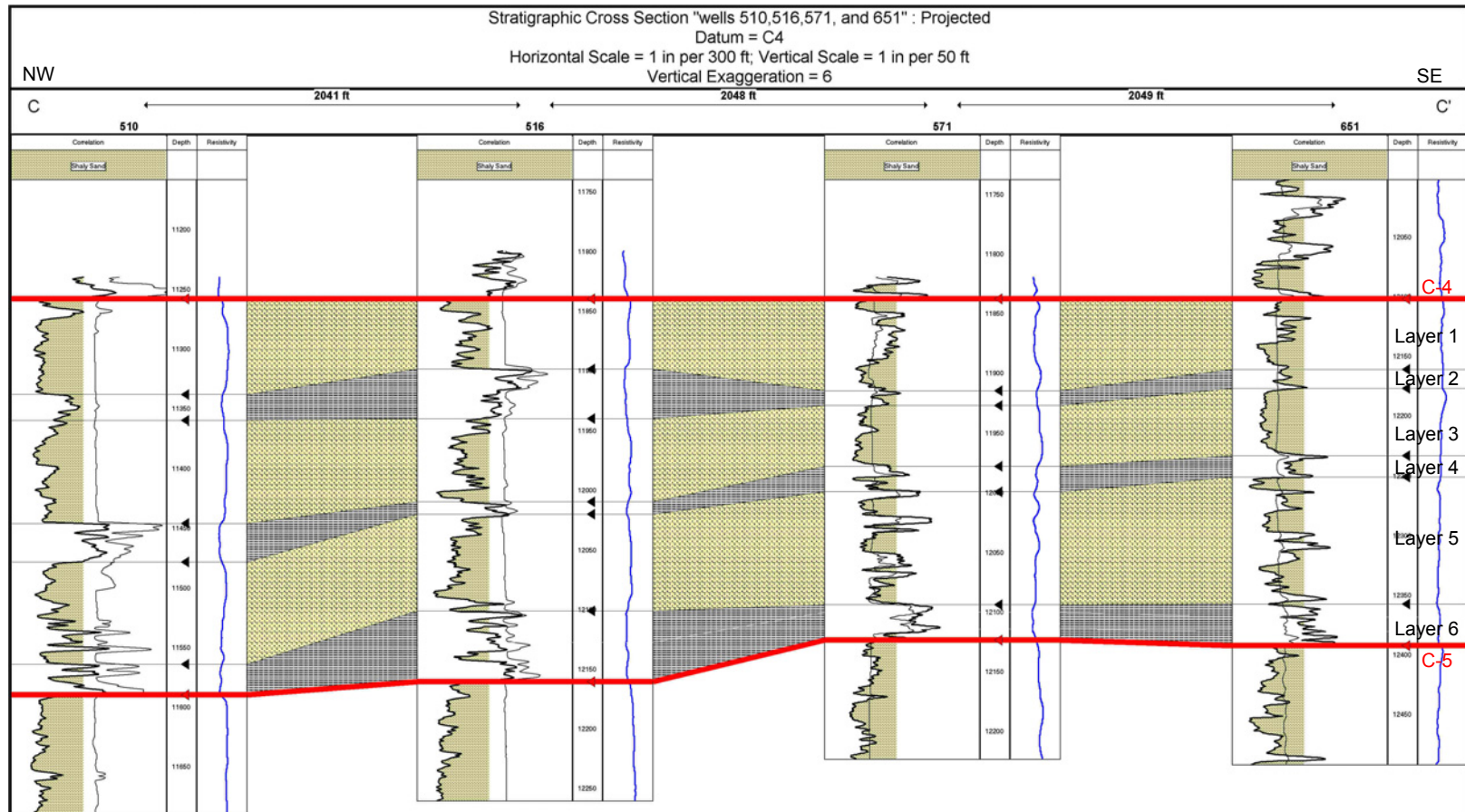


Figure 4.10 Stratigraphic cross-section C-C' along the depositional strike (northwest-southeast) (see Figure 1.2 for location). Sandy layers of C-4 interval have dominantly fining-upward, blocky, and serrate log responses. Layer 1 in well #571 also shows existence of distributary channel with its fining-upward log pattern and increasing sand thickness.

and inter-distributary channels (ranging from 30 to 50 ft) along the depositional dip (northeast-southwest). Channel fill sands are heterogeneous and cut by several thin shale beds. Comparison of net sand maps and cross sections also suggest that reservoir sandstones are more continuous in the east-west direction.

Previous studies indicate that the Lower Misoa strata deposited in a tide-dominated delta setting and sediment source was from the west or southwest (Talukdar and Marcano, 1994). Results of this study also suggest that the sediments in the VLE 196 area were deposited by a tide dominated delta plain to shallow marine sediments consisting of fluvial/distributary channel and delta front sandstones prograded eastward through the field. This interpretation is based on (1) log patterns of framework sandstones which are upward coarsening, block, and upward fining on the gamma ray trace; (2) sand body geometry and characteristics are shown on net sandstone, average porosity, gross thickness and log facies maps suggesting stacked fluvial channel-fill sandstones in the VLE 196 area and distributary sand bodies southeast of the field.

4.1.3 Results

- 1) C-4 interval in the Misoa sandstones were divided into three sandy and three shaly units based on type log responses and cross-sections. In each layer, sand thickness varies but they trend through paleo dip (southwest-northeast).
- 2) Layer 1 is predominantly sand and interbedded with thin shaly units. Maximum gross thickness of this layer 250 ft and average porosity 27%. Fining-upward and blocky log responses of Layer 1 indicate delta front environment.
- 3) Layer 3 consists of massive sand within shaly interbeds. Maximum gross thickness and average porosity of this layer are 100 ft and 30% respectively. Log facies map of Layer 3 has blocky, serrate, and coarsening-upward log characteristics.
- 4) Layer 5 is mostly sandy with shaly interbeds. Gross thickness of this layer is approximately 150 ft and elongated to southwest northeast direction and become thinner through to southeast. Average porosity of this layer is 30%. Layer 5 has upward-fining log response, which is indicator of distributary channel.
- 5) Shaly layers of C-4 strata interpreted as potential seals and they deposited in low-energy interdistributary, and shallow marine environments. The percentage of shale increases upward from C-5 to C-4. Shales are of variable thickness and extend and they make up almost 40% of the C-4 interval.
- 6) Layer 6 at the base of the C-4 interval is most extensive shaly layer in the section and most likely it represents a marine flooding surface which is identified in electric logs as low resistivity and high gamma peak. In contrast, many other shaly layers have

more sand content. Thus, the extend of shale layers as reservoir or no-flow units are vary from layer to layer.

- 7) In general, all C-4 layers exhibit southeast northwest sand thickness contour patterns in lithofacies maps, reflecting depositional control on the interval. Depositional axis in the C-4 interval defined by more than 250 ft of gross sandstone, occur in narrow, depositional dip parallel belts, separated by relatively sandstone-poor areas consisting less than 20 ft of gross sandstone. C-4 depositional axes coincide with blocky and upward-fining log responses, flanked by sandstone-poor deposits exhibiting upward-coarsening and serrate log responses.
- 8) The log patterns and their order of occurrence in C-4 strata suggest that the sandstone are delta front and fluvial/distributary channel facies of delta system. This conclusion supported by the sand-body geometry shown on net sandstone and gross thickness maps.

4.2 Seismic Stratigraphy

4.2.1 Principles

Seismic stratigraphy is the interpretation of stratigraphy and depositional facies from seismic data. Seismic reflection terminations and configurations are interpreted as stratification patterns, and are used for recognition and correlation of depositional sequences, interpretation of depositional environment, and estimation of lithofacies.

Seismic sequence analysis subdivides the seismic section into packages of concordant reflections, which are separated by surfaces of discontinuity defined by systematic reflection terminations. These packages of concordant reflection (seismic sequences) are interpreted as depositional sequences consisting of genetically related strata and bounded at their top and base by unconformities or their correlative conformities. Reflection terminations interpreted as stratal terminations include erosional truncation, toplap, onlap, and downlap (Figure 4.11 a) (Mitchum et al., 1977).

After seismic sequences are defined, environment and lithofacies within the sequences are interpreted from seismic and geologic data. Seismic facies analysis is the description and geologic interpretation of seismic reflection parameters, including configuration, continuity, amplitude, frequency, and interval velocity. Each parameter provides considerable information on the geology of the subsurface. After seismic facies units are recognized, their limits defined and areal associations are mapped, they are interpreted to express certain stratification, lithologic, and depositional features of the deposits that generated the reflections within the units. Major units of reflection

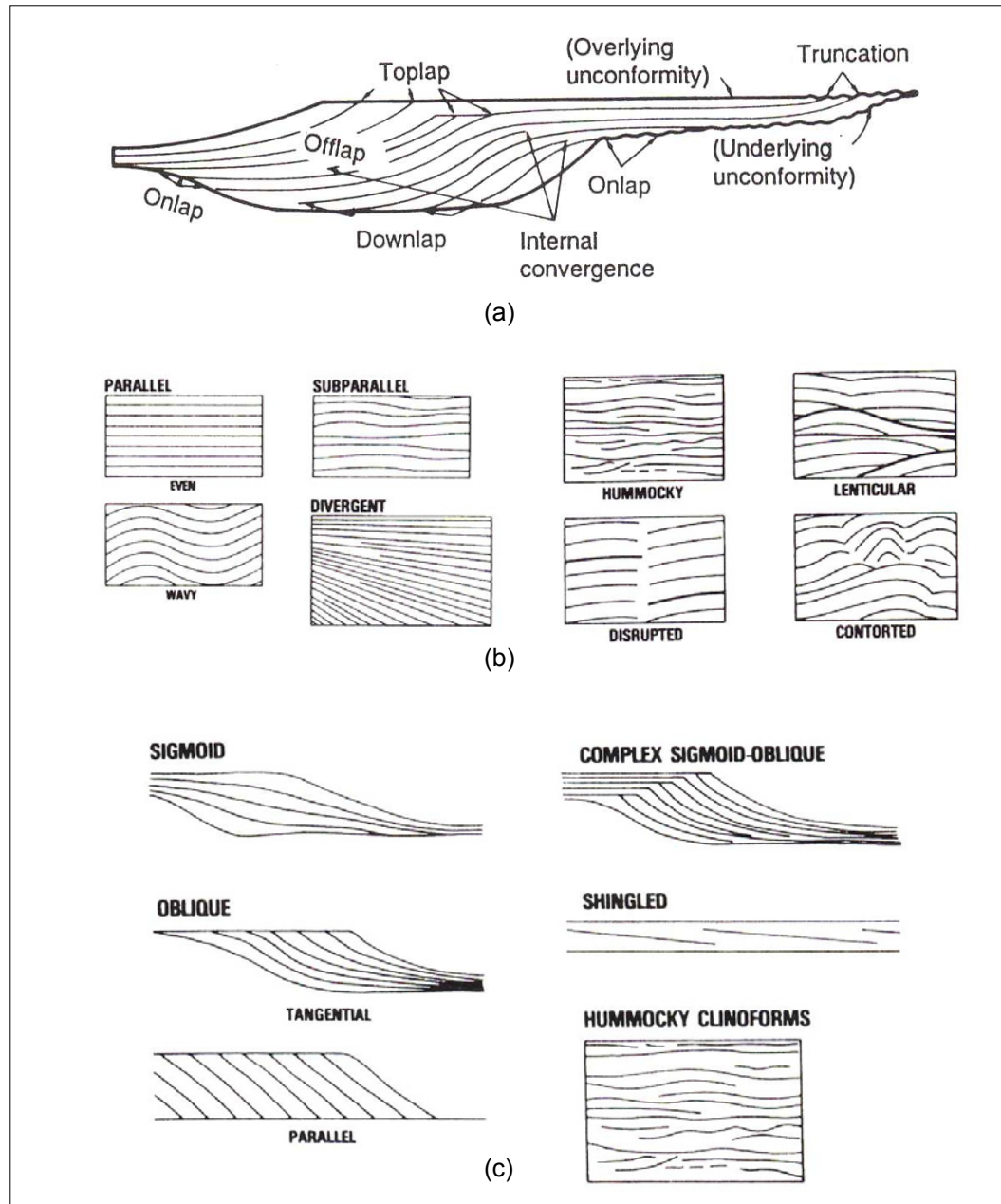


Figure 4.11 (a) Seismic stratigraphic reflection terminations within idealized seismic sequence. (b) Various seismic reflection configurations and modifications. (c) Seismic reflection patterns interpreted as prograding clinoforms (Mitchum et al., 1977).

configurations include parallel, subparallel, divergent, prograding, chaotic, and reflection-free patterns (Figure 4.11 b). Prograding configurations may be subdivided into sigmoid, oblique, complex sigmoid-oblique, shingled, and hummocky clinoform configurations (Figure 4.11 c) (Mitchum et al., 1977).

In delta depositional environments, each kind of delta has a distinct framework orientation and depositional pattern, which results in a characteristic seismic reflection pattern. Fluvial-dominated deltas are characterized by clinoform seismic reflection patterns which include; oblique (tangential), complex oblique (tangential), sigmoid, and complex sigmoid-oblique. Wave dominated-deltas are characterized by shingled seismic reflection patterns. Tide-dominated deltas are difficult to recognize in the subsurface and through seismic stratigraphic methods, but the clinoform seismic reflection patterns, which commonly appear on seismic data and they usually associated with delta systems (Mitchum et al., 1977) can be used to characterize tide-dominated deltas (Berg, 1982).

4.2.2 Seismic Stratigraphic Interpretation

In this part of the study, isochron, isopach, and seismic amplitude maps were used to interpret seismic stratigraphy of the study area. Because existing well logs only penetrated to C4 interval, associated maps were drawn only for top of the C4 and C5 layers. Beside conventional seismic amplitude maps, instantaneous phase display sections also used. Instantaneous phase is basically a measure of reflector continuity. Because it is independent of the magnitude of peak or through amplitudes, the magnitude of instantaneous phase is always same (0^0 for peak amplitude, $+180$ for

troughs). Therefore, instantaneous phase tend to balance the weak and strong reflectors and make the interpretation of weak coherent reflectors easier and is very effective for detecting the fault discontinuity, wedge-out, channels, fan and internal deposition geometry of the sedimentary layers and sequence boundaries. C4 interval isopach thickness were also correlated with thickness from well data to ensure seismic and well data coherence. Because well curves could not be tied to seismic data, time-depth relations from velocity survey (well #1101) was used to pick top of the C4 and C5 layers from seismic data and to create related iso-maps.

Because the scale of the depositional structures within the C4 layers is generally below seismic resolution, I was unable to interpret seismic stratigraphy of the C4 layers and correlate them with well data. To determine vertical resolution of the seismic data, dominant frequencies were calculated for the C-4 strata and Misoa Formation. As it can be seen in Appendix C, dominant frequency is approximately 20 Hz and average velocity of the Misoa sands was determined from velocity survey from well #1101 as 8600 ft/sec. Using velocity and dominant frequency, dominant wavelet ($\lambda = v/f$) was calculated as 430 ft. Average thickness of C4 layers change between values of 20 ft and 90 ft (Appendix B) but the vertical resolution of seismic data allows recognizing intervals more than or equal to 107 ft ($\lambda/4$).

Figure 4.12 shows isochron map of the C4 interval. As it can be seen in this figure, it is very difficult to interpret the area covers well logs but the general trend of the interval exhibits time thickening of contour patterns, which are indication of possible sand ridges, between arrows in southwest-northeast direction. The interval thickness

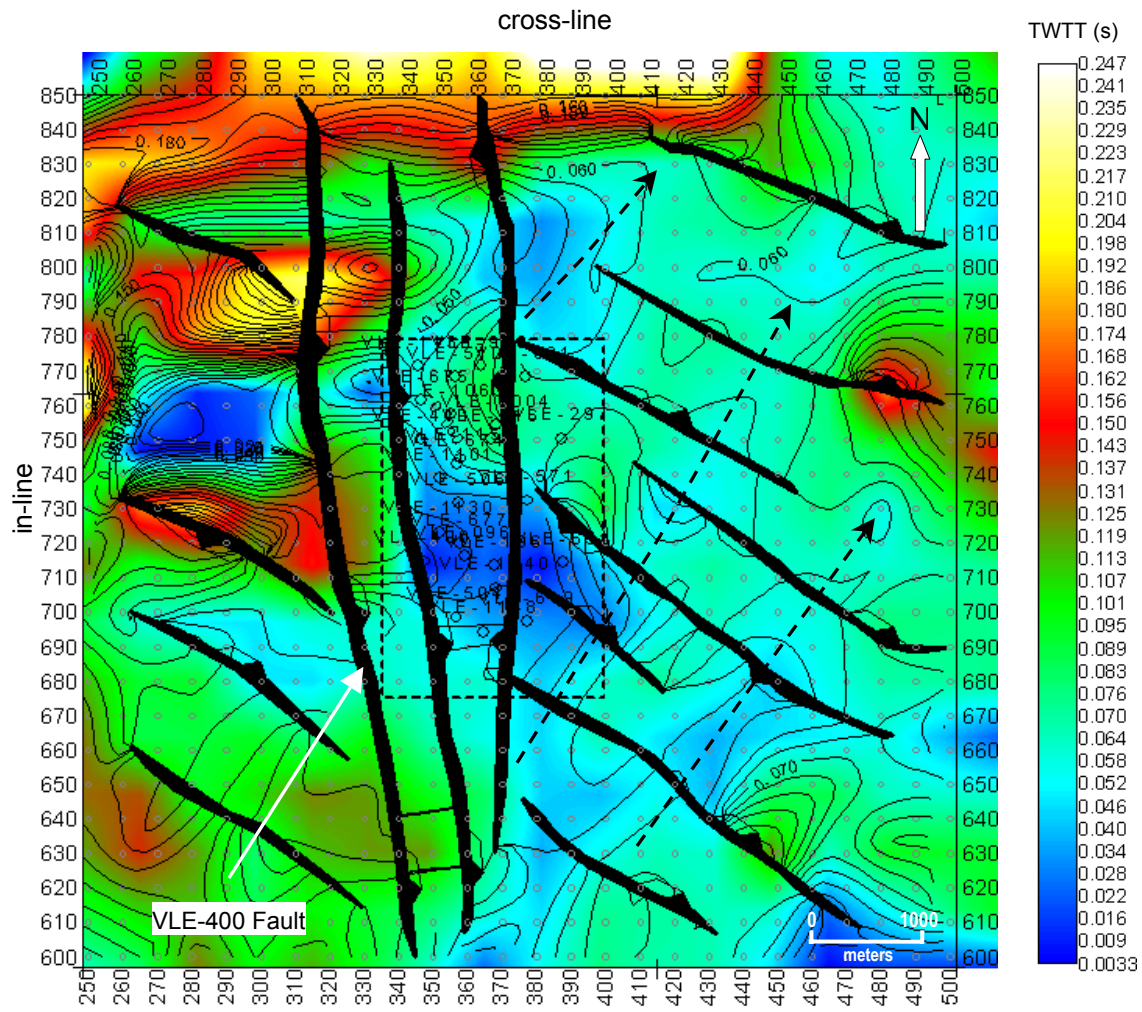


Figure 4.12 Isochron map of the C4 interval. Arrows indicate time thinning of the interval. As it can be seen in the figure, thickest parts located between the arrows and trend southwest-northeast direction. Dotted rectangular indicates well data extend. Contour interval is 10 ms.

maximum 250 ms TWTT. Isopach map of the C4 interval (Figure 4.13) also exhibits southwest-northeast trending contour patterns and some isolated lobes between en echelon faults in the east side of the area. The interval thickness of the C4 isopach map ranges from a minimum 300 ft to a maximum 700 ft. It is obvious that the C4 interval thickest (approximately 600 ft) in the west side (downthrown block) of the VLE 400 Fault and become thinner in the east side (approximately 250 ft). This is caused mainly by the reverse component of the VLE 400 Fault which made the “C” layers thinner in the east side (upthrown block) and the erosion created by Late Eocene unconformity. The isopach patterns also indicate that the sediments entered the study area from the southwest direction and they create some distributary channel fill structures between tidal sand ridges (see Figure 4.13).

Figure 4.14 shows enlarged image of the dotted line area which represents well log data extend in Figure 4.13. Contour patterns indicate that the thinning of the C4 interval in the middle of the area because of uplifting created by the VLE 400 Fault. Most of the “C” layers eroded in the vicinity of the VLE 400 Fault and they created toplap reflection patterns through the unconformity. Thickness values obtained from each well in this figure were used to correlate thickness form well data. Values on each well in isopach map of the C4 interval were plotted versus C4 thickness values from well data to correlate seismic and well log data. As it can be seen in Figure 4.15, thickness from well and seismic data show good correlation. Note that the in this figure, thickness below vertical seismic resolution and thickness have extremely high values were not considered (see Appendix D for details).

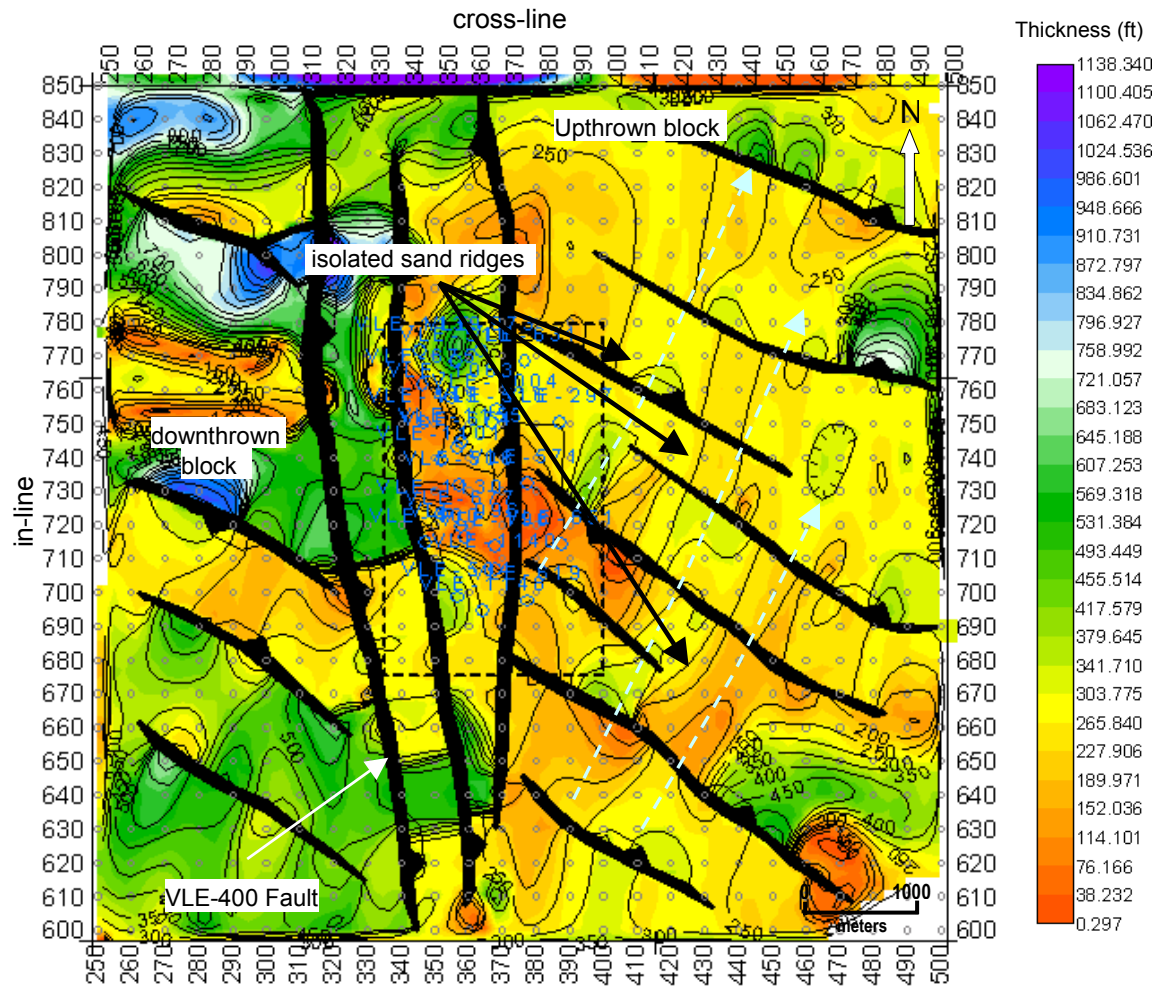


Figure 4.13 Isopach (true vertical thickness) map of the C4 interval. Contour patterns indicate that the sediment source in the area was southwest northeast direction. Thickening of the interval is also observable in the downthrown block whereas the C4 interval become thinner in the upthrwon block due to reverse componenet of the VLE 400 Fault and erosion created by Late Eocene unconformity. Dotted line indicates well data extend. Contour interval is 50 ft.

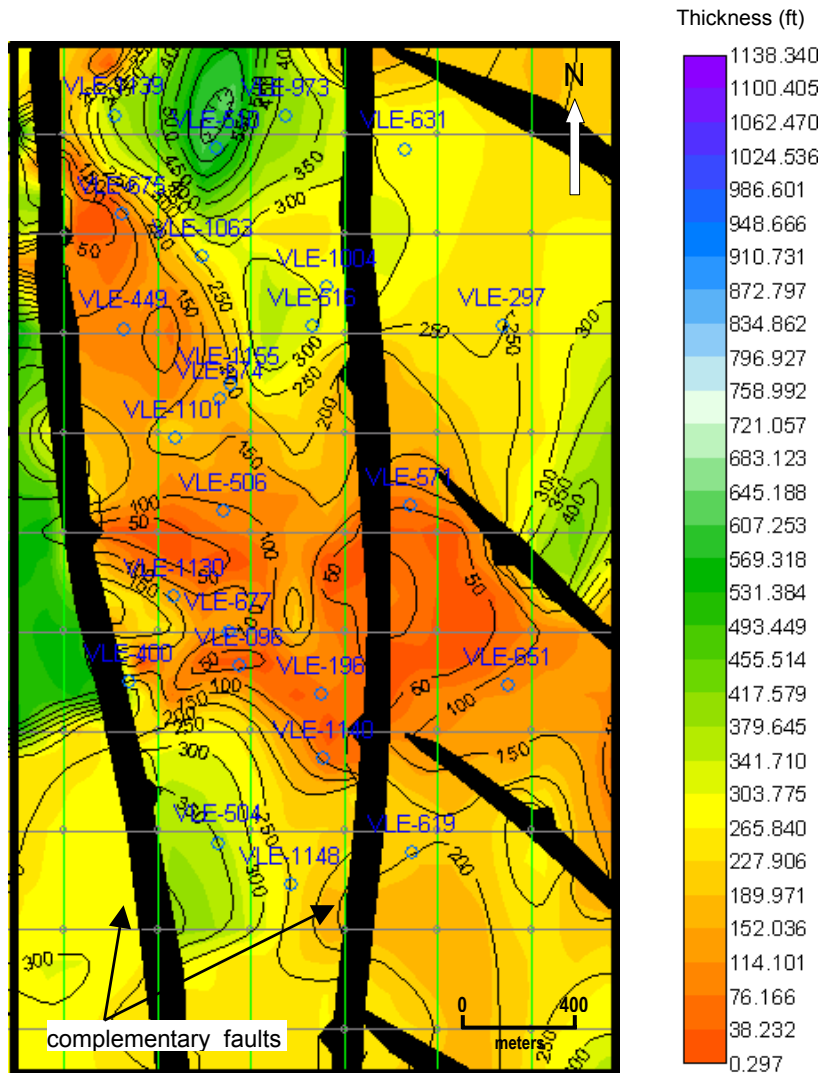


Figure 4.14 Enlarged image of the dotted line area in Figure 4.13. Contour patterns indicate that the thinning of the C4 interval in the middle of the area because of uplifting created by the VLE 400 Fault. Most of the “C” layers eroded in the vicinity of the VLE 400 Fault and they created toplap reflection patterns through the unconformity. Thickness values obtained from each well in this figure were used to correlate thickness form well data. Contour interval 50 ft.

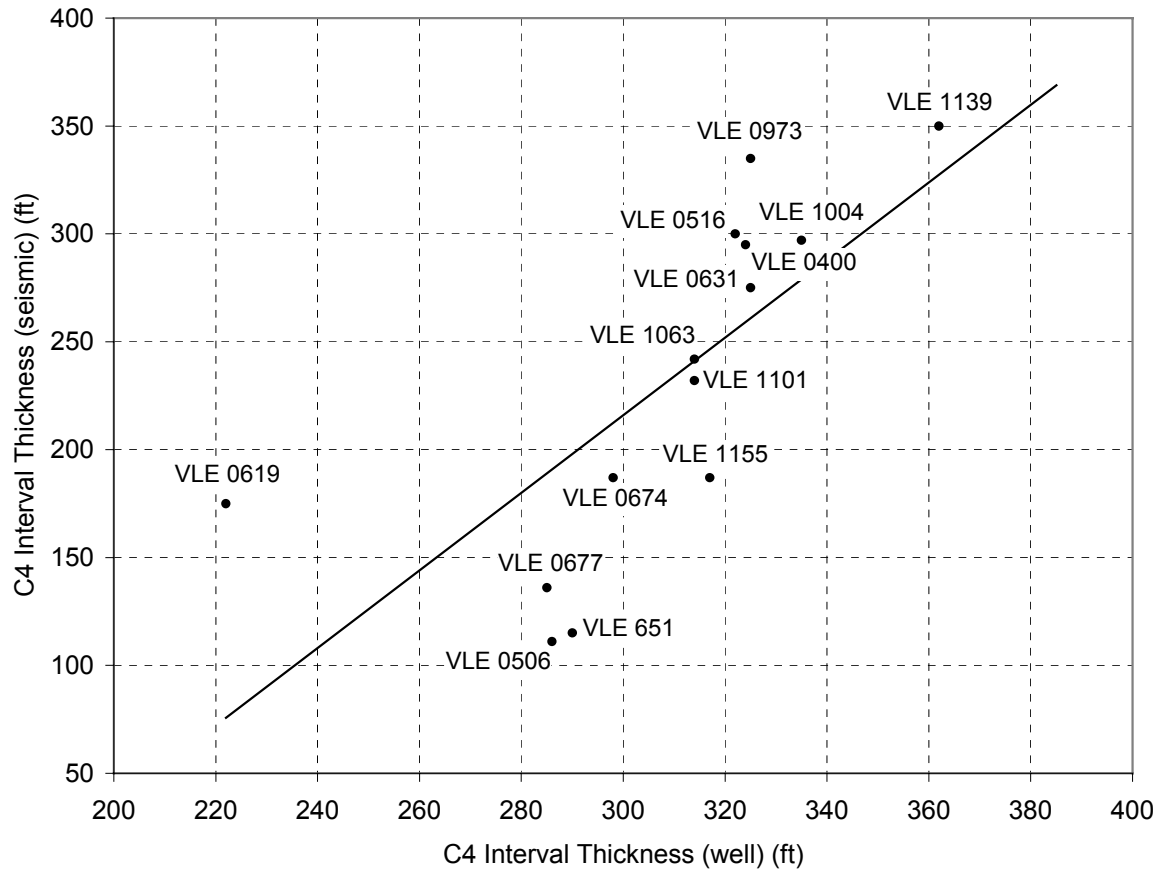


Figure 4.15 Correlation plot of the C4 interval thickness from well and seismic data. Thickness below vertical seismic resolution (see Appendix C) and thickness have extremely higher values were not considered in this plot (see Appendix D).

In the VLE 196 area, four main seismic facies are recognized (Figure 4.16). The seismic facies are better distinguished on the north-south seismic lines than the east-west ones because of northwest-southeast oriented reverse component of the VLE 400 Fault which made thinner the formations and created disturbed zones in this direction. Due to lack of well data in the target formations (Misoa and Guasare), the depositional environment of each seismic facies was interpreted using reflection amplitude, continuity, and configuration. Seismic stratigraphic interpretation techniques followed Mitchum, Vail, and Sangree (1977).

Seismic facies I is characterized by low-to-high or variable amplitude and poor-to-low continuity reflections with hummocky zones. Reflections with poor continuity and chaotic zones suggest that the rapid sedimentation of Miocene-to-recent age of the La Rosa, Lagunillas, La Puerta, and El Mirago formations. Erosion, which was created by the Late Eocene unconformity, was most probably led to fast sedimentation of recent formations. Seismic facies II is characterized by high amplitude, moderate-to-good continuity reflections. Parallel-to-subparallel reflections are dominant in the seismic facies II and discontinuous reflections (mostly truncations) can also be seen locally. This seismic facies represent the common reflection character of the Misoa Formation through the VLE 196 area. Because of the coastline of the Caribbean Sea during the Eocene time was in the vicinity of what is now the Lake Maracaibo (Bockmeulen et al., 1983), during the Middle Eocene time the great river built a stream flowed from southwest to northeast. It built a series of deltas, but subsidence of sea bottom was very rapid and the successive deltas did not prograde seaward, but piled on top of each other.

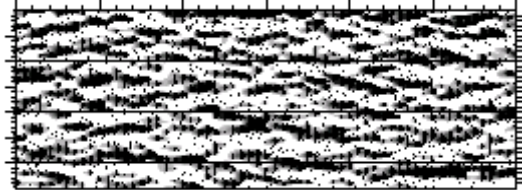
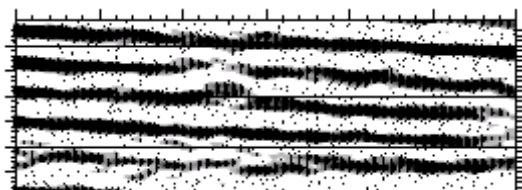
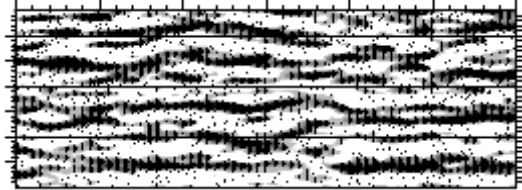
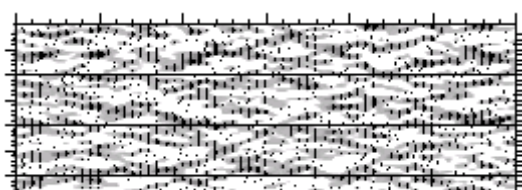
Seismic Facies	Characteristics	Geological Interpretation
 Seismic Facies I	Low-to-high or variable amplitude, poor-to-low continuity reflections with hummocky and/or structureless	Miocene-to-recent sediments of La Rosa, Lagunillas, La Puerta, and El Milagro formations, mostly shale interbedded with sand and coal
 Seismic Facies II	High amplitude moderate-to-good continuity reflections, mostly parallel-to-subparallel and disturbed by some truncations	Eocene age "C" sands of Misoa Formation, tidal-flat environment with regional erosion Limestones of Guasare and La Luna formations show similar pattern
 Seismic Facies III	Low-to-high amplitude, package of short, irregular, hummocky cliniforms	Delta environment, distributary channel fill and truncations within the Misoa Formation Some part of the Colon and Mito Juan formations (mostly shale) exhibit same pattern
 Seismic Facies IV	Chaotic, largely reflection free	Acoustic basement, igneous, metamorphic, and coarse continental clastic sediments

Figure 4.16 Seismic facies recognized in this study and their characteristics and geological interpretation.

(Zamora, 1977). The reason of parallel to subparallel reflection character of the tide-dominated deltaic sandstones of the Misoa Formation can be due to, as it stated above, piling of sediments to each other during the Eocene times. Another explanation for this situation can be the VLE 196 area is most probably situated in the tidal flat (delta plain) within the sequence of the tide-dominated delta structure.

Seismic facies III is characterized by low-to-high amplitude, package of short, irregular hummocky cliniforms. This reflection pattern is observable within the Misoa Formation and some part of the shaly sediments of the underlying Colon and sandy layers of the Mito Juan formations. Seismic facies III is referring to a distributary channel fills and tidal sand ridges and lobes, which were created by deltaic sandstones of the Misoa “C” sands. This interpretation was supported by seismic cross sections, which were discussed in the following pages. Seismic facies IV is characterized by chaotic, reflection free patterns which indicate the acoustic basement of the study area. Basement consists of igneous, metamorphic, and continental clastic sediments of the Cogollo, Rio Negro, and La Quinta formations.

To represent the seismic stratigraphy of the Misoa-Guasare interval, five seismic sections were selected over the study area. Figure 4.17 shows the location of the seismic sections. Figure 4.18 and 4.19 show the general reflection character of the Misoa “C” sands over the study area. As it can be seen in these figures, the Misoa Formation is unconformity bounded, Late Eocene unconformity on the top and the Guasare Formation on the bottom respectively. Misoa Formation shows high amplitude, moderate-to-good continuity reflections. These reflections are mostly parallel but they were disturbed by

some distributary channel fill and some truncations within the formation. Wedge shaped seismic features in Figure 4.18 and 4.19 can be corresponded to the distributary channel fill. Scale of channel fill similar structures vary within the formation, such as 750 m to 2 km wide and 0.5 ms to 2 ms (TWTT) deep. Reflection patterns of these channels reflect seismic facies III, which have low-to-high amplitude and hummocky reflections and they mainly bounded and eroded by the unconformity. Carbonates of the Guasare Formation show strong reflections and underlying unit have weak reflections because of its high shale content.

Figure 4.20 exhibits different reflection character than the other seismic sections. In this figure, sandy layers of the Misoa Formation have lobe shape characters with aggradational pattern which suggest that the continuous deposition of sand layers through the depositional dip (southwest-northeast) within the deltaic environment of study area. In this figure, on the other hand, bounding layers (unconformity on the top and Guasare Formation on the bottom) have almost parallel reflections relative to the Misoa Formation and general geometry of the “C” layers were not affected by faults. This shows that the aggradational reflections resulted from deposition other than the structure. Erosional truncations in the Misoa Formation were also observed that they were mainly created by the overlying unconformity. Figure 4.21 which lies along the depositional strike also shows some eroded channel similar structures within the Misoa Formation. Overlying and underlying units of the formation exhibit generally flat-lying reflections but as it can be seen in the interpreted part of the seismic section (Figure 4.21 b), a belt of dipping events forms a progradational pattern with some onlap surfaces.

Western side of the study area (downthrown block) represents different reflection character which is shown in Figure 4.22. As it can be seen in this figure, Misoa sands have high amplitude with package of irregular, hummocky cliniforms and onlapping the underlying unconformable surface of the Guasare Formation. Thickening of the Misoa Formation in northwest direction resulted from the oblique movement of the VLE 400 Fault other than the depositional environment. Therefore, it cannot be concluded that the northwest direction onlap patterns reflect the depositional axis in the study area which is inconsistent with the results obtained from well log interpretation (see Chapter IV, interpretation of depositional system). Eroded channel similar features also exist in the middle part of the seismic section in Figure 4.22 but they were believed to be created by the extensive faulting in the area.

In general, Guasare-Misoa interval in the VLE 196 area represents eroded channel structures with internal truncations in the direction of the depositional dip (southwest-northeast). But the absence of well logs and core data over the entire interval, it was unable to correlate results gathered from seismic stratigraphic interpretation with well data and represent more precise definition of the stratigraphy of the Guasare-Misoa interval.

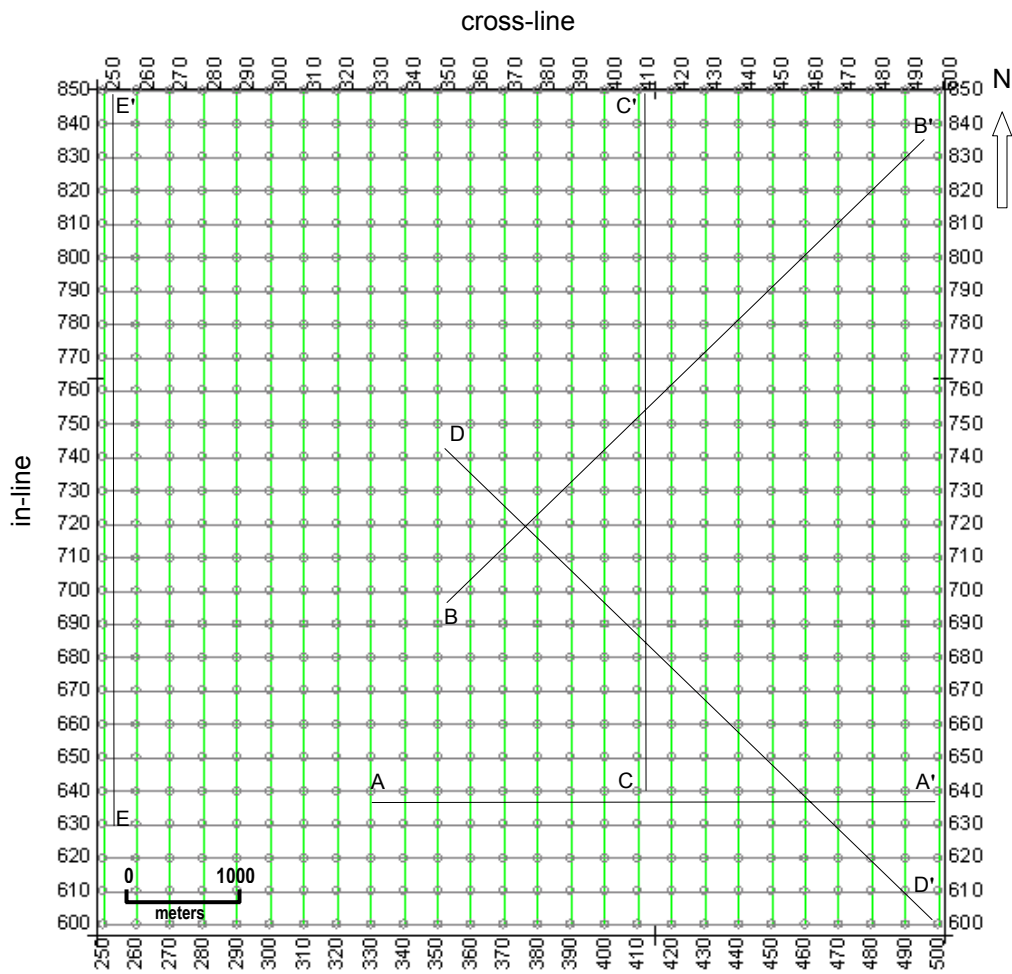


Figure 4.17 Locations of the seismic lines in Figure 4.18 to Figure 4.22 on the seismic basemap.

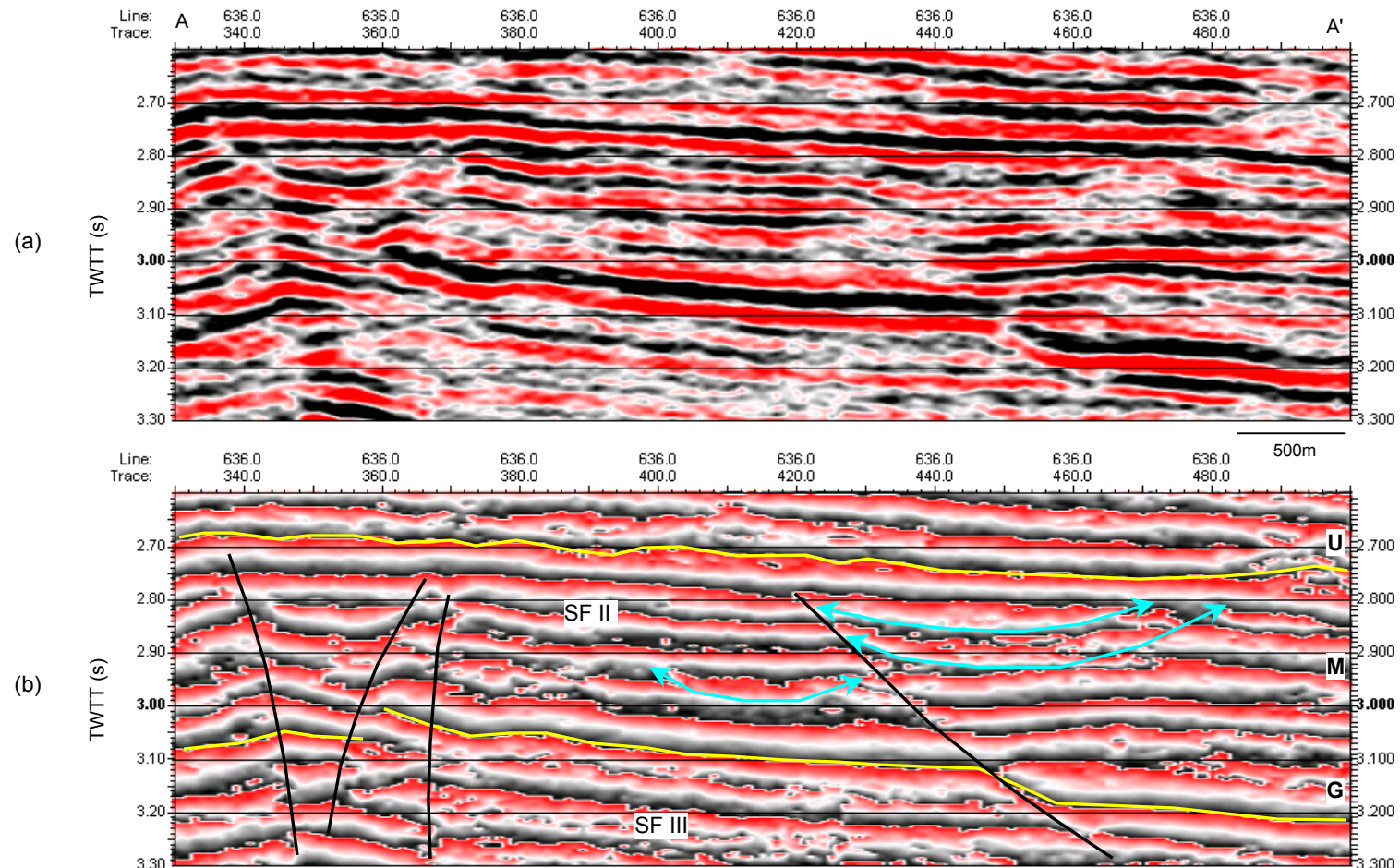


Figure 4.18 (a) Seismic line A-A' (amplitude display) showing the general reflection character of the Guasare-Misoa interval. (b) Interpreted phase display of the line A-A'. Within the Misoa Formation, eroded channel similar structures can be observable (see Figure 4.17 for location). U: unconformity, M: Misoa F., G: Guasare F., SF: Seismic Facies

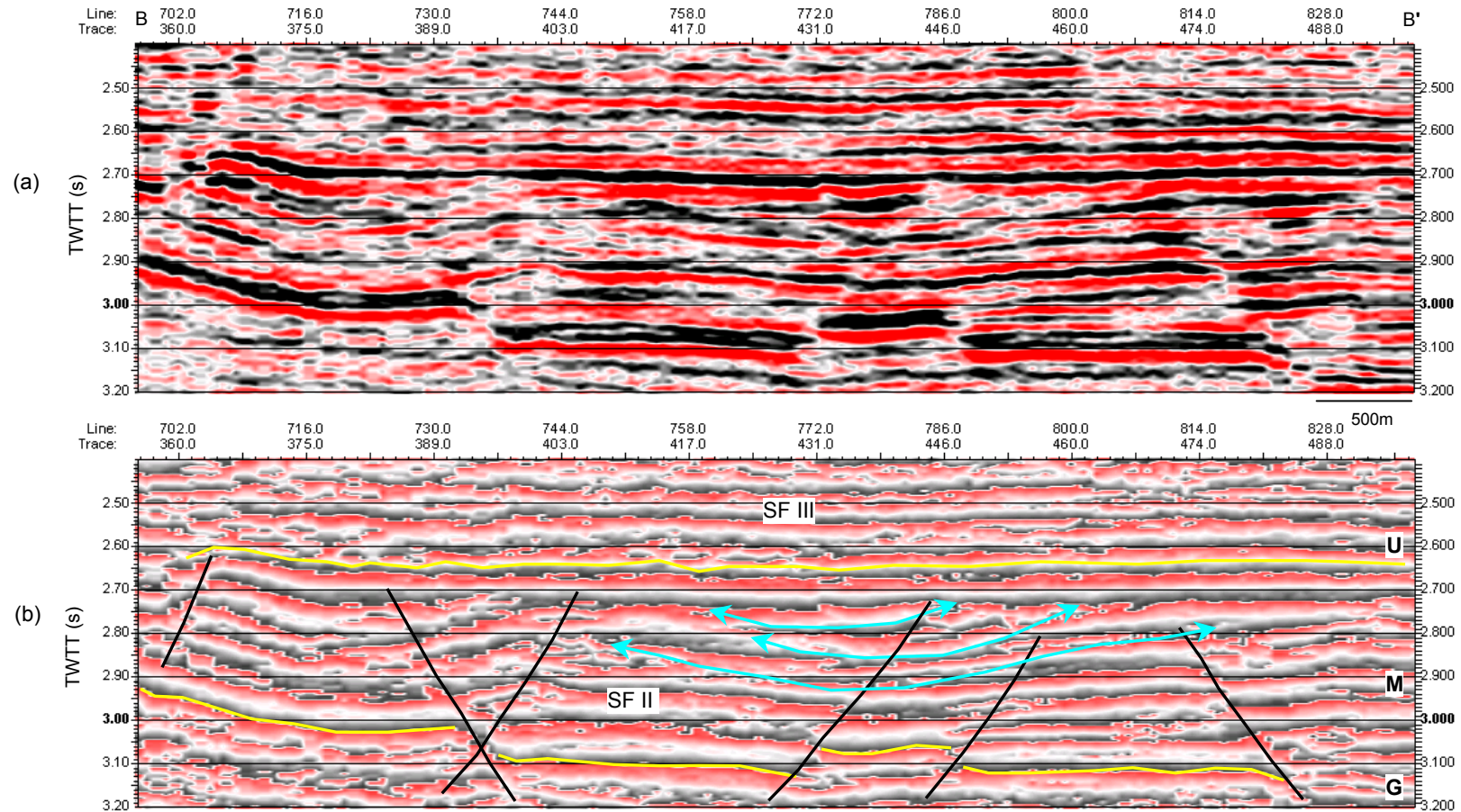


Figure 4.19 (a) Seismic line B-B' (amplitude display) along the depositional dip (southwest-northeast) showing the stacking pattern of the Guasare-Misoa interval. (b) Interpreted phase display of the line B-B' (see Figure 4.17 for location). U: unconformity, M: Misoa F., G: Guasare F., SF: Seismic Facies

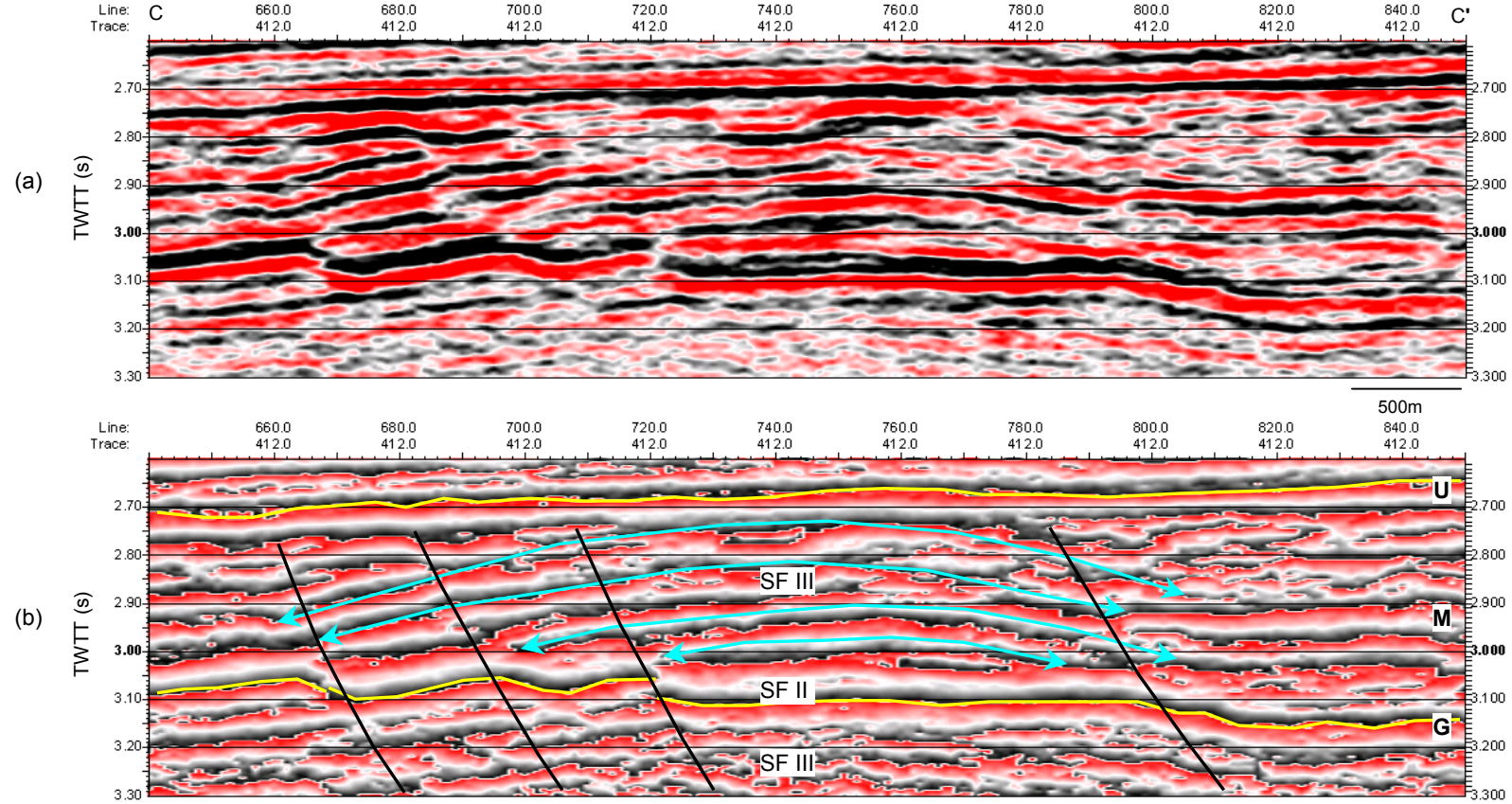


Figure 4.20 (a) Seismic line C-C' (amplitude display) showing the aggradational deposition of "C" sands in the Misoa Formation. (b) Interpreted phase display of the line C-C' (see Figure 4.17 for location). U: unconformity, M: Misoa F., G: Guasare F., SF: Seismic Facies

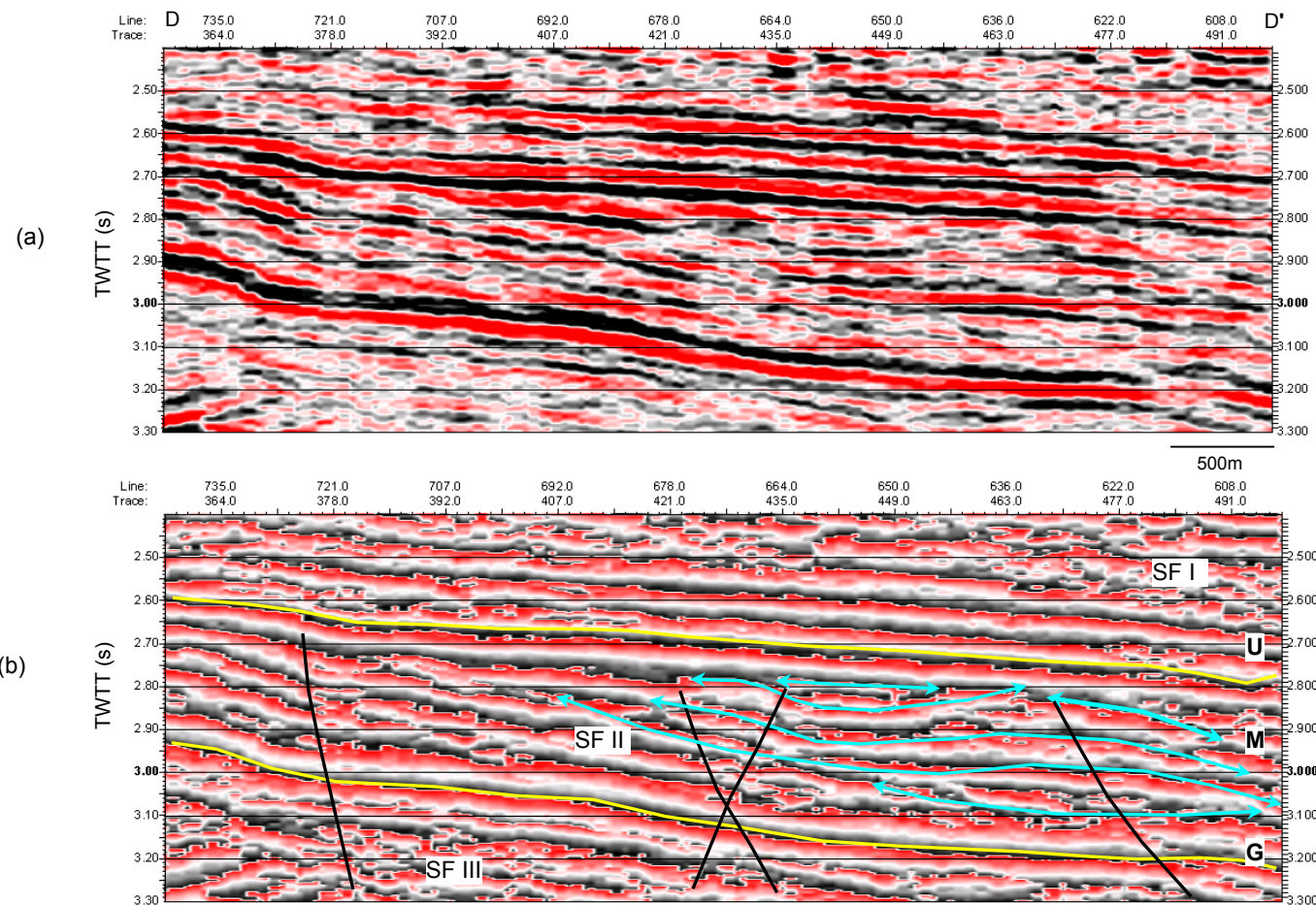


Figure 4.21 (a) Seismic line D-D' (amplitude display) along the depositional strike (southeast-northwest) showing progradational reflection patterns within the Misoa Formation. (b) Interpreted phase display of the line D-D' (see Figure 4.17 for location). U: unconformity, M: Misoa F., G: Guasare F., SF: Seismic Facies

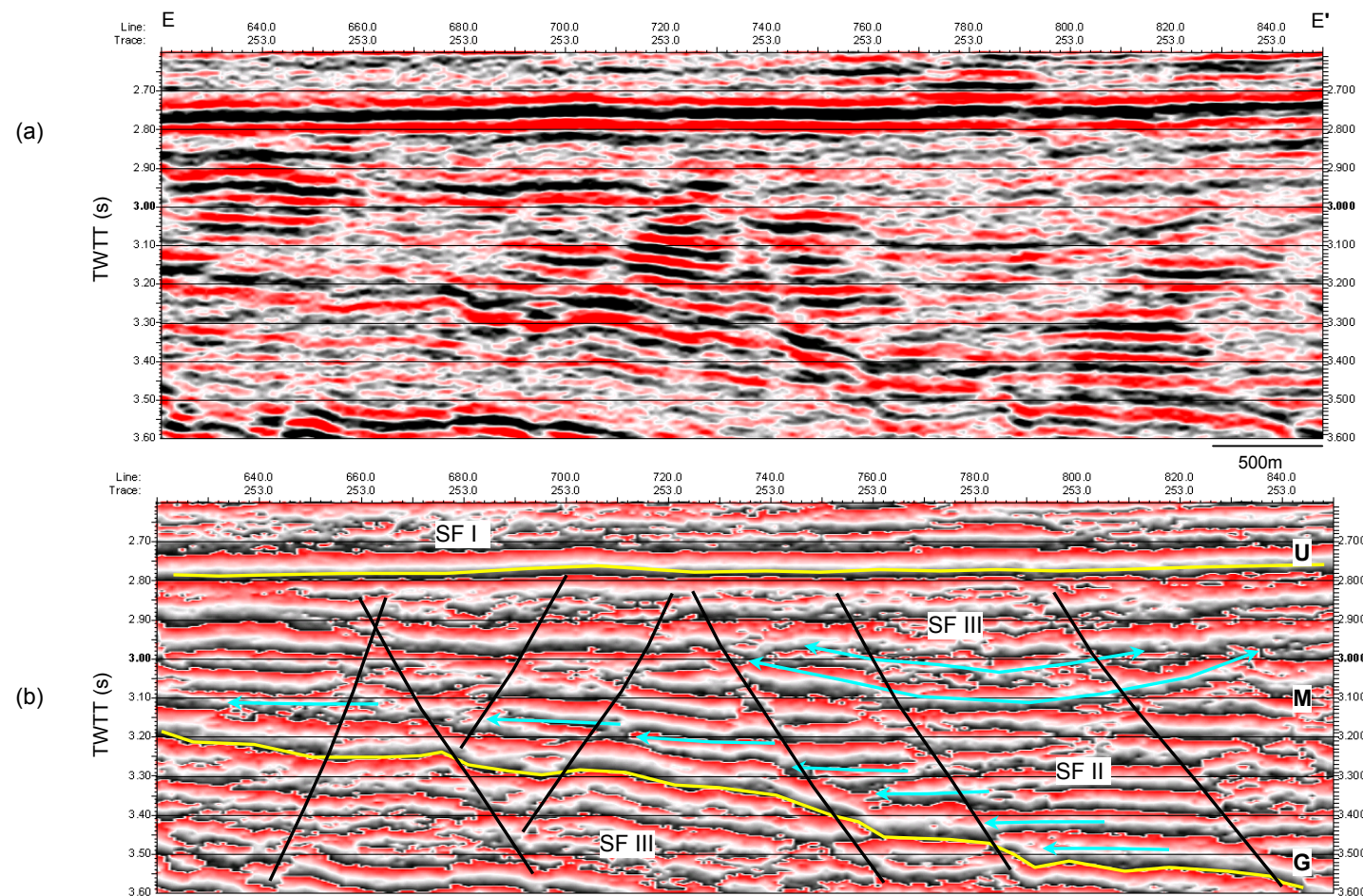


Figure 4.22 (a) Seismic line E-E' (amplitude display) showing the reflection pattern of the Misoa and Guasare formations in the west side of the area (downthrown block). (b) Interpreted phase display of the line E-E' (see Figure 4.17 for location). U: unconformity, M: Misoa F., G: Guasare F., SF: Seismic Facies

4.2.3 Results

- 1) In the VLE 196 area four main seismic facies are recognized. Seismic facies I is characterized by low-to-high or variable amplitude and poor-to-low continuity reflections with hummocky zones. Reflections with poor continuity and chaotic zones suggest that the rapid sedimentation of Miocene-to-recent age of La Rosa, Lagunillas, La Puerta, and El Mirago formations.
- 2) Seismic facies II is characterized by high amplitude, moderate-to-good continuity reflections. Parallel-to-subparallel reflections are dominant in the seismic facies II and discontinuous reflections (mostly truncations) can also be seen locally. This seismic facies represent the common reflection character of the Misoa Formation through the VLE 196 area. Seismic facies III is characterized by low-to-high amplitude, package of short, irregular hummocky cliniforms. This reflection pattern is observable within the Misoa Formation and some part of the shaly sediments of the underlying Colon and Mito Juan formations.
- 3) Seismic facies III is referring to a distributary channel fill and tidal sand ridges and lobes, which were created by deltaic sandstones of the Misoa “C” sands.
- 4) Seismic facies IV is characterized by chaotic, reflection free patterns which indicate the acoustic basement of the study area. Basement consists of igneous, metamorphic, and continental clastic sediments of the Cogollo, Rio Negro, and La Quinta formations.

- 5) Some channel similar structures with distributary pattern were also observed within the Misoa Formation but they were not continuous over the formation. Most probable reason for their discontinuity can be the intensive faulting in the area.
- 6) Seismic stratigraphy of the C4 layers could not be interpreted because of the vertical seismic resolution of the seismic data (see Appendix B and C).
- 7) The interval thickness of the C4 layer from seismic data ranges from 300 ft to 700 ft and exhibits SW-NE trending contour patterns and isolated sand lobes between the en echelon faults.

CHAPTER V

DISCUSSION

The VLE 196 area, Block V, Lamar Field represents a complex structure because of its previous long tectonic activity which was stated by most authors e.g. Sutton, 1946; Burke, 1988; Lugo and Mann, 1995; and Mann and Burke, 1984. In this study, as it stated in previous chapters, I proposed that the main deformation process created by the VLE 400 Fault which separates the area into two main parts. The VLE 400 Fault was interpreted as a complex left-lateral, strike-slip reverse fault (term adapted from Hill, 1947).

Dual classification of faults were explained by many authors e.g. Hill, 1947, 1959; Clark, 1943; and Crowell, 1959. Hill (1947 and 1959) stated that the “In dual classifications of faults, both dip- and strike-separation of faults are considered. The classification is principally geometric and gives, when both dip and strike-separation are evidence, a three dimensional concept of the apparent displacement. The classification could be used for both previously and newly mapped and described faults.”

Detailed interpretation of 3D seismic sections was revealed that the VLE 400 Fault appears as a left-lateral strike-slip fault in the southern part of the area but through the north it behaves as a reverse fault because of compressional structures which are created during the last period of deformation of the Lake Maracaibo. Kulke (1994) stated that “The last period of deformation in the Miocene-Pliocene-Recent is characterized by intense structural development in the area and this deformation in general related to the

oblique compression of the Caribbean plate with respect to the South American plate. Open folds, minor faults, and some uplifts were formed in the post-Eocene sedimentary rocks as well as the reactivation of the earlier structures in the Eocene and older rock units.”

Another possibility is that the VLE 400 strike-slip fault could be inverted during the last period of deformation, which is explained above, and gained a reverse component. As it can be seen in Figure 2.3, the VLE 196 area located between two syncline axes. It is believed that the occurrence of these anticlines was responsible for the possible inversion tectonics in the study area. Lugo Lobo (1991) also stated this situation as follows: “During the Cretaceous, extensional processes led to Cretaceous subsidence and normal displacement along major faults as evidence by thicker Cretaceous sections on the downthrown side of the faults. The Aptian-Albian K2 and K3 units do not have evidence of major activity along the faults, but in the Late Albian to Early Cenomanian the VLE fault system was reactivated. This allowed deposition of a thicker section of unit K4.”

The results that I gathered from well log interpretation to define depositional settings of the area were consistent with the previous works. Most of the authors (e.g., Martin et al., 1997; Talukdar and Marcano, 1994; Gonzales and Gustavo, 1991; Delgado, 1993; Ambrose et al., 1995; Munoz et al., 1994; Lugo and Ochoa, 1994; Link et al., 1996; Raeuchle et al., 1997; Carrizales et al., 2001) stated that that Lower Misoa strata were deposited in a tide-dominated delta setting and sediment source was from the west or southwest. The result of this study are also indicated that the sediments in the

VLE 196 area were deposited in tide dominated delta plain to shallow marine sediments consisting of fluvial/distributary channel and delta front sandstones prograded southwest to northeast (paleodip direction). This interpretation was based on log patterns of sandstones which are upward-coarsening, blocky, and upward-finishing on the gamma ray traces, and sandbody geometry shown on the gross thickness and net sand thickness maps.

CHAPTER VI

CONCLUSIONS

- 1) The VLE 196 area, Block V, Lamar Field, represents a complex structure because of its previous long tectonic activity.
- 2) The main deformation process in the area is the strike-slip movement created by the VLE 400 Fault, a left-lateral strike-slip reverse fault, separated the area in two main parts.
- 3) The trend of PDZ (principal displacement zone) is north south and dips westward.
- 4) Associated complementary faults have same trend with the VLE 400 Fault whereas en echelon normal and reverse faults are oriented approximately 50 degrees to the VLE 400 Fault and they compartment the reservoir.
- 5) General structural interpretation shows that the area was subjected northeast southwest compression and the VLE 196 area situated in the restraining bend.
- 6) Three main reflectors in the study area are the Late Eocene unconformity, Guasare Formation, and La Luna Formation. The unconformity is spread all over the field and because of it was not affected by faulting, it acted as a seal and inhibited the migration of the hydrocarbons. The Guasare and La Luna formations were affected by faulting especially in the vicinity of the VLE 400 Fault. The VLE 400 Fault created a significant vertical displacement of the Guasare and La Luna formations. Vertical separation is approximately 75 m (150 ms two-way travel time) and 150 m (250 ms two-way travel time) for Guasare and La Luna formations respectively.

- 7) The major trapping mechanism in the VLE 196 area is the four-way closure of the anticline and offset of strata created by the VLE 400 Fault.
- 8) C-4 interval in the Misoa sandstones were divided into three sandy and three shaly units based on type log responses and cross-sections. In each layer sand thickness varies but they trend through paleo dip (southwest-northeast).
- 9) Layer 1 is predominantly sand and interbedded with thin shaly units. Maximum gross thickness of this layer 250 ft and average porosity 27%. Fining-upward and blocky log responses of Layer 1 indicate delta front environment.
- 10) Layer 3 consists of massive sand within shaly interbeds. Maximum gross thickness and average porosity of this layer are 100 ft and 30% respectively. Log facies map of Layer 3 has blocky, serrate, and coarsening-upward log characteristics.
- 11) Layer 5 is mostly sandy with shaly interbeds. Gross thickness of this layer is approximately 150 ft and elongated to southwest northeast direction and become thinner through to southeast. Average porosity of this layer is 30%. Layer 5 has upward-fining log response, which is indicator of distributary channel.
- 12) Shaly layers of C-4 strata interpreted as potential seals and they deposited in low-energy interdistributary, and shallow marine environments. The percentage of shale increases upward from C-5 to C-4. Shales are of variable thickness and extend and they make up almost 40% of the C-4 interval.
- 13) Layer 6 at the base of the C-4 interval is most extensive shaly layer in the section and most likely it represents a marine flooding surface which is identified in electric logs as low resistivity and high gamma peak. In contrast, many other shaly layers have

more sand content. Thus, the extend of shale layers as reservoir or no-flow units are vary from layer to layer.

- 14) In general, all C-4 layers exhibit southeast northwest sand thickness contour patterns in lithofacies maps, reflecting depositional control on the interval. Depositional axis in the C-4 interval defined by more than 250 ft of gross sandstone, occur in narrow, depositional dip parallel belts, separated by relatively sandstone-poor areas consisting less than 20 ft of gross sandstone. C-4 depositional axes coincide with blocky and upward-fining log responses, flanked by sandstone-poor deposits exhibiting upward-coarsening and serrate log responses.
- 15) The log patterns and their order of occurrence in C-4 strata suggest that the sandstone are delta front and fluvial/distributary channel facies of delta system. This conclusion supported by the sand-body geometry shown on net sandstone and gross thickness maps.
- 16) In the VLE 196 area four main seismic facies are recognized. Seismic facies I is characterized by low-to-high or variable amplitude and poor-to-low continuity reflections with hummocky zones. Reflections with poor continuity and chaotic zones suggest that the rapid sedimentation of Miocene-to-recent age of La Rosa, Lagunillas, La Puerta, and El Mirago formations.
- 17) Seismic facies II is characterized by high amplitude, moderate-to-good continuity reflections. Parallel-to-subparallel reflections are dominant in the seismic facies II and discontinuous reflections (mostly truncations) can also be seen locally. This seismic facies represent the common reflection character of the Misoa Formation

through the VLE 196 area. Seismic facies III is characterized by low-to-high amplitude, package of short, irregular hummocky cliniforms. This reflection pattern is observable within the Misoa Formation and some part of the shaly sediments of the underlying Colon and Mito Juan formations.

- 18) Seismic facies III is referring to a distributary channel fill and tidal sand ridges and lobes, which were created by deltaic sandstones of the Misoa “C” sands.
- 19) Seismic facies IV is characterized by chaotic, reflection free patterns which indicate the acoustic basement of the study area. Basement consists of igneous, metamorphic, and continental clastic sediments of the Cogollo, Rio Negro, and La Quinta formations.
- 20) Some channel similar structures with distributary pattern were also observed within the Misoa Formation but they were not continuous over the formation. Most probable reason for their discontinuity can be the intensive faulting in the area.
- 21) Seismic stratigraphy of the C4 layers could not be interpreted because of the vertical seismic resolution of the seismic data (see Appendix B and C).
- 22) The interval thickness of the C4 layer from seismic data ranges from 300 ft to 700 ft and exhibits SW-NE trending contour patterns and isolated sand lobes between the en echelon faults.

REFERENCES CITED

- Ambrose, W. A., E. R. Ferrer, S. P. Dutton, F. P. Wang, A. Padron, W. Carrasquel, J. S. Yeh, and N. Tyler, 1995, Production optimization of tide-dominated deltaic reservoirs of the Lower Misoa Formation (Lower Eocene), LL-652 area, Lagunillas Field, Lake Maracaibo, Venezuela: The University of Texas at Austin, Bureau of Economic Geology, Report of Investigation n.226, 46 p.
- Ambrose, W. A., and E. R. Ferrer, 1997, Seismic stratigraphy and oil recovery potential of tide-dominated depositional sequences in the Lower Misoa Formation (Lower Eocene), Lagunillas Field, Lake Maracaibo, Venezuela: The Leading Edge, v.16, n.9, p.1331-1334.
- Ambrose, W. A., and E. Ferrer, 1997, Seismic stratigraphy and oil recovery potential of tide-dominated depositional sequences in the Lower Misoa Formation (Lower Eocene), LL-752 Area, Lagunillas Field, Lake Maracaibo, Venezuela: Geophysics, v.62, n.5, p.1483-1495.
- Azpíritxaga, I., 1991, Carbonate depositional styles controlled by siliciclastic influx and relative sea level changes, Lower Cretaceous central Lake Maracaibo, Venezuela: M.S. thesis, The University of Texas at Austin, p.1-80.
- Bartok, P., and T. Reijers, 1977, Sedimentología, diagenesis y potencial petrolífero del Grupo Cogollo, Cretaceo Inferior, Cuenca de Maracaibo: V Congreso Geol. Venez. Caracas, Noviembre 1977, Memoria A. Espejo et al., Editores, MEM-Soc. Venez. Geol., IV, p.529-557.
- Berg, O. R., 1982, Seismic detection and evaluation of delta and turbidite sequences, their application to exploration for the subtle trap: AAPG Bulletin, v.66, n.9, p.1271-1288.

- Bertagne, A. J., J. Rivas, M. Poupon, and J. O'Connor, n.d., The Maracaibo study in Bloque VIII: Compagnie Generale de Geophysique, <http://www.cgg.com/proserv/software/articles/MB1.htm> (October, 2001).
- Bockmeulen, H., C. Barker, and P. A. Dickey, 1983, Geology and geochemistry of crude oils, Bolivar coastal fields, Venezuela: AAPG Bulletin, v.67, n.2, p.242-270.
- Burke, K., 1988, Tectonic evolution of the Caribbean: Annual Review of Earth and Planetary Sciences, v.16, p.201-230.
- Carrazales, R., E. Sifonte, and T. Aguilar, 2001, Maximization of a field characterization using 3D Seismic: case study, C-2 Reservoir, Block VIII, Occidental Basin, Lake Maracaibo, Venezuela: Society of Petroleum Engineers Paper 69629, 12 p.
- Christe-Blick, N., and Biddle, K. T., 1985, Deformation and basin formation along strike-slip faults, *in* K.T. Biddle, and N. Christie-Blick, eds., Strike-slip deformation, basin formation, and sedimentation: SEPM Special Publication, p.1-34.
- Clark, S. K., 1943, Classification of faults: AAPG Bulletin, v.27, n.9, p.1245-1265.
- Coleman, J. M., and D. B. Prior, 1982, Deltaic environments of deposition, *in* P. A. Scholle and D. Spearing, eds., Sandstone depositional environments: AAPG Memoir 31, p.139-142.
- Crowell, J. C., 1959, Problems of fault nomenclature: AAPG Bulletin, v.43, n.11, p.2653-2674.
- Delgado, I., 1993, Lama Field - Venezuela, Maracaibo Basin, Zulia State, 1993 *in* N. H. Foster and E. Q. Beaumont, eds., Structural Traps VIII, Treatise of Petroleum Geology, Atlas of Oil and Gas Fields: AAAPG Special Publications, v.A022 , p.271-294.

- Einsele, G., 1992, Sedimentary basins – evolution, facies, and sedimentary budget, Berlin, Germany: Springer-Verlag, p.150-153.
- Galloway, W. E., and D. K. Hobday, 1996, Terrigenous clastic depositional systems, applications to fossil fuel and ground water resources: Berlin, Germany, Springer-Verlag, p.115-120.
- Garcia I., 1998, Different methodologies for obtaining a permeability distribution in the Misoa Formation, Venezuela: M.S. thesis, Texas A&M University, College Station, Texas, p.27-37.
- Gonzales, C., and F. Gustavo, 1991, Diagenesis and reservoir characterization of the Block V, Lamar Field, Maracaibo Basin, Venezuela: AAPG Bulletin, v.75, n.3, p.583.
- Gonzales de Juana, C., J. A. Arozeno, and X. Picard Cardillat, 1980, Geologia de Venezuela y sus cuencas petroliferas: Ediciones Foninves, Caracas, p.1031.
- Harding, T. P., R.C. Vierbuchen, and N. Christie-Blick, 1985, Structural styles, Plate tectonic settings, and hydrocarbon traps of divergent (transtensional) wrench faults, *in* K.T. Biddle, and N. Christie-Blick, eds., Strike-slip deformation, basin formation, and sedimentation: SEPM Special Publication, n.37, p.51-77.
- Hill, M. L., 1947, Classification of faults: AAPG Bulletin, v.31, n.9, p.1669-11673.
- Hill, M. L., 1959, Dual classification of faults, AAPG Bulletin, v.43, n.1, p.217-221.
- Holditch, S. A. & Associates Inc., 1997, Reservoir characterization of the C-4 and C-5 intervals, VLE 196 Area, Block V, Lamar Filed, Lake Maracaibo, Venezuela, v.1, p.1-40.

- James, K. H., 1990, The Venezuelan hydrocarbon habitat, *in* J. Brooks, ed., Classic petroleum provinces: Geological Society Special Publications, n.50, p.9-35.
- Kulke, H., 1994, Venezuela, *in* H. Kulke, ed., Regional petroleum geology of the World, Part II: Berlin, Gebruder Borntraeger, p.489-515.
- Link, M. H., C. K. Taylor, N. G. Munoz, J.E. Bueno, and P. Munoz, 1996, 3-D seismic examples from central Lake Maracaibo, Maraven's Block I Field, Venezuela, *in* P. Weimer and T. L. David, eds., Studies in geology 42: AAPG Special Publications, p.96-118.
- Lugo, J., and E. Ochoa, 1994, Sequence stratigraphic analysis of northeastern Maracaibo Basin, Venezuela: 14th World Petroleum Congress, preprint topic 2(5), Chichester, UK, J. Wiley&Sons, p.105-117.
- Lugo, J., and P. Mann, 1995, Jurassic-Eocene tectonic evolution of Maracaibo Basin, Venezuela, *in* A. J. Tankard, R. S. Sorucu, and H. J. Welsink, eds., Petroleum Basins of South America: AAPG Memoir 62, p.699-725.
- Lugo L. J. M., 1991, Cretaceous to Neogene tectonic control on sedimentation, Maracaibo Basin, Venezuela: Ph.D. dissertation, The University of Texas at Austin, 220 p.
- Maguregui, J. A., and N. Tyler, 1991, Evolution of middle Eocene tide-dominated deltaic sandstones, Lagunillas field, Maracaibo Basin, western Venezuela, *in* A. D. Miall, and N. Tyler, eds., The three-dimensional facies architecture of terrigenous clastic sediments and its implications for hydrocarbon discovery and recovery: SEPM Concepts in Sedimentology and Paleontology, v.3, p.233-244.
- Mann, P., and K. Burke, 1984, Neotectonics of the Caribbean: Reviews of Geophysics and Space Physics, v.22, n.4, p.309-362.

- Martin, R. B., W. B. Ayers, E. R. Jr. Hunt, D. A. Pursell, I. R. Diyashev, and D. A. McVay, 1997, An integrated reservoir model of the Early Eocene age Misoa Formation (C-4 and C-5 sands), VLE 196/Lamar Field, Block V, Lake Maracaibo, Venezuela: I Congreso LatinoAmericano De Sedimentologia, Porlamar, Isla de Margarita, Venezuela, 7 p.
- McClay, K., and M. Bonora, 2001, Analog models of restraining stepovers in strike-slip fault systems: AAPG Bulletin, v.85, n.2, p.233-260.
- Mitchum, R. M., P. R. Vail, and J. B. Sangree, 1977, Seismic stratigraphy and global changes of sea level, part 6: stratigraphic interpretation of seismic reflection patterns in depositional sequences, *in* C. E. Payton, ed., Seismic stratigraphy – applications to hydrocarbon exploration: AAPG Memoir 26, p. 117-133.
- Molina, A., 1993, Tarra Field, Maracaibo Basin, Zulia State, Venezuela, *in* N. H. Foster and E. Q. Beaumont, eds., Structural Traps VIII, Treatise of Petroleum Geology, Atlas of Oil and Gas Fields: AAPG Special Publications, v.A022 , p.255-269.
- Montgomery, H., E. A. Pessagno, Jr., and I. M. Munoz, 1992, Jurassic (Tithonian) radiolaria from La Desirade (Lesser Antilles), Preliminary paleontological and tectonic implications: Tectonics, v.11, p.1426-1432.
- Munoz J., N. G., M.H. Link, J. Delgado, P. J. Munoz, C. K. Taylor, and R. M. Mitchum, 1994, Integrated sedimentological and seismic studies, Eocene Misoa C sands, Maraven Block I, Maracaibo Basin, Venezuela: Memorias del VII Congreso Venezolano de Geofísica, p.259-266.
- Pindell, J. L., and S. F. Barret, 1990, Geologic evolution of the Caribbean: a plate-tectonic perspective, *in* G. Dengo and J. E. Case, eds., The Caribbean, Volume H: Decade of North American Geology, GSA, p.405-432.

- Pindell, J. L., 1991, Geologic rationale for hydrocarbon exploration in the Caribbean and adjacent regions: Journal of Petroleum Geology, v.14 (3), p.237-257.
- Pindell, J. L., J. P. Erikson, and S. Algar, 1991, The relationships between plate motions and sedimentary basin development in northern South America: Trans. 2nd Geol. Conf., Trinidad and Tobago Geological Society, Port-of-Spain, 1990.
- Raeuchle, S. K., W. A. Ambrose, M. S. Akhter, J. Cesas, L. Salamanca, P. Munoz, and A. Leon, 1997, Integrated reservoir study, Lower Eocene Misoa reservoirs, VLA-6/9/21 Area, Block I, Phase 2, Stage 2, Lagunillas Field, north-central Lake Maracaibo, Venezuela: Geophysics, v.62, n.5, p.1496-1509.
- Rosencrantz, E., M. Ross, and J. G. Sclater, 1988, Age and spreading history of the Cayman Trough as determined from depth, heat flow, and magnetic anomalies: Journal of Geophysical Research, n.93, p.2141-2157.
- Rosencrantz, E., 1990, Structure and tectonics of the Yucatan Basin, Caribbean Sea, as determined from seismic reflection profiles: Tectonics, v.9, p.1037-1059.
- Scheibling, M. H., and C. D. Atkinson, 1992, Lithofacies and environmental analysis of clastic depositional systems, *in* D. Morton-Thompson and A. M. Woods, eds., Development geology reference manual: AAPG Special Publications, Methods in Exploration 10, p.293-265.
- Speed, R. C., and G. K. Westbrook, 1984, Lesser Antilles Arc and adjacent Margin Drilling Program: Regional Atlas Series, Marine Science International, n.10, 27 p.
- Stauffer, Kark W., and G. D. Croft, 1995, A modern look at the petroleum geology of the Maracaibo Basin, Venezuela: Oil and Gas Journal, v.93, n.23, p.63-66.

Sutton, F. A., 1946, Geology of Maracaibo Basin, Venezuela: AAPG Bulletin, v.30, n.10, p.1621-1741.

Talukdar, S., O. Gallango, and M. Chin-A-Lien, 1985, Generation and migration of hydrocarbons in the Maracaibo Basin, Venezuela: Memoir, Second Bolivarian Symposium on petroleum exploration in Subandean Basin, Bogota, Colombia, v.2, 43 p.

Talukdar, S., O. Gallango, and A. Ruggiero, 1987, Generation and migration of oil in the Maturin Subbasin, Eastern Venezuelan Basin: Advances in Organic Geochemistry, v.13, n.1-3, p.537-547.

Talukdar, Suhas C., and F. Marcano, 1994, Petroleum systems of the Maracaibo Basin, Venezuela, *in* L.B. Magoon and W.G. Dow, eds., The petroleum system – from source to trap: AAPG Memoir 60, p.463-481.

Twiss, R. J., and E. M. Moores, 1992, Structural geology: New York, W. H. Freeman and Company, p.113-127.

Tyler, N., W. A. Ambrose, S. P. Dutton, F. Wang, J. S. Yeh, E. Ferrer, A. Padron, and W. Carrasquel, 1994, Characterization of Lower Eocene reservoirs in the LL-652 Area, Lagunillas Field: The University of Texas Austin, Bureau of Economic Geology, Final Report to Lagoven, S.A., 425 p.

Van Andel, T. H., 1958, Origin and classification of Cretaceous, Paleocene, and Eocene sandstones of western Venezuela: AAPG Bulletin, v.42, n.4, p.734-763.

Zambrano, E., E. Vasquez, B. Duval, M. Latreille, and B. Coffinieres, 1971, Sintesis paleogeográfica y petrolera del occidente de Venezuela: Memoir, Fourth Venezuelan Geological Congress, Caracas, Venezuela, Special Publication 5, p.483-545.

Zamora, L., 1977, Uso de perfiles en la identification de ambientes sedimentarios del Eocene del Lago de Maracaibo: V Cong. Geol. Venez., Noviembre, 1977, Memoria, A. Espejo et al., Editores, MEM-Soc. Venez. Geolo., v.IV, p.1359-1376.

APPENDIX A

Measured depth of the top of the C-4 strata and top of the C-5 strata based on well logs.

Well ID	Top C-4 (ft)	Top C-5 (ft)	Thickness
VLE 0096	11246	11540	294
VLE 0196	11675	11940	265
VLE 0400	11729	12053	324
VLE 0449	11074	11459	385
VLE 0504	-	11888	-
VLE 0506	11369	11655	286
VLE 0510	11258	11590	332
VLE 0516	11840	12162	322
VLE 0571	11837	12124	287
VLE 0619	12055	12277	222
VLE 0631*	12022	12347	325
VLE 0651	12102	12392	290
VLE 0674	11345	11643	298
VLE 0675	11170	11500	330
VLE 0677	11316	11601	285
VLE 0973	11460	11785	325
VLE 1004	11822	12157	335
VLE 1063*	11095	11409	314
VLE 1101	11208	11522	314
VLE 1130	11347	11707	360
VLE 1139	11205	11567	362
VLE 1140	11818	12082	264
VLE 1148	11823	-	-
VLE 1155	11352	11669	317

(*) Type Log

APPENDIX B

Measured depth and average thickness of the C-4 layers based on well logs.

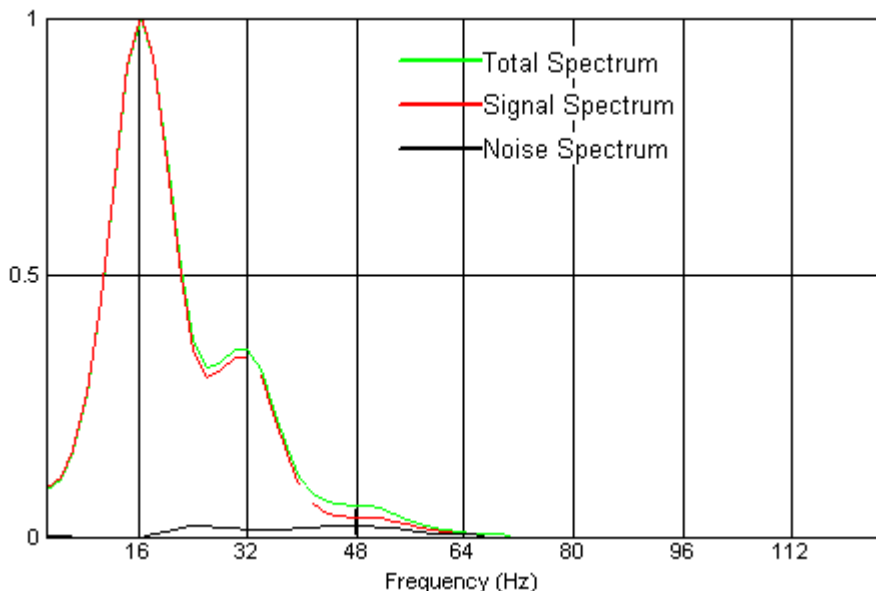
Well ID	Layer 1 Top (ft)	Layer 2 Top (ft)	Layer 3 Top (ft)	Layer 4 Top (ft)	Layer 5 Top (ft)	Layer 6 Top (ft)
VLE 0096	11246	11290	11323	11415	11424	11516
VLE 0196	11675	11734	11800	11841	11848	-
VLE 0400	11729	-	11837	11884	11919	12010
VLE 0449	11074	11178	11206	11290	11310	-
VLE 0506	11369	11427	11441	11519	11549	11644
VLE 0510	11258	11338	11360	11446	11478	11564
VLE 0516	11840	11899	11940	12009	12020	12101
VLE 0571	11837	11915	11927	11978	11999	12094
VLE 0619	12055	12100	12109	12183	12211	12256
VLE 0631*	12022	12074	12101	12193	12213	12309
VLE 0651	12102	12161	12177	12233	12251	12358
VLE 0674	11345	11408	11426	11495	11513	11573
VLE 0675	11170	11236	11259	11304	11313	11388
VLE 0677	11316	11395	11418	11450	11458	11567
VLE 0973	11460	11520	11586	11630	11667	11739
VLE 1004	11822	11910	11964	12008	12026	12117
VLE 1063*	11095	11169	11196	11270	11280	11379
VLE 1101	11208	11310	11333	11389	11402	11473
VLE 1130	11347	11438	11451	11554	11576	11671
VLE 1139	11205	11324	11365	11447	11468	11546
VLE 1140	11818	11880	11889	11965	11973	12048
VLE 1148	11823	11937	11962	12045	12058	12130
VLE 1155	11352	11409	11437	11490	11530	11592
Average Thickness (ft)	73	28	66	19	83	41

(*) Type Log

APPENDIX C

Determination of Vertical Seismic Resolution

Dominant frequency for the Misoa sadns in VLE 196 area calculated extracting wavelet from seismic in-line 750 using SynPak tool of Kingdom Suite software. Two dominant frequencies were determined both for Misoa interval and C-4 strata.



Frequency spectrum of the Misoa sands.

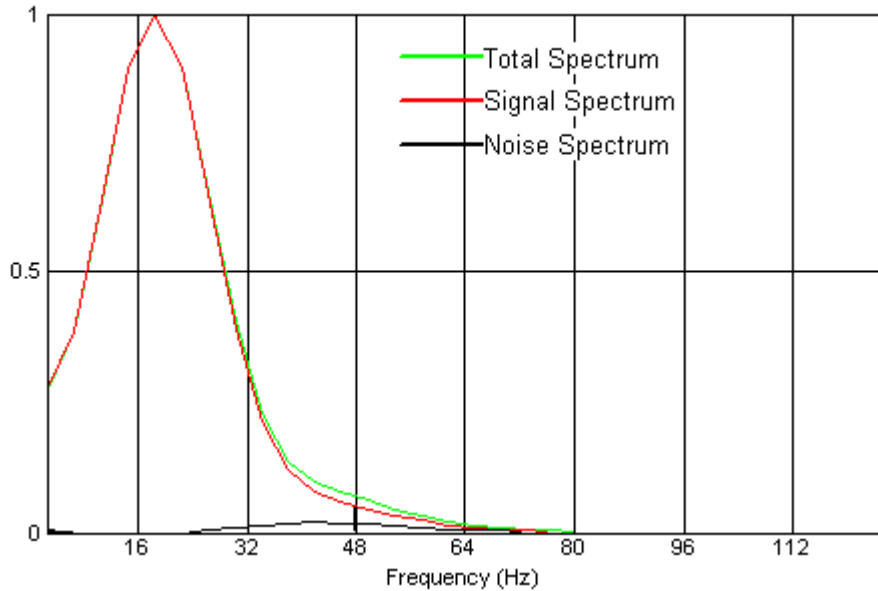
In-line: 750

Start time: 2.731

End time: 3.064

Starting trace: 437

Ending trace: 466



Frequency spectrum of the C-4 strata.

In-line: 750

Start time: 2.869

End time: 3.005

Starting trace: 413

Ending trace: 498

The dominant wavelength of seismic waves given by $\lambda = \frac{v}{f}$ where v is the velocity and f

f is the dominant frequency. From above figures, dominant frequency is approximately 20 Hz and seismic velocity of the Misoa sands was calculated as 8600 ft/s, then λ is 430 ft and the acceptable vertical resolution for seismic data is approximately $(\lambda/4)$ 107 ft.

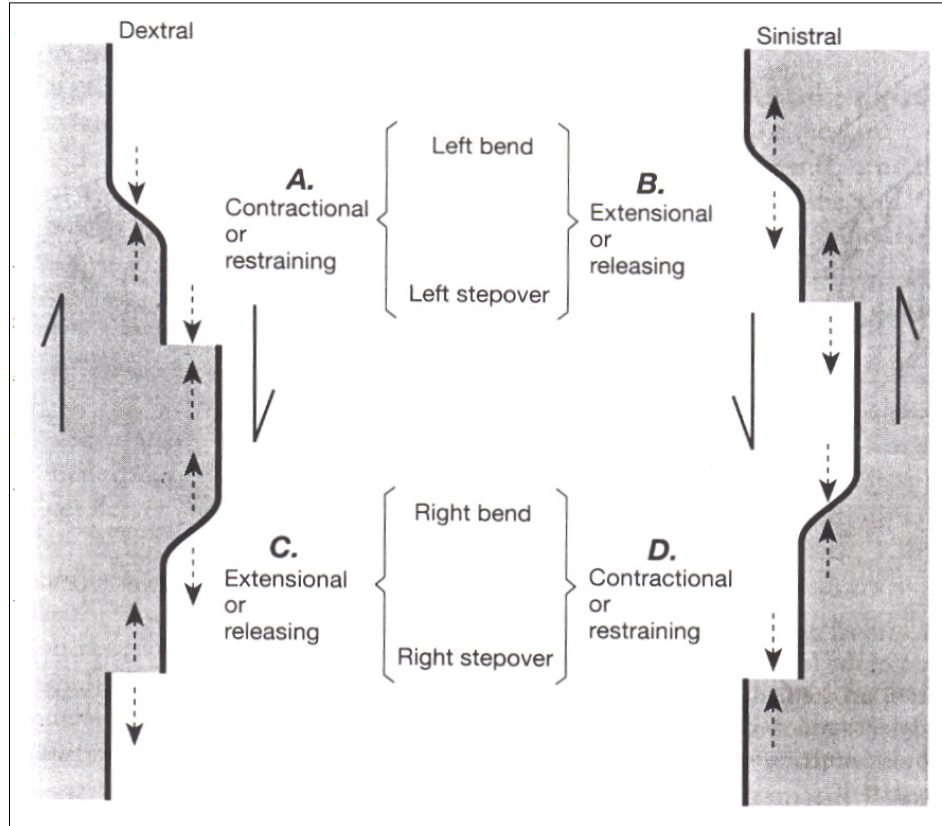
APPENDIX D

Well ID	Thickness values for C4 interval from well (ft)	TWTT values for C4 interval isochron map (s)	Thickness values for C4 interval isopach map (ft)
VLE 0096	294	0.022	18*
VLE 0196	265	0.022	70*
VLE 0400	324	0.007	295
VLE 0449	385	0.038	113*
VLE 0506	286	0.027	111
VLE 0510	332	0.067	597*
VLE 0516	322	0.076	300
VLE 0571	287	0.037	77*
VLE 0619	222	0.032	191
VLE 0631	325	0.070	293
VLE 0651	290	0.005	115
VLE 0674	298	0.076	187
VLE 0675	330	0.067	31*
VLE 0677	285	0.022	136
VLE 0973	325	0.087	384
VLE 1004	335	0.076	297
VLE 1063	314	0.038	242
VLE 1101	314	0.028	232
VLE 1130	360	0.007	152*
VLE 1139	362	0.067	337
VLE 1140	264	0.035	67*
VLE 1155	317	0.076	187

(*) Values that were not considered for seismic-well log correlation plot.

TWTT: Two way travel time

APPENDIX E



The geometry and terminology for right and left bends and stepovers. Large arrows show relative shear on the fault. Pairs of dashed arrows indicate the extension or contraction across the bends and stepovers (Twiss and Moores, 1992).

VITA

Sadun Arzuman received his Bachelor of Science degree in geophysical engineering from Istanbul Technical University (ITU) in 1998. Upon graduation, he started his master's education, pursuing a degree in geophysical engineering at the same university. During his master's work at ITU, he was awarded a Turkish Petroleum Company (TPAO) scholarship to study abroad. He enrolled in Texas A&M University, Department of Geology and Geophysics, to pursue a Master of Science degree in geology and graduated in December 2002. He is currently employed by TPAO and working as a seismic interpreter at the International Project Group. His current address is TPAO International Project Group, Mustafa Kemal Mah. 2. Cad No: 86 06520 Ankara Turkey.